SYSTEM MONITORING BY TRACKING FRACTIONAL ORDER

A Dissertation

Submitted to the Graduate School
of the University of Notre Dame
in Partial Fulfillment of the Requirements
for the Degree of

Doctor of Philosophy

by

Kevin Leyden

Bill Goodwine, Director

Graduate Program in Aerospace and Mechanical Engineering
Notre Dame, Indiana
April 2018

SYSTEM MONITORING BY TRACKING FRACTIONAL ORDER

Abstract

by

Kevin Leyden

Mechanical systems are often combinations of many interacting components. Examples of such systems include gas turbines, washing machines, machine tools, and cars. These systems' vibrations are commonly analyzed with numerical methods, but the complexity makes mathematical analysis challenging. This research has pursued a mathematical framework to relate applied force and displacement in mechanical systems of this type by modeling them as networks.

Fractional differential equations are a simplifying tool for complex systems. The overall dynamics of a mechanical (or mechanically behaving) system with many moving parts can be modeled as having a fractional order, circumventing any need to include the many intermediate degrees of freedom explicitly. Damage to a complex system of this type can be assessed by measuring the change in its fractional order.

This research has yielded a system identification procedure to compute fractional-order models from frequency data. In analyzing simulated systems representing multi-robot vehicle formations, shifts in fractional order are evident in response to changes in both the severity and the location of damage. These results support the primary goal of this research: a monitoring method that can diagnose damage without complete sensor coverage, instead measuring fractional order to infer operational changes.

If fractional calculus can be likened to monomials in the derivative D — for example, first derivative D, second derivative D^2, and half derivative $D^{1/2}$ — implicit

operators are the next frontier: general expressions in D. In this research, implicit operators have been used for concise models describing the dynamics of complex vibrating systems. These models are promising for ease of accurate simulation and control of such systems. Along with this mathematical extension, the concept of fractional order as a defining parameter in modeling and control has been extended toward application in simulated trajectory-following control of a dynamically walking two-legged robot. Both extensions are meant to demonstrate the breadth of previously undiscovered utility for fractional and implicit operators in engineering.

To all who thirst for knowledge

CONTENTS

FIGURES

ACKNOWLEDGMENTS

I extend many thanks to Bill Goodwine, my advisor, as well as to Panos Antsaklis, Jim Schmiedeler, and Mihir Sen, the members of my committee. I also thank my research group colleagues, my instructors, and everyone else I have had the pleasure of knowing in the Aerospace and Mechanical Engineering department and, more broadly, at the University of Notre Dame. I thank the University, the National Science Foundation, and the Office of Naval Research for funding my graduate school years. Last but not least, I am grateful to my family and friends for their support.

CHAPTER 1

INTRODUCTION

A dissertation generally reflects a search for useful information. In that regard, this one is no different; however, searching for said information between derivative and integral operators is not so common. High-order mechanical systems are ubiquitous throughout engineering. It is the goal of this work to present ideas that will advance the modeling of these systems and, in turn, the control and design of these systems. The conduit for this evolution is fractional calculus, a transformative branch of mathematics that presents atypical interpretations of centuries-old principles.

Chapter 2 presents two types of background as foundation for this work. The first is a mathematical overview of the concepts central to fractional calculus. The second is a review of literature featuring these concepts in areas related to this work: systems theory, control, dynamics, and robotics, among others.

Chapter 3 illustrates the finding on which the following results are built: that damage to a high-order mechanical system can be observed through the lens of fractional order. This discussion includes details of the mathematical analysis that justifies this exploration. Computational results in the frequency and time domains follow, along with supporting ideas to develop these observations into a monitoring method.

Chapter 4 reinforces the observations of detected damages with a system identification procedure. This is included for the purpose of lending insight into the fractional-order dynamics that may be present throughout the class of systems with mechanical models. Future application of system monitoring by fractional order in experimental settings will need to rely upon a computational procedure of this nature.

Chapter 5 is concerned with determining operators to describe complex mechanical networks. Networks of this type are cast in the form of nodes having mass and branches consisting of massless linear springs and dampers. The behaviors of finite and infinite versions of systems in arrangements resembling trees and ladders are analyzed. It is shown that the overall dynamics of infinite systems can be represented using implicitly defined integro-differential operators, and it is suggested that this approach may be beneficial compared to high-order differential equations. Results from the proposed models compare favorably with numerical results from finite systems. This research is a mathematical extension of the work of the preceding chapters.

Chapter 6 presents research seeking greater efficiency for walking robots. Efficiency can be improved in two ways: better performance (i.e., less wasted motion) and reduced energy consumption. Fractional-order control is a pathway to both of these improvements because of the flexibility it offers in designing a control strategy. Compared to the existing proportional-derivative architecture, changing the order of the derivative — the number of derivatives taken — to real numbers other than 1 has yielded both types of improvement for a simulated walker. The evidence of better performance is the leg angles' improvement in maintaining a desired relationship with respect to one another. Depending on the controller chosen, the walker can also be made to achieve the original level of performance with reduced control signals and less torque delivered to the hip joint, implying greater energy efficiency. This research demonstrates the potential of fractional-order control even in a setting where fractional-order dynamics are not apparent, further highlighting its promise in controlling known fractional-order behavior.

Chapter 7 outlines the steps that may follow from this research. A mathematical framework to relate effects on mechanical components to order changes on the system level is proposed as a contribution that will make this monitoring more versatile. This versatility can be verified by enhancing the identification procedure and applying

it to additional systems, to include experimental data. It is also suggested that fractional calculus can be exploited for systems modeling in a distinct but related way: constructing a model from integer-order elements that responds at any order desired. These ideas are intended as future research directions that can proceed from this dissertation.

CHAPTER 2

MATHEMATICAL AND CONTEXTUAL BACKGROUND

Fractional calculus is a shock to the mind. Students of calculus are no strangers to derivatives and integrals, nor to the idea that they can be performed multiple times, resulting in a series of functions that are progressively the derivatives or integrals of one another. Still, until led to the metaphorical water at the outset of this work, this author never considered the possibility that a derivative or integral could be performed a *noninteger* number of times.

This chapter presents that revelation in two ways: the fundamentals behind the operators of fractional calculus and the effects that those operators have had on the research community in systems, control, dynamics, robotics, and similar areas. These discussions are meant to reveal the context in which the ideas and results outlined in the following chapters take their place.

2.1 Fractional Calculus

As stated above, it is common enough to perform repeated differentiation. Some types of functions are conducive to concise, closed-form expressions for the second derivative, the third, and so on; sine and cosine come to mind. As detailed in [22], an example function that foreshadows the derivation of the fractional derivative is a monomial. Consider $f(x) = x^k$, where k is an integer greater than or equal to zero. It follows that

$$\frac{df}{dx}(x) = kx^{k-1},$$

$$\frac{d^2 f}{dx^2}(x) = k(k-1)x^{k-2},$$

and so on. To this point, the restrictions on k are unnecessary, but they are needed for the following generalization. For a derivative order q that is an integer less than or equal to k,

$$\frac{d^q f}{dx^q}(x) = \frac{k!}{(k-q)!}x^{k-q}. \tag{2.1}$$

Factorial arguments must be integers greater than or equal to zero. Fractional calculus, however, is a rebuttal to the claim that k and q must be integers, or indeed, that any restrictions within the real numbers need be imposed on them at all.

The factorial operator has a generalization to the real numbers; this is the gamma function,

$$\Gamma(k) = \int_0^\infty z^{k-1}e^{-z}\,dz.$$

The analogy between the gamma function and the factorial is shown in Figure 2.1. The factorials of 0 to 4 are 1, 1, 2, 6, and 24; indeed, these values of the gamma function are marked in the figure. Their corresponding arguments are shifted by one from the factorial arguments. In other words, for a nonnegative integer k, $k! = \Gamma(k+1)$, or $\Gamma(k) = (k-1)!$ (though $\Gamma(0)$ does not converge).

Naturally, the true merit of the gamma function in this context is that it provides a factorial equivalent for noninteger arguments. This is needed to free Equation (2.1) from the restriction of integer k and q. The substitutions that accomplish this are

$$\frac{d^q}{dx^q}x^k = \frac{k!}{(k-q)!}x^{k-q} \quad \rightarrow \quad \frac{d^q}{dx^q}x^k = \frac{\Gamma(k+1)}{\Gamma(k-q+1)}x^{k-q}. \tag{2.2}$$

The gamma function converges for all real arguments except nonpositive integers.

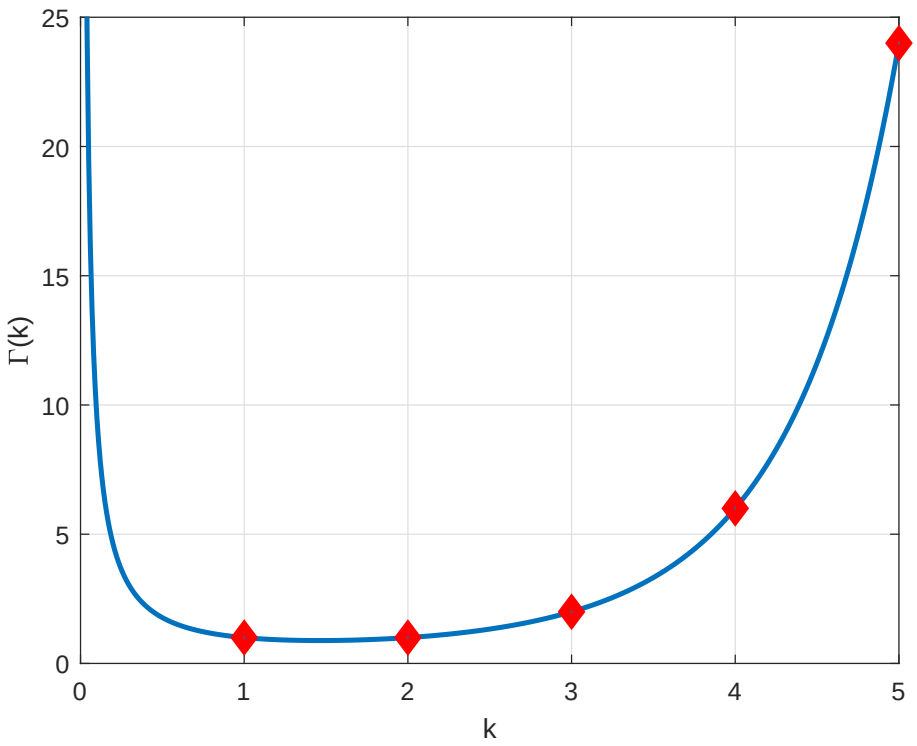

Figure 2.1. Gamma function for positive arguments with factorials marked.

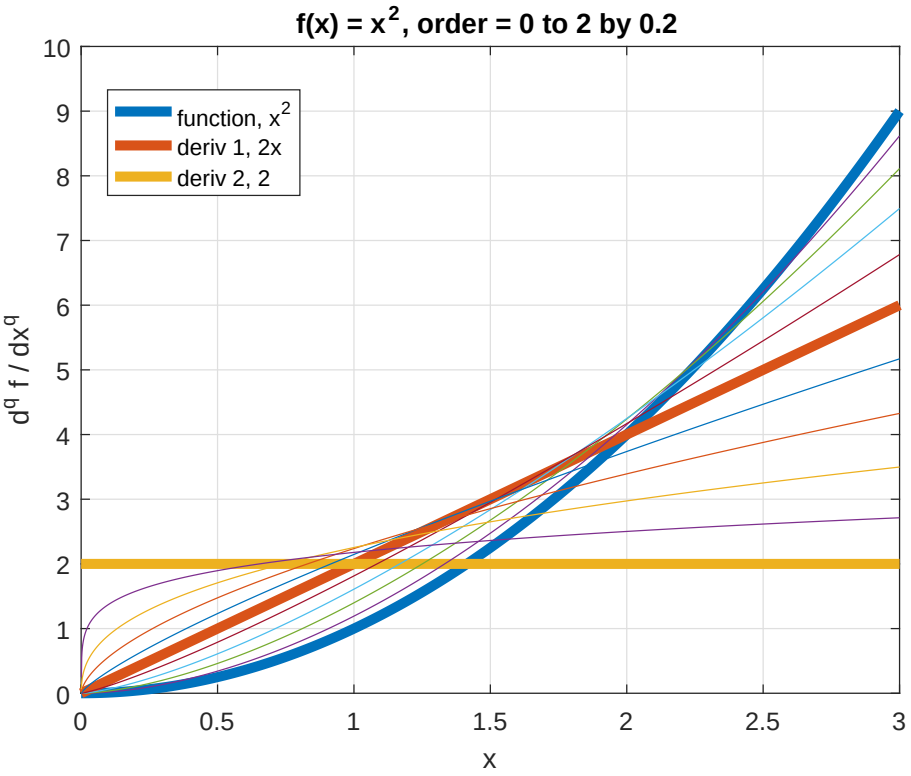

Figure 2.2. Many derivatives of x^2.

Equation (2.2) can be used to compute fractional derivatives for a monomial. An example of a popular monomial plotted with some of its integer and fractional derivatives is shown in Figure 2.2. As can be seen in the figure, the fractional derivative is not simply a linear interpolation between integer derivatives; one may instead think of it as a *mathematical* interpolation representing the result of stopping part of the way through the derivative operation.

The gamma function's utility is not limited to this example. Rather, it is essential in deriving the Riemann-Liouville fractional derivative. As in [50], this derivation begins with Cauchy's formula for repeated integration.

Repeated integration can be considered differentiation of a negative integer order.

If this order is called q ($q < 0$) and the formula is applied to a function $g(x)$, then

$$\frac{d^q g}{dx^q}(x) = q \text{ integrals} = \frac{1}{(-q-1)!}\int_0^x (x-y)^{-q-1} g(y)\, dy.$$

By substituting the gamma function, this formula can be extended to negative *real* orders, not exclusively integers, q:

$$\frac{d^q g}{dx^q}(x) = \frac{1}{\Gamma(-q)}\int_0^x (x-y)^{-q-1} g(y)\, dy. \tag{2.3}$$

This is the Riemann-Liouville fractional integral. If a fractional derivative that is truly a derivative, with $q \geq 0$, is desired, it can be computed by repeated differentiation of Equation (2.3). This step is given by

$$\frac{d^q g}{dx^q}(x) = \frac{d^n}{dx^n}\left(\frac{d^{q-n} g}{dx^{q-n}}(x)\right)$$

for an integer $n > q$. Further information about this and other definitions, as well as a detailed explanation of the fundamentals of fractional calculus, can be found in [50].

The Riemann-Liouville definition began with an integration formula. One alternative definition can be reached by starting from a formula for repeated differentiation; this is the Grünwald-Letnikov derivative. As derived in [38], the first and second derivative definitions of

$$\frac{df}{dt}(t) = \lim_{\Delta t \to 0} \frac{f(t) - f(t-\Delta t)}{\Delta t}$$

and

$$\frac{d^2 f}{dt^2}(t) = \lim_{\Delta t \to 0} \frac{f(t) - 2f(t-\Delta t) + f(t-2\Delta t)}{(\Delta t)^2}$$

can be generalized to an integer number of derivatives q:

$$\frac{d^q f}{dt^q}(t) = \lim_{\Delta t \to 0} \frac{\sum_{0 \le j \le q} (-1)^m \binom{q}{j} f\left(t + (q-j)\,\Delta t\right)}{(\Delta t)^q}.$$

The gamma function can be employed to compute an equivalent binomial coefficient for a real, instead of exclusively integer, first argument q. These substitutions are

$$\binom{q}{j} = \frac{q!}{j!\,(q-j)!} \quad \rightarrow \quad \binom{q}{j} = \frac{\Gamma(q+1)}{\Gamma(j+1)\Gamma\left(q-j+1\right)}.$$

Following from this generalized binomial coefficient, the Grünwald-Letnikov fractional derivative is given by

$$\frac{d^q f}{dt^q}(t) = \lim_{\Delta t \to 0} \frac{1}{(\Delta t)^q} \sum_{j=0}^{\infty} (-1)^j \binom{q}{j} f\left(t + (q-j)\,\Delta t\right). \tag{2.4}$$

The explanation in [38] offers some beneficial approximations for a numerical context. Specifically, for small Δt (much less than 1), and under the assumption that the derivative order q is not large (greater than about 10), the quantity $q\Delta t$ within the function argument in Equation (2.4) can be neglected. This is because $q\Delta t$ is dwarfed in magnitude by t and $j\Delta t$. Neglecting $q\Delta t$ does not save computational time at first glance; however, in the context of numerical methods, values of the function f are generally only available at times that are integer multiples of Δt ($t = p\Delta t$), so an adjustment of this nature is often needed.

A fundamental distinction between fractional- and integer-order derivatives is that finite-difference approximations for fractional-order derivatives are not strictly local. As can be seen in Equation (2.4), computing fractional derivatives of a function

requires knowledge of its history. However, if $t = p\Delta t$ and initial conditions are zero, then the summation need not continue incrementing to $j = \infty$, corresponding to $t = -\infty$; it can instead be bounded by $t = 0$, stopping at $j = p$. Thus, a computationally friendly version of this definition is

$$\frac{d^q f}{dt^q}(t) \approx \frac{1}{(\Delta t)^q} \sum_{j=0}^{p} (-1)^j \binom{q}{j} f\left(t - j\Delta t\right),$$

along the lines of the discussion in [14]. This particular approximation is used for time-domain solutions of fractional-order differential equations throughout this work.

2.2 Literature Review

The background presented in this section shows how fractional calculus has made, and can continue to make, its way into the literature throughout the disciplines of engineering. This overview begins with references covering the fundamentals of fractional calculus and results of studies grounded in these mathematics. Following is a selection of literature addressing problems in modeling and control of multi-robot systems.

The discussion continues with research efforts connecting fractional calculus and systems engineering, establishing the niche to be occupied by Chapter 3 and beyond. The first set of contributions of this nature represents a variety of control and robotics settings, both analytical and experimental, while the next has an emphasis on system identification so as to illustrate the ways in which the content of Chapter 4 is distinct among existing methods. The section concludes by discussing the references that preceded the contributions of this work along a common line of inquiry, as well as the publications generated from the efforts leading to this dissertation.

2.2.1 General Fractional Calculus References

An accessible textbook recommended as a starting point for the study of fractional calculus is [50]. It is concise and has a structure much like that of a typical calculus textbook. Examples of topics covered, in addition to the vital definitions of the fractional derivative and integral operators, include techniques such as the product and chain rules, adaptations to numerical methods, and selected solution procedures for differential equations.

A text with less emphasis on background but otherwise similar in content is [56]. Differential equation solutions are the focus of this book. The Mittag-Leffler function, a generalization of the exponential function that plays a role in these solutions, is discussed in the opening chapter. Numerical approximations, extensions to control, and applications of the mathematics are given thorough attention as well. An overview of mathematical applications is given in [68].

The collection [3] contains recent results exploiting fractional calculus by dozens of scholars in the fields of systems, control, and applied mathematics and physics. Some entries in this collection are concerned with linear control such as fractional PID or nonlinear methods such as backstepping and model predictive control. While these are simulation-based, other contributions present results that indicate the advantages of incorporating fractional calculus in engineering research.

One such chapter, from the area of numerical methods, is "A Fractional Order Dynamical Trajectory Approach for Optimization Problem with HPM." This method solves nonlinear programming problems by the homotopy perturbation method (HPM), casting such a problem as a system of fractional differential equations. For the problem of minimizing $f(x) = 100(x_1^2 - x_2)^2 + (x_1 - 1)^2$ such that $h(x) = x_1(x_1 - 4) - 2x_2 + 12 = 0$, the solution is $x_1 = 2$ and $x_2 = 4$. The HPM of order 0.9 returns $x_1 = 1.9991$ and $x_2 = 3.9996$ after 100 iterations, while the same method of order 1 and the fourth-order Runge-Kutta method both take over 300 iterations to reach that

proximity. A second example problem affirms the conclusion of faster convergence with a noninteger order.

Diffusion is another subject where fractional calculus has taken root. An example from [3] is the chapter "Numerical Solution of a Two-Dimensional Anomalous Diffusion Problem." Anomalous diffusion is described by a generalized diffusion equation, a partial differential equation that can contain fractional derivatives. In a problem where the time derivative of order 1 is equal to the sum of the two spatial derivatives of orders 0.3 (for x) and 1.8 (for y), for initial condition $u(x, y, 0) = \sinh(x + y)$, exact agreement is shown between the analytical solution and one computed by a Grünwald-Letnikov approximation. This approximation is then used to compute two- and three-dimensional representations of u for varied parameters as a function of space and time.

The role of fractional calculus in a bioengineering application can be found in the chapter of [3] titled "Analyzing Anomalous Diffusion in NMR Using a Distribution of Rate Constants." Specifically, the two experiments discussed are nuclear magnetic resonance (NMR) imaging of various gels and of a human brain. A fractional order parameter is part of a stretched exponential model to represent signal attenuation as a result of diffusion. The data analysis results for these experiments show that the model orders for the gels (0.71 ± 0.06, 0.80 ± 0.05, and 0.91 ± 0.08), white matter (0.600 ± 0.008), gray matter (0.78 ± 0.03), cerebral spinal fluid (0.910 ± 0.005), and distilled water (1.000 ± 0.003, suggestive of classical diffusion) all differ in expectation or distribution. These findings align with the hypothesized differences in diffusion behavior, and it is suggested that they may portend advances in monitoring of tissues.

Further engineering applications are discussed in [52]. Among resources other than books, a comprehensive overview of the properties of fractional derivatives can be found in [53], which also presents several definitions. The article [51] is an informative introduction to the effects of fractional derivatives and integrals on the area of linear

systems, specifically the impulse and step responses. It also discusses applications and provides an extensive assortment of references. A thorough list of additional resources throughout the disciplines of science and engineering can be found in [42].

2.2.2 Multi-Robot System References

The following references do not incorporate fractional calculus, but they are representative of the questions being asked by scholars about cooperating robots. This is the context of the example system that begins to frame the contributions of this dissertation in Chapter 3. As such, knowledge of how these contributions may fit into the area of multi-agent robotics is informative.

The article [60] is cast as a tutorial about consensus algorithms, the procedures by which groups of agents make collective decisions. It can also serve as a literature review on the subject. A deeper examination of distributed multi-robot systems, presenting both concepts and recent research findings, is [7]. This article begins with consensus but extends the discussion to formation control, optimization of this control, and state estimation.

An article establishing a control strategy for a group of vehicles is [19]. This work decouples the communication between vehicles from their dynamics, promoting stability of the formation and giving rise to localized control that is robust to faulty communication links. A review article of a similar nature that discusses many efforts toward control of multi-agent systems is [48].

In [37], interactions between vehicles are established with the constructions of artificial potentials and dissipative control. Conceptually, these measures are connected to the example system of Chapter 3, in which the interactions are modeled as springs and dampers. A formation control strategy that is implemented experimentally with a camera mounted on each robot is discussed in [13]. This is a modular approach that is designed for scalability to large groups of robots.

These references have a common interest in the pursuit of strategies by which robots in a formation or group can work together. The contributions of this dissertation exploit fractional calculus to manage the high-order nature of such systems. Innovation in modeling, such as that detailed in this work, may precede advances in control of these systems and, in turn, physical implementation of those strategies.

2.2.3 Other Interacting System References

There is hesitation to model systems with many vibrating degrees of freedom in closed form, as reflected in the literature. Extracting information from gas turbine vibrations is sufficiently intricate to invoke the use of machine learning, as presented in [62]. Vibration signals in washing machines are analyzed in [24]; that approach seeks to detect faults from the data but not to generate mathematical models. Machine tools are modeled computationally in [2] under the premise that coupled simulation is essential as a result of the complexity of the vibrations. Analytical models of machine tool vibrations are considered in [33], but those are differential equations with terms delayed in time; nonlinear operators are required in that analysis. In [69], a mechanical model is used for an automobile vibration application, but it is a deliberate simplification, considering only part of the vehicle where some analysis of the whole would be preferred if feasible. Each of these is an example of a system that can be considered in a new light with the approach of Chapter 5. Many of the systems that are possible applications for this research are cyber-physical systems; the dynamical perspective introduced here could complement the modeling frameworks discussed in [34, 36, 16].

The appeal of mechanical networks arises from the appearance of compelling properties in arrangements of mechanical components. Scaling in mechanical systems with random properties is discussed in [47]. The idea that a large network's behavior can remain essentially the same irrespective of its size, perhaps always sending signals at

a particular frequency, is a motivation for these studies and is discussed for electrical networks in [74]. Concepts stemming from infinite models of systems are presented in an electrical context in [73]. A network structure similar to the tree arrangement considered in this chapter is used to model blood flow in [1] and [20], showing the versatility of such a structure.

2.2.4 Walking References

Development of humanoid robots, dating back to early advances such as [28], is motivated by a desire for robots to perform tasks in the full set of environments accessible by humans. Several approaches have been taken toward governing the walking motions of a humanoid. Incorporating upper-body movements occurring simultaneously with dynamic walking is the subject of [72]. Reducing complexity of the control problem by defining a trajectory for the robot's center of gravity is discussed in [32].

Accounting for the discrete impacts of the feet during control design for a walker has been accomplished by considering the walker to be a hybrid system. One such approach, hybrid zero dynamics (HZD), was introduced in [70] and expanded in [71], and it is central to the choice of trajectory in Chapter 6. Control-related robotics efforts strengthened by HZD include hopping, as in [58]; running, as in [67]; and 3D walking, as in [26]. Rejection of disturbances in translational velocity for a robot governed by HZD-inspired control is the subject of [57]. In addition to control for robots, applications of HZD include predicting gait properties for humans at different speeds, as in [43].

The closest precedent for the work of Chapter 6 in the literature, found in [64], uses fractional-order control, but that algorithm takes the ground reaction forces at the heel and toe as control variables and is thus limited by large, flat feet. That walker also has ankle and knee actuation. In contrast, this research simulates a two-link

compass-gait walker with point feet and hip actuation. The walker is underactuated. Such a model has been the basis for several walking research efforts, such as [8].

2.2.5 Integer-Order System Identification References

The system identification method of Chapter 4 is intended to inform a health monitoring strategy for engineered systems with a large number of components. Modal characterization of systems of this type undergoing operational changes is the subject of [61] and [59]. Further research efforts in this direction include [10], regarding systems with nonlinear elements, and [63], regarding actively switching systems. Chapter 4 is concerned with linear systems with one or more properties that change permanently, perhaps unexpectedly. Furthermore, the utility of the resulting fractional-order differential equation models in suggesting engineering adjustments after damage is a motivation for this work to be established alongside other monitoring techniques.

System identification tools connected to structural health monitoring take several forms. There are methods for output-only systems such as [55]. Reduced-order modeling from structural response data is an objective of [31]. Nonlinear and multivariable methods include [9] and [30], respectively. In contrast to these sources' chosen ways to incorporate damage, the approach of Chapter 4 tracks it by measuring fractional order. It may be considered a fractional-order approach to the problem presented in [11]: determining a model from frequency response data. In situations with other types of data, the methods of [55, 31, 9, 30] could potentially be extended to yield fractional-order models, adding flexibility to the current model forms.

2.2.6 References on Fractional Calculus in Systems and Control

Examples of fractional calculus in the broad context of systems are as follows. Efficiency in modeling complex mechanical systems can be achieved with fractional-

order differential equations. Simplifying dynamics with fractional-order operators is the motivation for studies in several engineering fields. These studies include [35] for vibration, [29] for impedance in biological structure, and [4] for mechanical dynamics. Fractional-order differential equations are used as exact models in continuum mechanics, as in [17], and in multiphase materials, as in [18]. Other platforms for fractional-order differential equation models include scale-free networks and linear friction welding, as discussed in [21, 23].

On a more fundamental level, the article [12] presents stability conditions for fractional-order systems with delay. These findings rely upon Lambert functions for analytical solutions to fractional-order differential equations. On the topic of control theory, [75] gives a method for choosing gains in fractional-order proportional-integral-derivative (PID) control with noninteger orders on the integrator and differentiator. This is shown to perform better than conventional PID on fractional-order plants in simulation.

Experimental implementation of fractional PID tuning is the subject of [46]; this article includes results from controlling a water circuit and a servo motor. For the former, the transfer function of the plant whose input is a servo valve voltage and whose output is the water level is given by

$$G(s) = \frac{3.13}{433.33s + 1}\mathrm{e}^{-50s},$$

so it is first-order with a time delay of 50 seconds. The control parameters are chosen by constrained optimization of crossover frequency relative to a desired frequency, where the constraints represent specifications for phase margin, slope of phase at the crossover frequency (a flat slope indicates robustness to changes in the plant gain), and rejection of high-frequency noise and output disturbance. The resulting

controller is

$$C(s) = 0.6152 + \frac{0.0100}{s^{0.8968}} + 4.3867 s^{0.4773},$$

and all specifications are met.

The servo motor is a testing platform for the approach for auto-tuning a fractional PID controller in [46]. This procedure is developed for control of plants with unknown dynamics. The controller computed during the experiment is a product of fractional PI and PD controllers, namely

$$C(s) = \left(\frac{0.4348s + 1}{s}\right)^{0.8468} \left(\frac{4.0350s + 1}{0.0039s + 1}\right)^{0.8160}.$$

This controller satisfies specifications of a desired crossover frequency, phase margin, and slope of phase at the crossover frequency. It also leads to step responses exhibiting less overshoot than is seen in simulation results with a conventional PID tuned by the Ziegler-Nichols method.

Two studies presenting control of formations of agents with fractional-order dynamics are [5, 6]. The work of [5] proposes a control algorithm and discusses its convergence for different choices of damping in the algorithm. Varying the fractional order present in the components and coordination structure is the focus of [6]. In these studies, fractional order is part of the construction of the problem; in contrast, the coverage formation system of Chapter 3 and beyond is observed to have fractional order despite being constructed from only integer-order dynamics.

In addition to [64], first mentioned in Section 2.2.4, works merging fractional calculus and robotics include [65], which is concerned with a hexapod walker. In this case, fractional order is exploited as an avenue for greater flexibility in control, specifically proportional-derivative control. Another example of this control advantage is given in [15], where the robot of interest is a flexible manipulator. In that article, the control setting where incorporation of fractional order proves beneficial is sliding

mode control.

2.2.7 Fractional-Order System Identification References

Chapter 4 is motivated by practical concerns. For applicability to a wide variety of systems, a computational identification procedure must play a key role in any version of the monitoring proposed in this dissertation. The following are several examples of fractional-order system identification from the literature, including the one from which the method of Chapter 4 draws its inspiration.

An analytical treatment of the topic is [25], which details the determination of a continuous order distribution to describe a system. The results are, in essence, functions of order (in this context, a real number) that illustrate the concentration of dynamic response. Another mathematically grounded approach to fractional-order system identification is detailed in [41]. In this case, a series of modulating functions convolved with time-domain data creates the system of equations to be solved for governing equation parameters.

The method in [14] constructs a matrix equation to be solved, resulting in a discrete order distribution. In principle, the method holds promise for efforts similar to that of this dissertation; indeed, it can be stated that the quantities to be monitored comprise a discrete order distribution. However, this particular formulation appears to have limited robustness across initial choices of frequency resolution.

Computationally intensive methods include the iterative optimization approach of [49], which simultaneously computes estimates for a system's order and other parameters, including time delay. Genetic algorithms are the tool of choice in [76] for determining fractional-order governing equations. While these methods are effective, the investigations of this work have proceeded as desired with a simpler formulation.

The book [54] is an extensive text that, if the reader does not mind the French language, should be included among [50] and [56] as recommended overviews of fractional

calculus. The system identification method discussed therein presents the framework that has given rise to the method of Chapter 4. The latter has been modified significantly from the approach of [54], but the explanation behind that approach still lends itself well to the aims of this dissertation. The connection between the two methods is illustrated further in Chapter 4.

2.2.8 References of Precedent and Association

The example system that serves as backdrop for the contributions of Chapter 3 and beyond is a bifurcating tree network system. The importance of such systems is motivated in [44] and [45]. Settings for models of this nature include biological transport, river basin drainage, microchannel electronic cooling, and viscoelasticity, among others. In particular, viscoelasticity can be modeled with a self-similar arrangement of springs and dampers or their equivalents; this is shown in [27].

This arrangement is adapted for the context of multi-robot systems in [22], where it is shown that the positional relationship of interest has fractional order. Order changes are observed as effects of damage to this system model; this discussion is the subject of [38]. The system identification method of Chapter 4 is explained in publication form in [39].

This chapter has given two types of background for the contributions to be presented in the remainder of this dissertation. The operators of fractional calculus and examples of how these operators have been employed in the literature speak to the versatility of this branch of mathematics. The other publications referenced are meant to illustrate both the interest level in findings from this scholarly vein and the placement of this dissertation within the context of systems, control, robotics, and similar fields.

CHAPTER 3

USING FRACTIONAL-ORDER DIFFERENTIAL EQUATIONS TO MONITOR COOPERATING AGENTS

Mechanical systems are commonly modeled with mass, damper, and spring elements. Collectively, these are called lumped elements. Masses denote bodies or particles that are moving, while dampers and springs connect those masses whose movements are related. From a model of this nature, a differential equation can be formulated to capture the motion of the system as a whole. This chapter presents an example system modeled in this way that demonstrates the utility of fractional-order differential equations as a monitoring tool. Much of this content appears in [38], while some figures and accompanying discussions appear in [39].

3.1 Motivational Example

Consider a spill of toxic waste and a group of robots deployed to clean the contaminated area, as shown in Figure 3.1, from [38]. It is clear that the robots should be placed throughout the area, but the spillage is not uniform. It is deemed most useful to have about half of the robots near the source of the spill to stop further spreading of the waste, with the remaining robots placed at greater distances to address the damage already done. Thus, a formation is established with 2^n (perhaps $n = 4$, so 16) robots nearest the spill, with the number of robots in each subsequent layer being half that of the previous layer. This progression terminates with one robot in a layer by itself.

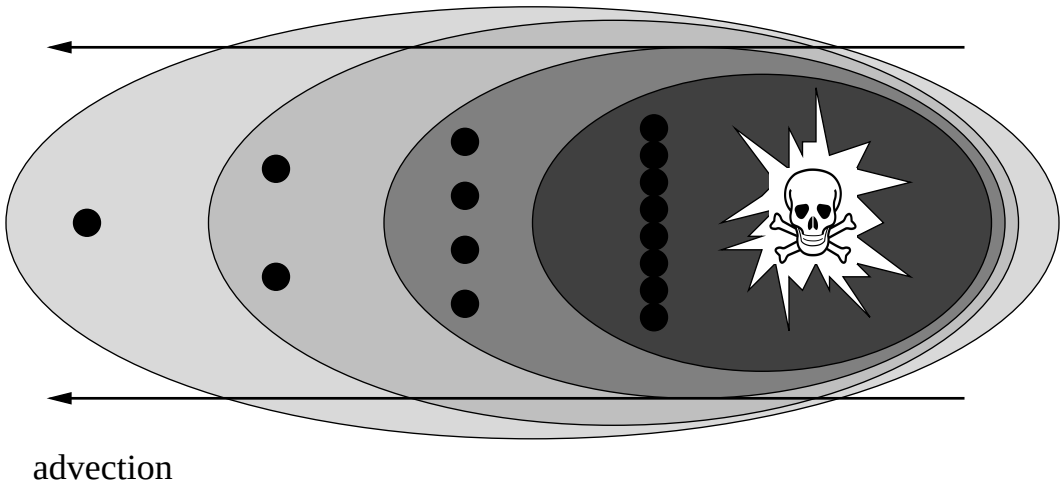

Figure 3.1. Contamination example with level of shading indicating proximity to the source.

This is a coverage problem; these robots must work together. If they do not, the cleaning is likely to be inefficient or, worse, the robots will collide with each other. To mitigate the possibility of collision, the communication between the robots is established such that the positional relationships between robots in neighboring layers are spring-like or damper-like, as in Figure 3.2, from [39]. In other words, the more any two robots connected in this way deviate from one another in the state variables of position (relative to a set equilibrium spacing) or velocity, the more effort is to be put toward correcting their differences in state. The robot in a layer by itself is in charge of the formation; its movements direct the other robots forward and backward according to these relationships.

This tree-like formation's dynamics have a self-similar nature. Each robot is connected to two robots in the next layer, one connection being a spring and the other a damper. From a mathematical modeling perspective, the relationship of interest is one of input and output between the first robot's position, x_{11}, and that of all 2^n robots nearest the spill, x_{last}. The latter robots are considered locked together, but this is with respect to the equilibrium spacing, so in a real cleanup scenario their

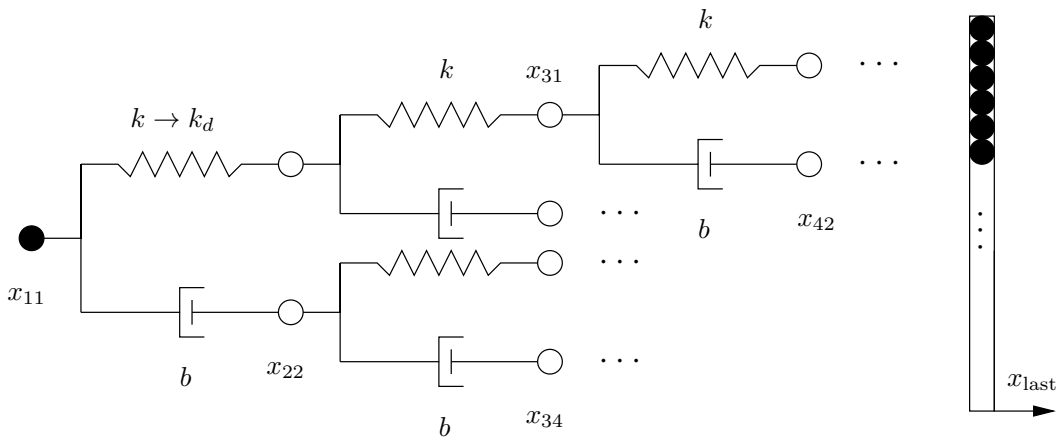

Figure 3.2. Robotic formation with spring and damper connections.

actual positioning would be set arbitrarily.

Springs and dampers have constants for stiffness and damping, respectively, that indicate their strength. Here, at least in this initial construction, the springs all have stiffness constant k, while the dampers all have damping constant b. The mass of the one robot in the first layer is taken to be the same as the combined mass of the 2^n robots in the last layer, with all masses of the robots between them considered negligible. This mass distribution, albeit unlikely to reflect any physical experiment, ensures that the movement of the intermediate robots is influenced primarily by that of the first robot and the springs and dampers. That notion would be feasible in an experimental setting with a more realistic mass distribution among the group of robots.

For this example, the component constants are chosen to be $k = 2$ (force per length or mass per time squared) and $b = 1$ (force per velocity or mass per time). The transfer function (TF) $G(s)$, or the complex multiplier applied to an input sinusoid to compute the output sinusoid, can be shown on a Bode plot as a function of frequency. For any $n \geq 4$, there exists a band of frequencies over which the magnitude of the TF decreases with a slope of -10 dB/decade and the phase difference between output

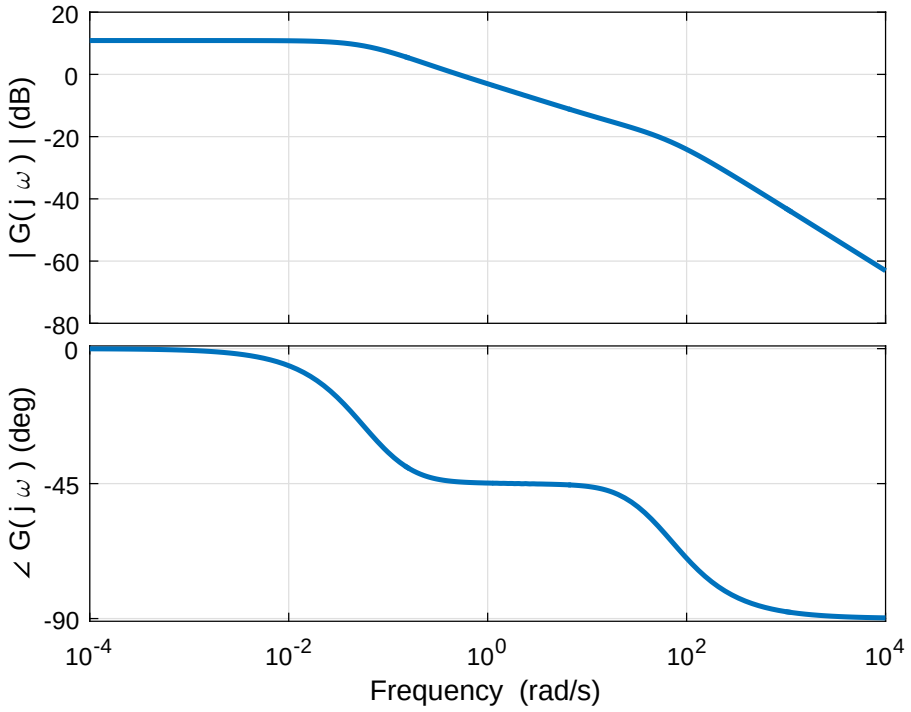

Figure 3.3. Frequency response of robotic formation.

and input plateaus at -45 degrees. These behaviors are shown in Figure 3.3 and were first noticed in [22]. This result is atypical in the presumed context of linear systems, where in most cases, the magnitude has slopes that are exclusively integer multiples of -20 dB/decade, while the phase difference decreases steadily toward an integer multiple of -90 degrees.

3.2 Mathematical Analysis

The property of the system dynamics that causes this unexpected frequency response can be discovered by examining the formulation of the transfer function $G(s)$. Consider the motion of a mass attached to one spring. The governing equation for

this system is

$$m\ddot{x}(t) + kx(t) = f(t)$$

where $x(t)$ is the displacement between the two ends of the spring relative to equilibrium and $f(t)$ is the input force on the mass as a result of the spring. After undergoing the Laplace transform, assuming initial conditions of zero,

$$ms^2X(s) + kX(s) = F(s).$$

In turn,

$$G_k(s) = \frac{X(s)}{F(s)} = \frac{1}{ms^2 + k} \approx \frac{1}{k}$$

with the approximation arising because, in this case, the spring force is assumed to dominate inertia.

In analogous fashion, the governing equation for a mass-damper system is

$$m\ddot{x}(t) + b\dot{x}(t) = f(t).$$

The Laplace transform with initial conditions of zero is

$$ms^2X(s) + bsX(s) = F(s).$$

With the damping force dominating inertia, the transfer function is

$$G_b(s) = \frac{X(s)}{F(s)} = \frac{1}{ms^2 + bs} \approx \frac{1}{bs}.$$

Hereafter, $G_k(s) = 1/k$ and $G_b(s) = 1/bs$.

3.2.1 Undamaged Coverage Formation

By combining G_k and G_b in parallel, the tree formation is established for $n = 1$. Its transfer function is

$$G_1(s) = \frac{1}{\frac{1}{G_k(s)} + \frac{1}{G_b(s)}} = \frac{1}{\frac{1}{\frac{1}{k}} + \frac{1}{\frac{1}{bs}}}.$$

Extending to $n = 2$ requires adding a spring-damper parallel combination in series with both the spring and damper of layer 1. As a result, the transfer function is

$$G_2(s) = \frac{1}{\frac{1}{G_k(s) + \frac{1}{\frac{1}{G_k(s)} + \frac{1}{G_b(s)}}} + \frac{1}{G_b(s) + \frac{1}{\frac{1}{G_k(s)} + \frac{1}{G_b(s)}}}},$$

and the pattern continues for larger trees:

$$G_\infty(s) = \frac{1}{\frac{1}{G_k(s) + \frac{1}{\frac{1}{G_k(s)+\ldots} + \frac{1}{G_b(s)+\ldots}}} + \frac{1}{G_b(s) + \frac{1}{\frac{1}{G_k(s)+\ldots} + \frac{1}{G_b(s)+\ldots}}}}.$$

As mentioned previously, the structure of the tree is self-similar. If the tree is extended to infinitely many layers, a substitution can be made to illustrate the self-similarity in a transparent fashion. The transfer function then becomes

$$G_\infty(s) = \frac{1}{\frac{1}{G_k(s) + G_\infty(s)} + \frac{1}{G_b(s) + G_\infty(s)}}.$$

Furthermore, simplifying the fraction leads to a closed-form expression for $G_\infty(s)$:

$$G_\infty(s) = \frac{1}{\frac{G_b(s) + G_\infty(s) + G_k(s) + G_\infty(s)}{(G_k(s) + G_\infty(s))(G_b(s) + G_\infty(s))}};$$

$$G_\infty(s) = \frac{(G_k(s) + G_\infty(s))(G_b(s) + G_\infty(s))}{G_b(s) + 2G_\infty(s) + G_k(s)};$$

$$G_\infty(s)(G_b(s)+2G_\infty(s)+G_k(s)) = G_k(s)G_b(s)+G_k(s)G_\infty(s)+G_b(s)G_\infty(s)+G_\infty(s)^2;$$

$$\begin{aligned} G_b(s)G_\infty(s) + 2G_\infty(s)^2 + G_k(s)G_\infty(s) \\ = G_k(s)G_b(s) + G_k(s)G_\infty(s) + G_b(s)G_\infty(s) + G_\infty(s)^2; \end{aligned}$$

$$G_\infty(s)^2 = G_k(s)G_b(s);$$

$$G_\infty(s) = \pm\sqrt{G_k(s)G_b(s)} = \pm\sqrt{\frac{1}{kbs}}.$$

From the hypothetical viewpoint of the person deploying the robotic formation in a physical setting, the positive solution is of exclusive interest; if the first robot is displaced to the right, all of the others settle to the right of their original positions as well. The Laplace-domain operator s^{-1} maps to integration in the time domain, and a system with a TF whose leading polynomial degree in the denominator is 1 is classified as first-order. It follows, as in [22], that the operator $s^{-1/2}$ maps to *half-integration* and that the corresponding system is of order 1/2.

3.2.1.1 Convergence to Order One-Half

The connection of this result to that of the finite tree is illustrated by the frequency response of this 1/2-order system. The Bode plot given in Figure 3.3 shows magnitude decreasing at -10 dB/decade and a corresponding constant phase difference of -45 degrees. Given behavior of order 1/2, these response characteristics are expected

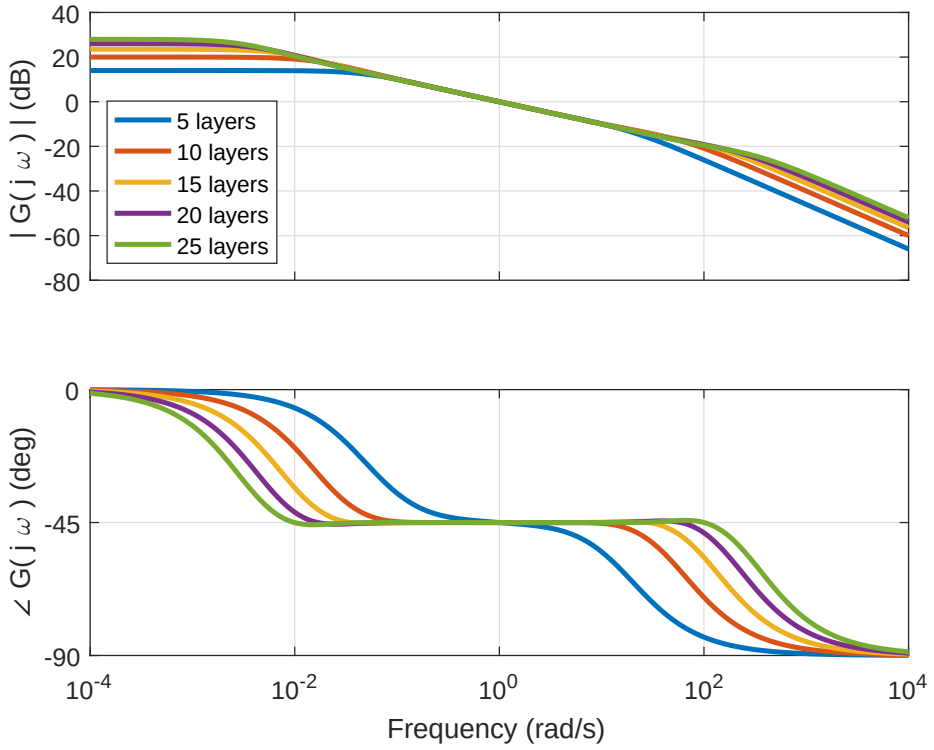

Figure 3.4. Elongation of frequency band suggesting half-order behavior.

because they are halfway between those for order zero (0 dB/decade and 0°) and order one (−20 dB/decade and −90°). In the case of the finite tree, the inclusion of more layers in the tree elongates the frequency band representative of a half-order system. A plot showing varied choices for the number of layers and the resulting changes in length to the frequency band of interest is given in Figure 3.4.

The frequency band indicative of order 1/2 can be measured in units of powers of 10 rad/s. Here, the frequency band is said to begin when the phase difference becomes less than or equal to −42.5 degrees, that is, close to −45 degrees, and end when it is no longer greater than −47.5 degrees. The width of the half-order frequency band as a function of tree depth (number of layers) is plotted in Figure 3.5.

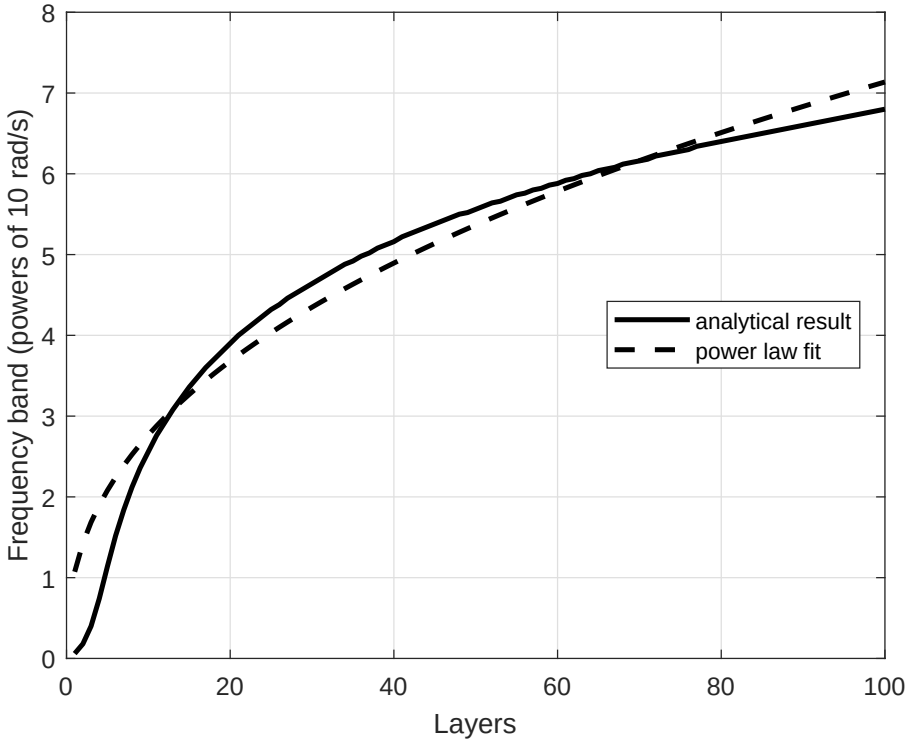

Figure 3.5. Length of frequency band suggesting half-order behavior.

In these measurements, the frequency domain is adjusted as needed to capture the frequency band of interest for different choices of k and b. The results do not change with k and b, but the frequency band shifts, with the ratio of k to b as its center. The upper bound of 100 layers is chosen to limit the influence of the outliers having the lowest numbers of layers: one, two, and three. These are outliers because they do not have enough components to exhibit fractional-order behavior, as discussed in [22]. Still, since these systems each possess a frequency band with a phase difference near -45 degrees, their inclusion is merited.

The relationship in Figure 3.5 appears quantifiable by fitting the curve to a power model cn^p, where n is the number of layers. Regardless of the choices of k and b examined (with the most extreme of these choices being $k = 0.001$ and $b = 1000$ and vice versa), the constants are $c = 1.0731$ and $p = 0.4114$. This fit has a determination coefficient of $r^2 = 0.9568$. However, the error for low numbers of layers and the unbounded growth of error on the high end imply that the power law is not an appropriate fit for this curve. Indeed, when different spans of tree depths are considered, the constants change too much for confidence to be placed in any one power model. No other type of simple curve fit considered is any more promising.

A truly half-order system would have a phase difference of -45 degrees for all frequencies. The truncation of the tree at some finite number of layers makes that impossible at the lowest and highest frequencies. When assembled from connections of springs and dampers, the transfer function of the tree has a numerator and a denominator that are polynomials in s of orders $2^n - 2$ and $2^n - 1$, respectively, with a nonzero term for each power of s. For low frequencies, the constants in these polynomials dominate, leading to a phase difference of 0 degrees. For high frequencies, the highest-order terms dominate. The transfer function behaves as a constant multiplied by $1/s$, leading to a phase difference of -90 degrees. It follows that these two trends in phase difference are seen in every frequency response plot for

the finite tree regardless of its number of layers; however, adding more layers makes the -45-degree phase difference more prominent and the progressions to 0 and -90 degrees less so.

3.2.1.2 Approximation by Fractional-Order Transfer Function

In light of these results, approximation of the full system's TF by the half-order TF is a natural pursuit. This approximation appears most promising when the system receives inputs in the medium-frequency range. By way of motivation, the tree as constructed from springs and dampers is a high-order system; exact models would scale poorly. For n layers of springs and dampers, the order is $2^n - 1$.

Meanwhile, the infinite tree is governed by a differential equation with far fewer terms. The transfer function

$$G_\infty(s) = \frac{X(s)}{F(s)} = \frac{X_{11}(s) - X_{\text{last}}(s)}{F(s)} = \sqrt{\frac{1}{kbs}}$$

is as determined. Considering that the input force is the force applied to the last layer of robots, a Newtonian force balance yields

$$f(t) = m\ddot{x}_{\text{last}}(t).$$

The substitution in the Laplace domain and further manipulations give

$$\frac{X_{11}(s) - X_{\text{last}}(s)}{ms^2 X_{\text{last}}(s)} = \sqrt{\frac{1}{kbs}};$$

$$ms^2 X_{\text{last}}(s) = \sqrt{kbs}(X_{11}(s) - X_{\text{last}}(s)),$$

or, in the time domain,

$$m\ddot{x}_{\text{last}}(t) + \sqrt{kb}\frac{d^{1/2}x_{\text{last}}}{dt^{1/2}}(t) = \sqrt{kb}\frac{d^{1/2}x_{11}}{dt^{1/2}}(t). \tag{3.1}$$

The advantage of this step is ease of computation for purposes of modeling and simulation.

The validity of the approximation is borne out in time-domain simulations. This discussion overlaps in part with [38]. Given an initial condition of zero and the input

$$\ddot{x}_{11} = \begin{cases} 1, & 0 \leq t < 1; \\ -1, & 1 \leq t < 2; \\ 0, & t \geq 2, \end{cases} \tag{3.2}$$

a step response of the tree with the components modeled individually is produced with a linear differential equation solver. This form of step response is chosen for practicality. In a physical setting, one cannot displace a robot from position 0 to 1 in zero time. However, one can enact that displacement by imparting a positive force, then a negative force, then zero force to yield the acceleration profile of Equation (3.2).

Each intermediate robot has an equation of motion solved simultaneously with Equation (3.2) to compute the step response. This equation takes one of two forms:

$$\ddot{x}_{\text{odd}} = \frac{1}{m}\left(k(x_{\text{left}} - x_{\text{odd}}) + k(x_{\text{right}_1} - x_{\text{odd}}) + b(\dot{x}_{\text{right}_2} - \dot{x}_{\text{odd}})\right); \tag{3.3}$$

$$\ddot{x}_{\text{even}} = \frac{1}{m}\left(b(\dot{x}_{\text{left}} - \dot{x}_{\text{even}}) + k(x_{\text{right}_1} - x_{\text{even}}) + b(\dot{x}_{\text{right}_2} - \dot{x}_{\text{even}})\right). \tag{3.4}$$

Here, the label of odd or even refers to the robot's index. For example, the robots in the second layer have indices 21 and 22; those in the third have indices 31 to 34. The distinction is simply that odd-numbered robots are connected to the left by springs and even-numbered ones by dampers. The labels of left and right denote the specific robots connected in the formation to the left and right of the one governed by the equation. Each of these robots is connected to two others on the right; "right_1" refers to the one connected by a spring and "right_2" that connected by a damper. The

robot's mass for dynamical purposes is m. It is assumed that k and b are constant throughout the tree, but if that is not the case, the individual stiffness and damping constants must replace k and b in these equations in a manner corresponding to the spring and damper locations. For n layers of springs and dampers, the total number of intermediate robots is $2^n - 2$.

The equation of motion of the last layer of robots is

$$\ddot{x}_{\text{last}} = \frac{1}{m_{\text{last}}} \sum_{j=1}^{2^{n-1}} \left(k_{n,j}(x_{n,j} - x_{\text{last}}) + b_{n,j}(\dot{x}_{n,j} - \dot{x}_{\text{last}}) \right).$$

The tree has n layers of springs and dampers, so the last layer is connected to the left by 2^{n-1} springs and 2^{n-1} dampers. The indexing is consistent with the other equations; commas are in place to ensure that n and j are not multiplied and to allay any concerns about digit overflow for $j \geq 10$. In total, the number of second-order differential equations is 2^n (one for each intermediate robot as well as the first and last). Thus, casting this problem as a system of first-order differential equations for solution by MATLAB's `ode45` function requires 2^{n+1} equations.

The response of the half-order system to the same input is determined by stepping through time according to

$$\begin{aligned} x_{\text{last}}(N\Delta t) \approx & \frac{1}{\dfrac{m_{\text{last}}}{(\Delta t)^2} + \dfrac{\sqrt{kb}}{\sqrt{\Delta t}}} \\ & \times \left(\frac{m_{\text{last}}}{(\Delta t)^2} \left(2x_{\text{last}}((N-1)\Delta t) - x_{\text{last}}((N-2)\Delta t) \right) \right. \\ & - \frac{\sqrt{kb}}{\sqrt{\Delta t}} \sum_{j=1}^{N} (-1)^j \binom{1/2}{j} x_{\text{last}}((N-j)\Delta t) \\ & \left. + \frac{\sqrt{kb}}{\sqrt{\Delta t}} \sum_{j=0}^{N} (-1)^j \binom{1/2}{j} x_{11}((N-j)\Delta t) \right). \end{aligned} \tag{3.5}$$

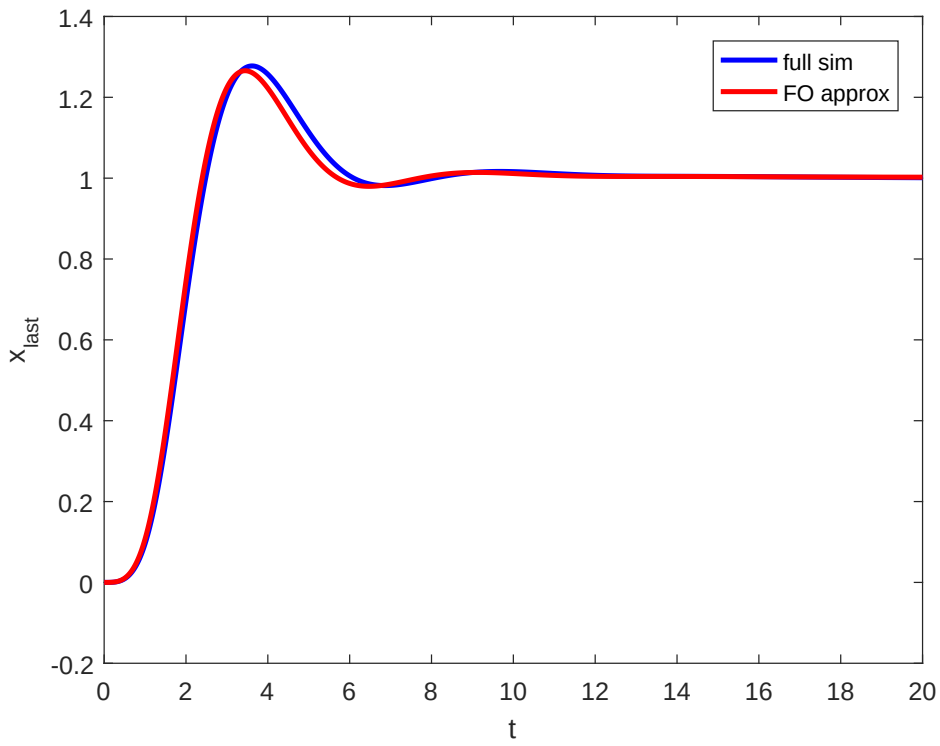

Figure 3.6. Comparison of step response of system with fractional order 1/2, according to Equation (3.5), to full simulation response.

This comes from Equation (3.1) and the Grünwald-Letnikov derivative of Equation (2.4), adjusted for computational viability. Here N is the number of the instance in time for which the solution is computed. Given eight layers of robots, $k = 2$, $b = 1$, and each mass between the first and last layer (having total mass $m_{\text{last}} = 1$) equal to 0.001, it is shown in Figure 3.6 that the match is accurate. Therefore, it may be concluded that the tree system with those parameters behaves in a manner suggestive of order 1/2. Discussion of intermediate mass justifying the choice of $m = 0.001$ is forthcoming; that amount of mass is shown to be small enough to be considered negligible. In theory, all frequencies are excited by a step input, so even though the step considered here is nonideal, any arbitrary input other than a low- or high-frequency sinusoid is expected to yield a similar match.

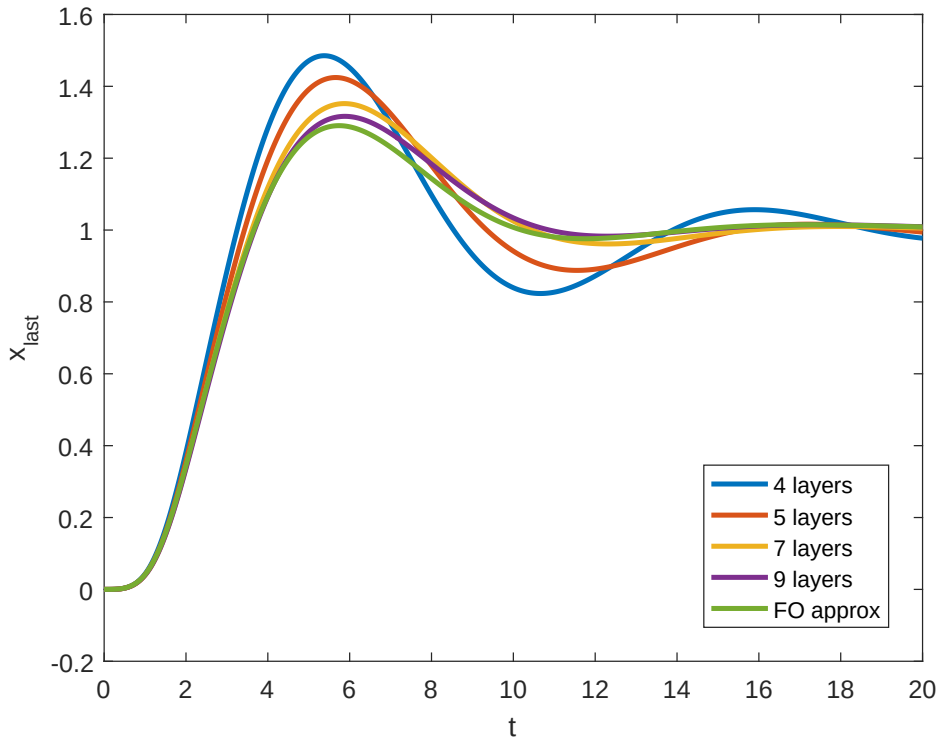

Figure 3.7. Comparison of step response of system with fractional order 1/2 to those of simulated trees with varying robot layers but constant mass.

The depth of the tree affects the strength of the match between the step responses of the tree and the half-order system. Including more layers renders the tree more similar to the infinite tree that is the basis for the approximation, so it is expected to produce a better match. This is shown to be the case in Figure 3.7. The four trees whose responses are plotted all have $k = 1$, $b = 0.25$, and equal mass. The last layer of robots locked together has total mass 1, while the remaining mass is distributed evenly among the intermediate robots. (The first robot is simply the location of the force input, so its mass is irrelevant.) For n layers of springs and dampers in the tree, each intermediate mass is $0.015/(2^{n-1} - 1)$; it follows that, with six layers of robots and $n = 5$, each of those masses would be 0.001. Computational limits affect the choices of mass and tree depth.

This treatment of the mass distribution is meant to expose the underlying significance of including the intermediate masses in the simulations of the tree. The intermediate masses are nonzero purely for numerical reasons; if they are taken to be zero, then all of the second-order derivative terms in the equations of motion for those tree nodes, all multiplied by $1/m$, fail to converge. (Nonzero but sufficiently small masses present computational challenges for similar reasons.) The presented structure of the system of equations is viable only because small masses are assigned to the intermediate robots. However, these numbers represent nothing related to the hypothetical physical system. The local control schemes governing the spring- and damper-like connections between robots are assumed to act in spite of the robots' actual masses and without adding any artificial inertia, as discussed in the opening of Section 3.2.

For the approximation of half-order behavior to hold, it is desirable to keep the intermediate masses small enough to be considered negligible. If the choice of mass is too large, the solution of the system of equations simulating the tree may not match well with the solution of the approximating fractional-order equation. Figure 3.8 shows some example simulation solutions with eight robot layers, $k = 1$, $b = 1$, and various mass choices, and compares them to the approximation. The highest mass choice, $m = 0.01$, is somewhat excessive in the sense that the intermediate masses are far from negligible; in fact, they are greater than those in the last layer. There, a total mass of 1 is distributed over 128 robots. It can be seen that more mass in the system dynamics raises the settling time of the solutions to their steady state.

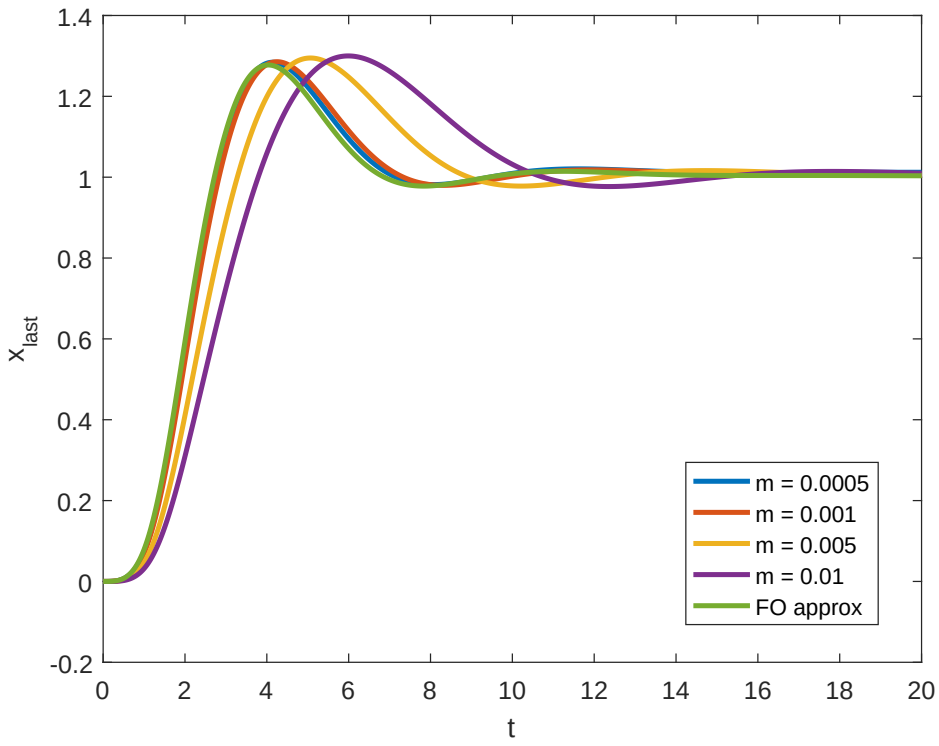

Figure 3.8. Comparison of step response of system with fractional order 1/2 to those of simulated trees with varying mass.

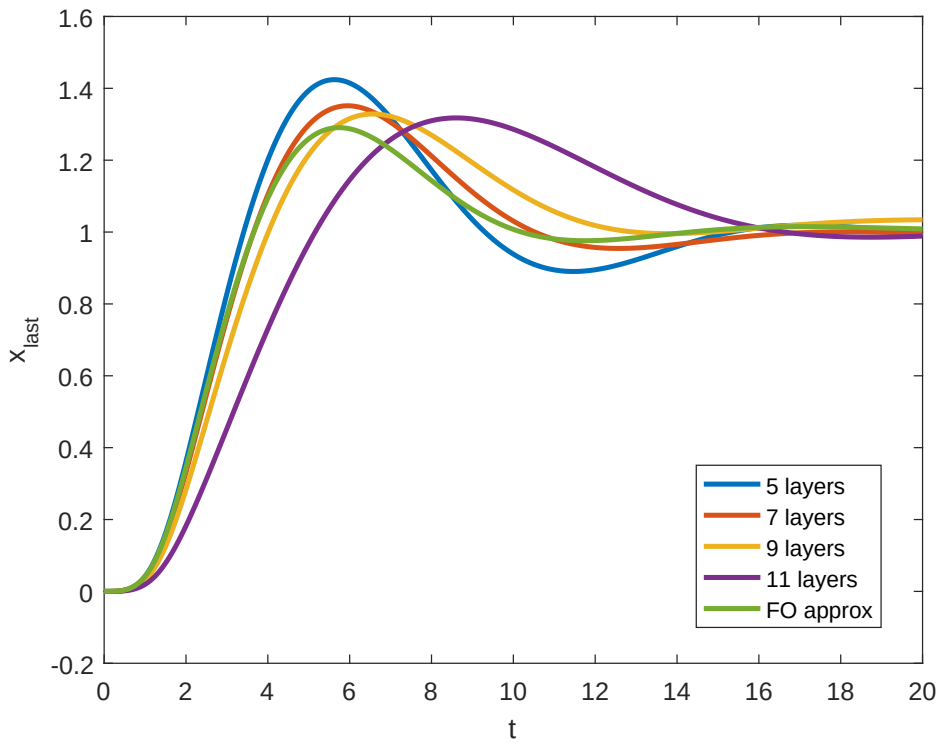

Figure 3.9. Comparison of step response of system with fractional order 1/2 to those of simulated trees with varying robot layers and constant individual robot mass.

Naturally, such an increase in settling time also occurs when holding the intermediate masses constant but adding more layers, thereby increasing the total mass of the system. In this case, the effect is not as obvious because adding layers *improves* the match between the full simulation and the approximation. Still, in excess of some number of layers, the amount of mass being added to the system is too great to be overcome by the increased fractionality of the tree. Some response characteristics may better resemble those of the fractional-order equation solution, but the longer settling time is evident, as shown in Figure 3.9 for $k = 1$, $b = 0.25$, and $m = 0.001$. From these results, it should not be concluded that there is an optimal number of layers, but rather that the comparisons of these versions of the tree are not informative.

For valid comparisons of trees of different depths, the quantity to be preserved is the total mass in the simulation of the tree system, as opposed to each intermediate robot mass. When this is upheld, the comparisons confirm that the solution from simulating the tree matches the approximation better as more layers are added, such as in Figure 3.7. The trend that may be perceived from the four trees of different depths suggests nearly exact convergence to the approximation; the slight discrepancy can be attributed to the inclusion of intermediate mass in the simulations.

The tree system can be simulated with zero intermediate mass. This requires a structure for the node equations that differs from Equations (3.3) and (3.4). If those equations are multiplied by m and evaluated for $m = 0$, they become

$$0 = k(x_{\text{left}} - x_{\text{odd}}) + k(x_{\text{right}_1} - x_{\text{odd}}) + b(\dot{x}_{\text{right}_2} - \dot{x}_{\text{odd}});$$
$$0 = b(\dot{x}_{\text{left}} - \dot{x}_{\text{even}}) + k(x_{\text{right}_1} - x_{\text{even}}) + b(\dot{x}_{\text{right}_2} - \dot{x}_{\text{even}}).$$

The highest-order derivative present in these equations is the first. One may consider a solver-friendly form of these equations to be

$$\dot{x}_{\text{odd}} = \frac{1}{b}\left(k(x_{\text{left}} - x_{\text{odd}}) + k(x_{\text{right}_1} - x_{\text{odd}}) + b\dot{x}_{\text{right}_2}\right); \tag{3.6}$$
$$\dot{x}_{\text{even}} = \frac{1}{2b}\left(b\dot{x}_{\text{left}} + k(x_{\text{right}_1} - x_{\text{even}}) + b\dot{x}_{\text{right}_2}\right). \tag{3.7}$$

These look somewhat similar to Equations 3.3 and 3.4. (As mentioned in that discussion, these must be altered slightly if k and b are not uniform throughout the tree; for instance, $2b$ becomes the sum of b_{left} and b_{right}.) However, the solution of the system of equations from this form is not straightforward. This follows from the reduced order of the equations; as simulation time progresses, $\dot{x}_{\text{left}}$ and $\dot{x}_{\text{right}_2}$ are not preserved as state variables because there is no need to compute *their* derivatives. The only exceptions to this occur when $x_{\text{left}} = x_{11}$ or $x_{\text{right}_2} = x_{\text{last}}$; the derivatives of

those two positions are state variables.

The complication arising from this reduction of order is dynamical coupling; some subsets of node velocities must be determined simultaneously. Paths of consecutive dampers dictate this grouping; the velocities of all intermediate nodes along a path of consecutive dampers must be computed together. This is a result of the dependence on the left and right node velocities shown in Equation (3.7), as opposed to that on only the right node velocity shown in Equation (3.6).

Matrix equations can be solved for these subsets of node velocities. These equations, with one exception, take the form

$$\begin{bmatrix} 1 & -1 & 0 & \cdots & 0 \\ -1/2 & \ddots & -1/2 & \ddots & \vdots \\ 0 & \ddots & \ddots & \ddots & 0 \\ \vdots & \ddots & \ddots & \ddots & -1/2 \\ 0 & \cdots & 0 & -1/2 & 1 \end{bmatrix} \begin{bmatrix} \dot{x}_{i,\text{ odd}} \\ \dot{x}_{i+1,\text{ even}} \\ \dot{x}_{i+2,\text{ even}} \\ \vdots \\ \dot{x}_{n,\text{ even}} \end{bmatrix} = \begin{bmatrix} \frac{1}{b}k(x_{\text{left}} + x_{\text{right}_1} - 2x_{i,\text{ odd}}) \\ \frac{1}{2b}k(x_{\text{right}_1} - x_{i+1,\text{ even}}) \\ \frac{1}{2b}k(x_{\text{right}_1} - x_{i+2,\text{ even}}) \\ \vdots \\ \frac{1}{2b}k(x_{\text{right}_1} - x_{n-1,\text{ even}}) \\ \frac{1}{2b}(k(x_{\text{last}} - x_{n,\text{ even}}) + b\dot{x}_{\text{last}}) \end{bmatrix},$$

where the left-hand matrix is $(n-i+1)$-by-$(n-i+1)$. A more natural way to write the first entry of the right-hand vector (that, alas, consumes too much space to fit into the matrix equation) is

$$\frac{1}{b}(k(x_{\text{left}} - x_{i,\text{ odd}}) + k(x_{\text{right}_1} - x_{i,\text{ odd}})).$$

The exception applies to the bottom path consisting of only dampers. Its matrix

equation is

$$\begin{bmatrix} 1 & -1/2 & 0 & \cdots & 0 \\ -1/2 & \ddots & \ddots & \ddots & \vdots \\ 0 & \ddots & \ddots & \ddots & 0 \\ \vdots & \ddots & \ddots & \ddots & -1/2 \\ 0 & \cdots & 0 & -1/2 & 1 \end{bmatrix} \begin{bmatrix} \dot{x}_{22} \\ \dot{x}_{34} \\ \dot{x}_{48} \\ \vdots \\ \dot{x}_{n,2^{n-1}} \end{bmatrix} = \begin{bmatrix} \frac{1}{2b}(b\dot{x}_{11} + k(x_{33} - x_{22})) \\ \frac{1}{2b}k(x_{47} - x_{34}) \\ \frac{1}{2b}k(x_{5,15} - x_{48}) \\ \vdots \\ \frac{1}{2b}k(x_{n,2^{n-1}-1} - x_{n-1,2^{n-2}}) \\ \frac{1}{2b}(k(x_{\text{last}} - x_{n,2^{n-1}}) + b\dot{x}_{\text{last}}) \end{bmatrix},$$

and the left-hand matrix is $(n-1)$-by-$(n-1)$.

The caveat concerning variations in k and b within the tree recurs here; these forms assume uniform stiffness and damping. If k and b are not uniform, the matrix and right-hand vector change. The extent of these changes is not made entirely transparent here, but the derivations from Equations (3.6) and (3.7) (with the necessary modifications) are straightforward.

In both versions of the matrix equation, the right-hand vector follows a pattern: each entry contains $\frac{1}{2b}k(x_{\text{right}_1} - x_{\text{curr}})$, where x_{curr} denotes the position of the node whose velocity is the corresponding entry of the left-hand vector. Note that while the notation x_{right_1} appears in all but one entry, it is each time referring to a different node, the one connected to the right of x_{curr} by a spring. (For all but the bottom path, the first entry is multiplied by $\frac{1}{b}$ instead of $\frac{1}{2b}$; that holds in this discussion.) The first and last entries each have an additional term: $\frac{1}{b}k(x_{\text{left}} - x_{\text{curr}})$ (or $\frac{1}{2b}b\dot{x}_{11}$) and $\frac{1}{2b}b\dot{x}_{\text{last}}$, respectively. In some cases, the matrix and both vectors are 1-by-1; when this occurs, the matrix is 1, $x_{\text{curr}} = x_{n,\text{ odd}}$ (or x_{22} if $n = 2$), and both additional terms are added to the right-hand side. In cases where the matrix is 2-by-2, it is the upper-left 2-by-2 block of the larger general form.

These matrices combine to produce $2^n - 2$ first-order differential equations, one for each intermediate robot. The governing equations for the first and last robot

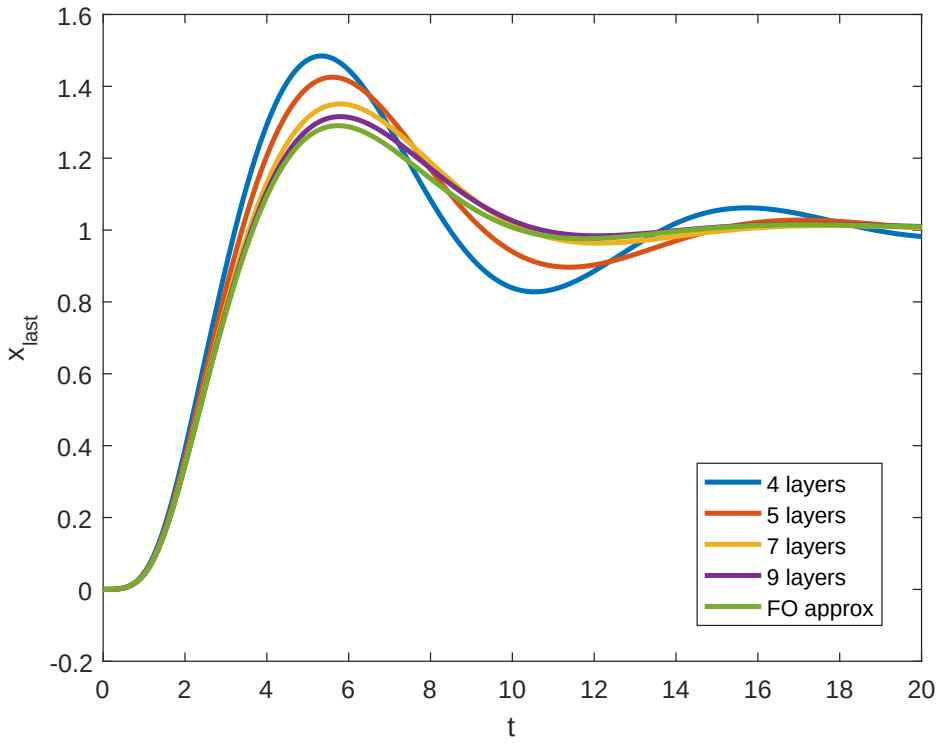

Figure 3.10. Comparison of step response of system with fractional order 1/2 to those of simulated trees with varying robot layers and zero intermediate mass.

layers do not change, so the total number of first-order equations for the tree system is $2^n + 2$. With relative and absolute tolerances on the order of 10^{-14}, MATLAB's `ode45` function can solve the equations and verify that adding layers causes the step response to approach that of a half-order system. This is shown in Figure 3.10; the figure is similar to Figure 3.7, but the trend toward the approximation is slightly more convincing, as expected.

The accuracy of the fractional-order equation solution as an approximation of the full system response exhibits some robustness to variations in the choices of stiffness k and damping b. Figure 3.11 demonstrates this for seven layers of robots with $m = 0.001$ for each robot in the intermediate layers. For each simulation,

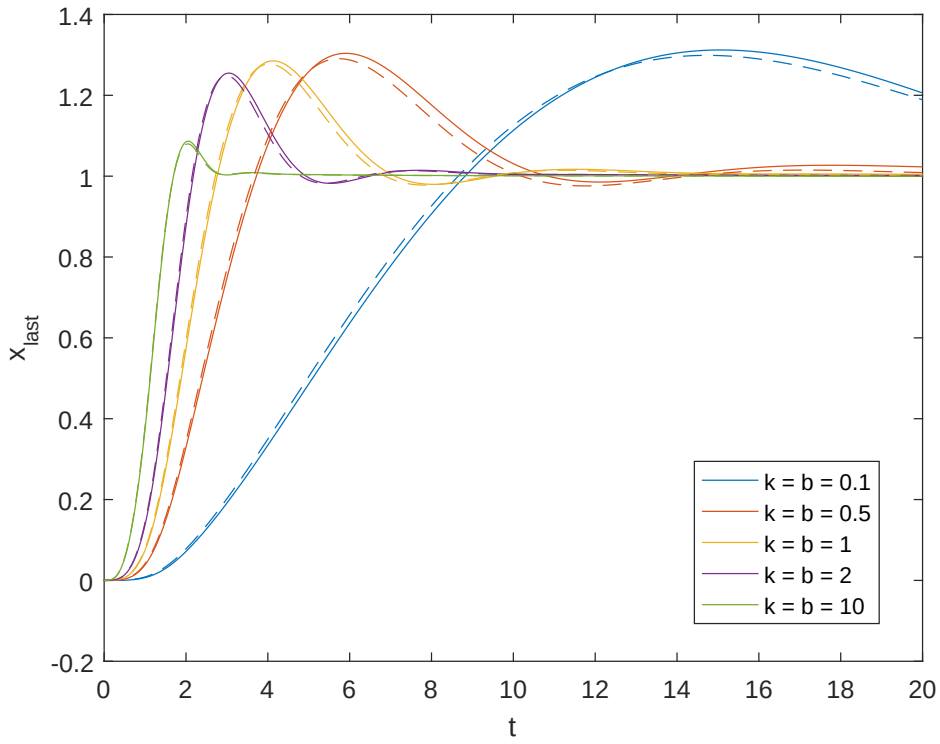

Figure 3.11. Step responses of system with fractional order 1/2 shown by dashed lines and compared to those of simulated trees with different stiffness and damping.

an approximation is computed from a fractional-order differential equation with the corresponding k and b, and all of these (shown with dashed lines) match well.

Equation (3.5) clearly reveals that k and b do not have individual significance in its solution; rather, the influential quantity is the product kb. As approximations for responses of the full tree systems, solutions of Equation (3.5) are viable only if k and b are somewhat close to one another. This is illustrated in Figure 3.12 for seven robot layers and $m = 0.001$, as in Figure 3.11, for pairs of k and b that multiply to $kb = 1$. It can be seen that there is more flexibility for differences between k and b if b is the larger of the two.

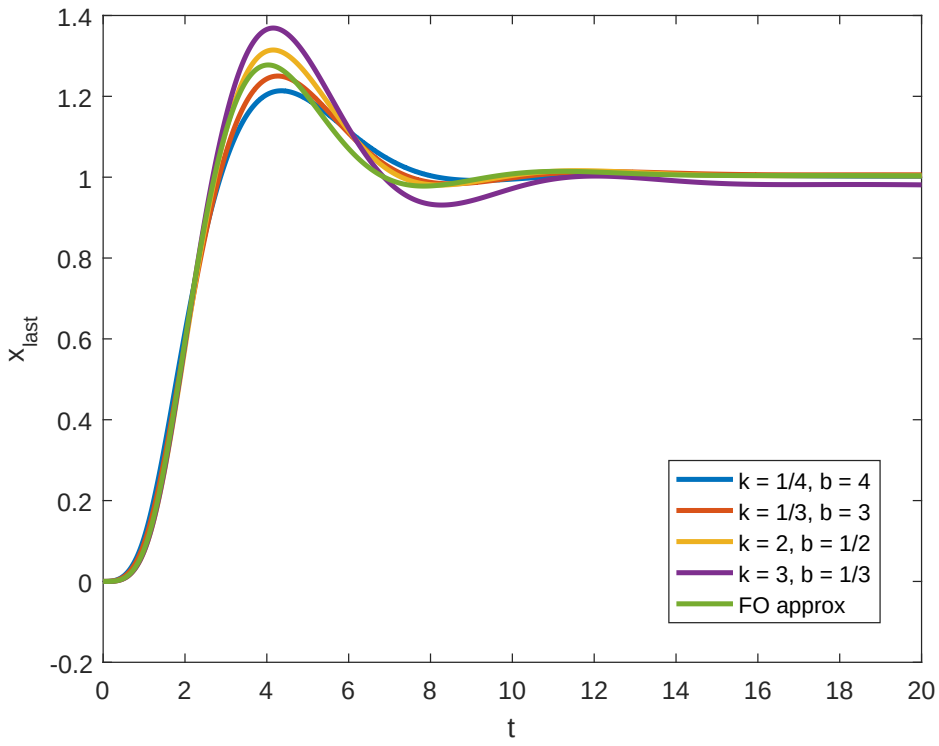

Figure 3.12. Comparison of step responses of system with fractional order 1/2 to those of simulated trees with constant kb.

Eventually, the robustness expires; the more extreme examples shown in Figure 3.12 likely render the approximation not accurate enough for many purposes. In those cases, the resistive property, stiffness or damping, with the larger constant is dominant over the other. With an eye toward ease of control of the overall system and monitoring it through the lens of fractional order, it would not be desirable to create such a strong imbalance in the system. Still, under minor imbalances, the solution of the fractional-order differential equation holds as an approximation to the simulated response of the full system.

It is thus established that the tree formation is of order 1/2, or rather, it is expected to be. However, a system's frequency response and corresponding responses to time-domain inputs can change if there is damage to the components. This is the next problem of interest: what happens to the tree when its component constants are not uniformly the same and how the fractional-order governing equation may differ as a result.

3.2.2 Damaged Coverage Formation

A spring with reduced stiffness or a damper with a reduced damping constant acts with less force on the two masses attached to it. In the context of the toxic waste spill, damage to these mechanical components in the model corresponds to a weakening of the network's control effort to maintain the desired spacing between the robots. The components with the greatest effect on the overall system response are the spring and damper in the first layer because they are each directly connected to the driving robot, which means that the effects resulting from damage propagate through the entirety of the tree.

3.2.2.1 Finite Formation

The constants of the first spring and damper are referenced as k_{11} and b_{11} respectively. The default constants throughout the tree remain k and b, and there are eight layers of robots. First consider damage to the first spring: $k_{11} = 0.1k$. In the Bode plot for this system, a notably new result is present: the frequency band that previously demonstrated a phase difference of -45 degrees now causes a phase difference of approximately -60 degrees. This is reflective of a system of order 2/3; the distinction is illustrated in Figure 3.13, from [39]. A comparison between the time-domain responses of this tree and the approximation, a system of order 2/3, shows agreement between the two, as illustrated in Figure 3.14, also from [39]. The time-domain response for the approximation is given by

$$\begin{aligned} x_{\text{last}}(n\Delta t) \approx & \frac{1}{\frac{m_{\text{last}}}{(\Delta t)^2} + \frac{M(kb)^{2/3}}{(\Delta t)^{2/3}}} \\ & \times \left(\frac{m_{\text{last}}}{(\Delta t)^2} \left(2x_{\text{last}}((n-1)\Delta t) - x_{\text{last}}((n-2)\Delta t)\right) \right. \\ & - \frac{M(kb)^{2/3}}{(\Delta t)^{2/3}} \sum_{j=1}^{n} (-1)^j \binom{2/3}{j} x_{\text{last}}((n-j)\Delta t) \\ & \left. + \frac{M(kb)^{2/3}}{(\Delta t)^{2/3}} \sum_{j=0}^{n} (-1)^j \binom{2/3}{j} x_{11}((n-j)\Delta t) \right). \end{aligned}$$

Here M is a magnitude adjustment, in this case -7 dB. This is incorporated to improve the approximation by matching its frequency response magnitude to that of the full system at a frequency of 1 rad/s. That frequency is chosen because it is logarithmically central and therefore expected to be part of the frequency band showing fractional-order behavior. In practice, it is seen in Figure 3.13 that 1 rad/s is close to the edge of that frequency band. By matching at a different frequency, a

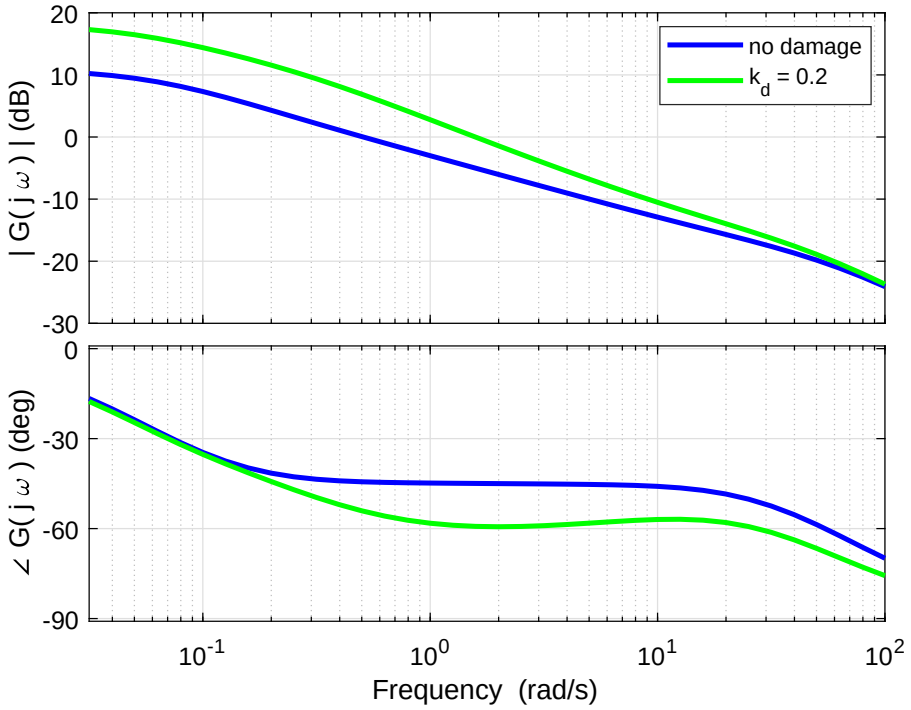

Figure 3.13. Bode plot for undamaged system and system with damage to first spring, $k_{\mathrm{d}} = 0.1k$.

higher one (such as 3 rad/s) in this case, there is room for improvement in the match of Figure 3.14 as a result of a different choice of M.

The magnitude adjustment is justified by the inflation in frequency response magnitude from the undamaged case to the damaged case, as shown in Figure 3.13. The combination of springs and dampers is weakened in the damaged case, so the motion of the first robot is not resisted as strongly by the components; this may be likened to a circuit with reduced impedance. Thus, more of the force on the first robot is transmitted to the last layer of robots. From a nominal transfer function of $(kbs)^{-1/2}$, the hypothesis for the damaged system's transfer function is not truly $(kbs)^{-2/3}$ but rather an amplification thereof. Introducing M implements this amplification within the computation of the time-domain response.

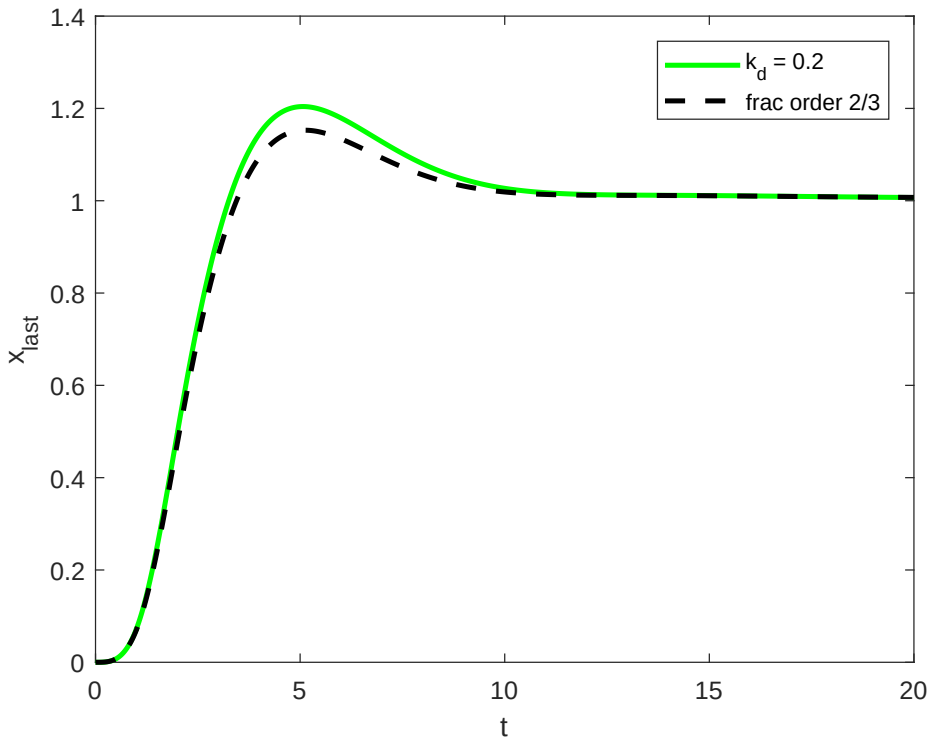

Figure 3.14. Comparison of time-domain response of 2/3-order system to that of full system with damage to first spring.

If the spring is restored to its normal stiffness k while $b_{11} = 0.1b$, a result of similar nature appears. In this instance, the Bode plot shows a phase difference near -30 degrees, indicative of a system of order 1/3; this Bode plot is given in Figure 3.15, from [39]. As in the previous case, the time-domain responses of the tree and an approximation, a system of order 1/3, match well; these are shown in Figure 3.16. The response for this approximation is given by

$$\begin{aligned} x_{\text{last}}(n\Delta t) \approx & \frac{1}{\frac{m_{\text{last}}}{(\Delta t)^2} + \frac{M(kb)^{1/3}}{(\Delta t)^{1/3}}} \\ & \times \left(\frac{m_{\text{last}}}{(\Delta t)^2} \left(2x_{\text{last}}((n-1)\Delta t) - x_{\text{last}}((n-2)\Delta t)\right) \right. \\ & - \frac{M(kb)^{1/3}}{(\Delta t)^{1/3}} \sum_{j=1}^{n} (-1)^j \binom{1/3}{j} x_{\text{last}}((n-j)\Delta t) \\ & \left. + \frac{M(kb)^{1/3}}{(\Delta t)^{1/3}} \sum_{j=0}^{n} (-1)^j \binom{1/3}{j} x_{11}((n-j)\Delta t) \right). \end{aligned}$$

The magnitude adjustment M is -3 dB, again included to draw the approximation's frequency response magnitude closer to the full system's at a frequency of 1 rad/s. These two results are fully analogous in spite of the fact that $k = 2$ and $b = 1$; this suggests some sort of duality between the damage cases without dependence on the magnitudes of the constants.

The order shifts perceived here align with intuition. A decrease in stiffness increases the order from 1/2; in other words, it pushes the order toward 1, the same order native to the damping elements. Likewise, a decrease in damping lowers the order toward 0, implying that the springs attain greater influence over the system.

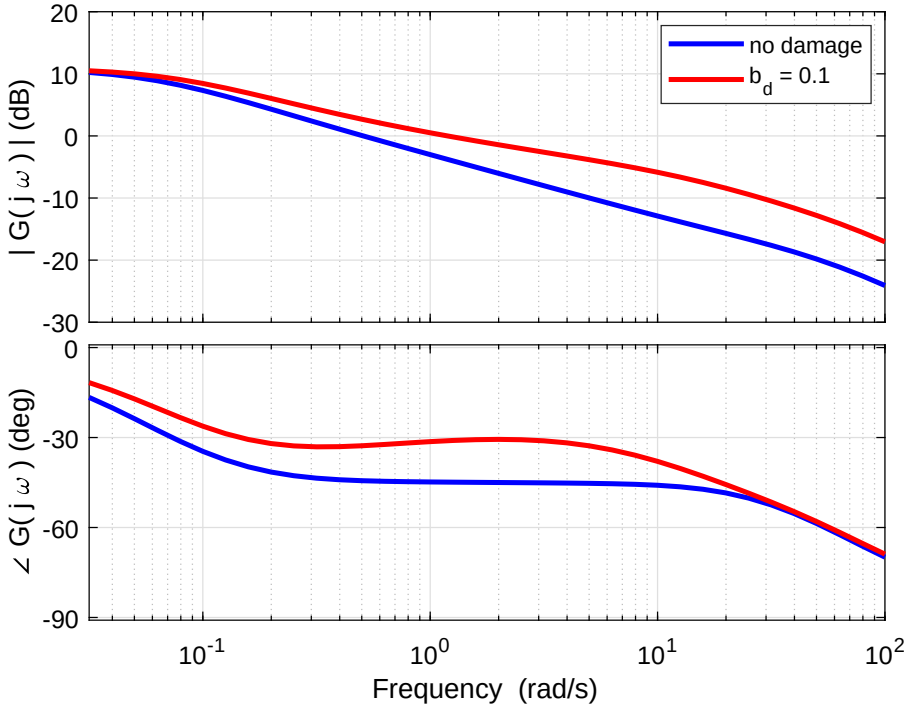

Figure 3.15. Frequency responses for undamaged system and system with damage to first damper.

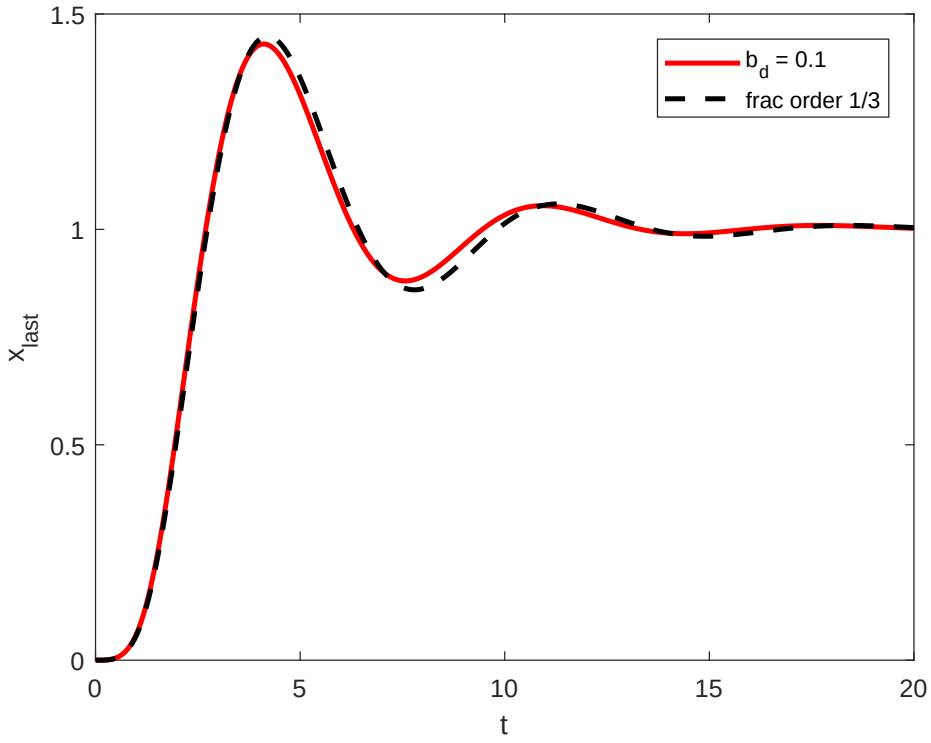

Figure 3.16. Fractional and exact time-domain responses for system with damage to first damper.

3.2.2.2 Infinite Formation: Asymptotic Damage

This discussion concerns a formation of the same type, but having infinitely many layers, to show that the damage results from the finite formation, an approximation of a system of order 1/2, are to be expected from a system that truly has order 1/2. Here, the leftmost stiffness and damping constants, k_1 and b_1 respectively, are changed separately to either zero or infinity; only the leftmost components are discussed because those cases present the effects of damage most clearly.

Without damage, that is, if $k_1 = k$ and $b_1 = b$, the components can be combined in parallel and series, and self-similarity can be invoked. The transfer function satisfies

$$\begin{aligned} G_\infty(s) &= \frac{1}{\frac{1}{\frac{1}{k_1}+G_\infty(s)} + \frac{1}{\frac{1}{b_1 s}+G_\infty(s)}} \\ &= \frac{1}{\frac{k_1}{1+k_1 G_\infty(s)} + \frac{b_1 s}{1+b_1 s G_\infty(s)}}. \end{aligned}$$

The result for $G_\infty(s)$ is as before:

$$G_\infty(s) = \frac{1}{\sqrt{kbs}}, \tag{3.8}$$

so the system has order 1/2. Hereafter, this transfer function resulting from the limiting case of infinitely many generations is called $G_{1/2}(s)$.

If either component's constant is changed such that $k_1 \neq k$ or $b_1 \neq b$, then G_∞ is no longer equal to $G_{1/2}$. Reducing k_1 to zero alters the formation; with the spring having no effect, the damper acts as though it is in series with a formation having one fewer layer but still having transfer function $G_{1/2}(s)$:

$$G_\infty(s) = \frac{1}{b_1 s} + G_{1/2}(s) = \frac{1}{b_1 s} + \frac{1}{\sqrt{kbs}},$$

a straightforward combination of a first-order system and a 1/2-order system. By

analogy, when b_1 is reduced to zero,

$$G_\infty(s) = \frac{1}{k_1} + G_{1/2}(s) = \frac{1}{k_1} + \frac{1}{\sqrt{kbs}},$$

i.e., the spring of order 0 is placed in series with a tree formation of order 1/2.

Correspondingly, when k_1 goes to infinity, that half of the formation behaves as the undamaged full formation of order 1/2. Therefore, $G_{1/2}(s)$ is placed in parallel with a series combination of a damper and another instance of $G_{1/2}(s)$:

$$G_\infty(s) = \frac{1}{\frac{1}{G_{1/2}(s)} + \frac{1}{\frac{1}{b_1 s} + G_{1/2}(s)}} = \frac{1}{\sqrt{kbs} + \frac{1}{\frac{1}{b_1 s} + \frac{1}{\sqrt{kbs}}}}.$$

Likewise, when b_1 goes to infinity, $G_{1/2}(s)$ is placed in parallel with a series combination of a spring and another transfer function of order 1/2:

$$G_\infty(s) = \frac{1}{\frac{1}{\frac{1}{k_1} + G_{1/2}(s)} + \frac{1}{G_{1/2}(s)}} = \frac{1}{\frac{1}{\frac{1}{k_1} + \frac{1}{\sqrt{kbs}}} + \sqrt{kbs}}.$$

The frequency responses for these parameter variations are displayed in Figures 3.17 and 3.18, from [39]. The curves labeled "no damage" show the frequency response for the system of Equation (3.8) that has order 1/2 and, in turn, a phase difference of $-45°$ and a magnitude slope of -10 dB/decade. The other cases exhibit other orders, as evidenced by their varying magnitude slopes and phase difference values. These scale linearly with order; order 0 maps to 0 dB/decade and 0°, order 1 maps to -20 dB/decade and $-90°$, and so on.

The curve representing $k_1 = k_d = 0$ in Figure 3.17 has a phase difference more negative than $-45°$, suggesting an order greater than 1/2; this is consistent with the physical interpretation that reduced stiffness results in a relatively heightened influence from the damper, drawing the overall order closer to 1. Analogously, the curve representing $b_1 = b_d = 0$ has a phase difference less negative than $-45°$; reduced

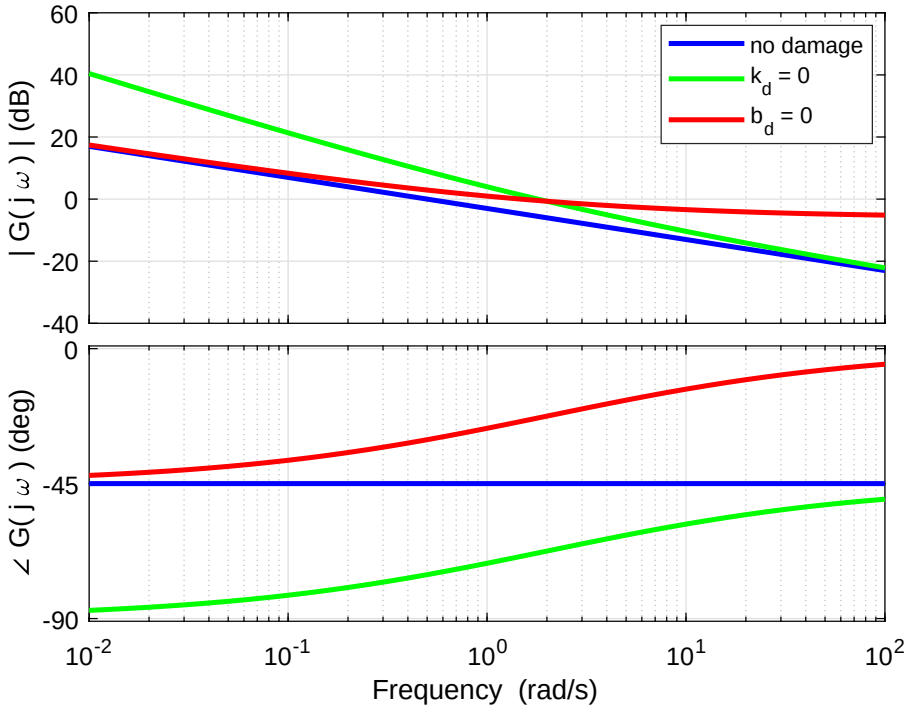

Figure 3.17. Frequency responses for limiting cases of extreme damage.

damping pushes the overall order toward 0, the order characteristic of a spring.

The frequency responses for the systems in which one constant goes to infinity are shown in Figure 3.18. If k_1 is made infinite, the order somewhat greater than 1/2 is explained by a greater damping effect that follows from placing a replica of the original system, having order 1/2, in parallel with a series combination of a damper and another replica system of order 1/2. An infinite b_1 has the analogous effect of combining two 1/2-order systems and a spring, yielding an overall order less than 1/2.

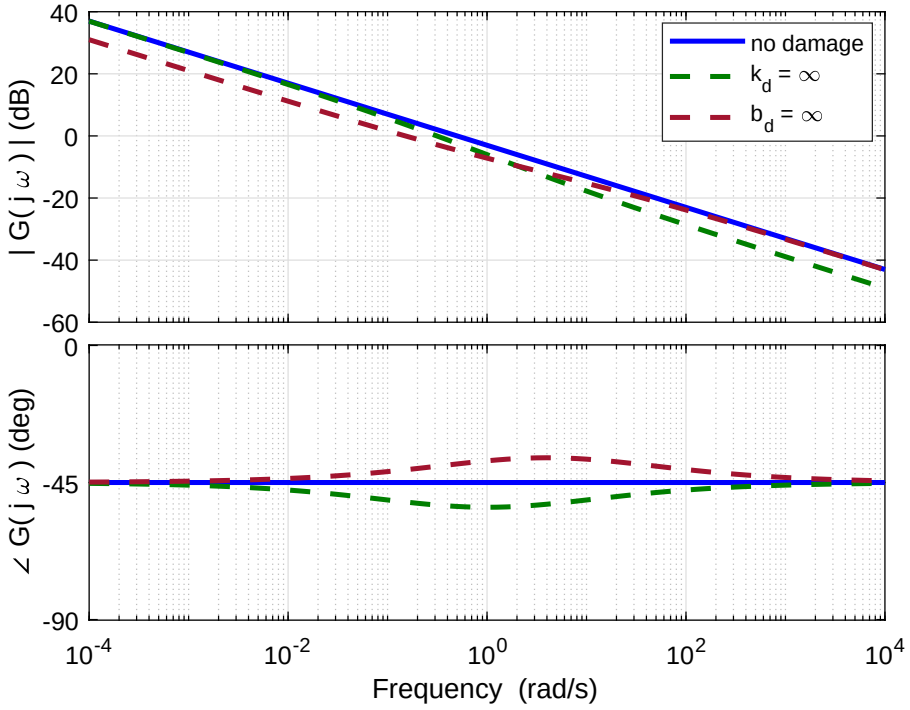

Figure 3.18. Frequency responses for limiting cases of extreme stiffness and damping increase.

To make this contribution more thorough, analysis of parameter variations falling between these limiting examples is needed. Chapter 4 outlines a fractional-order system identification procedure to measure changes in order resulting from damage or any other operational change. First, though, the need for such a procedure is demonstrated with responses from varying damage cases.

3.2.2.3 Infinite Formation: Intermediate Damage

The limiting cases of zero or infinite stiffness or damping lead to transfer functions suggesting that the component's new value effectively changes the construction of the system. In contrast, intermediate changes to k_1 or b_1 preserve the construction, but the component constants are no longer uniform, so self-similarity is lost. In general, changes to k_1 and b_1 give rise to the transfer function

$$\begin{aligned} G_\infty(s) &= \frac{1}{\frac{1}{\frac{1}{k_1}+G_{1/2}(s)} + \frac{1}{\frac{1}{b_1 s}+G_{1/2}(s)}} \\ &= \frac{1}{\frac{1}{\frac{1}{k_1}+\frac{1}{\sqrt{kbs}}} + \frac{1}{\frac{1}{b_1 s}+\frac{1}{\sqrt{kbs}}}}. \end{aligned}$$

While this transfer function cannot be simplified further, it can be evaluated for arbitrary constants k_1 and b_1. With default constants of $k_1 = k = 2$ and $b_1 = b = 1$, the frequency responses under varying stiffness, $k_1 \in \{2 \times 10^{-4}, 2 \times 10^{-3}, \ldots, 2 \times 10^{4}\}$, are shown in Figure 3.19, and the frequency responses of the same transfer function for $b_1 \in \{10^{-4}, 10^{-3}, \ldots, 10^{4}\}$ are shown in Figure 3.20; both figures appear in [39]. These damage cases are extensions of those displayed in Figures 3.13 and 3.15, the difference being that those two are concerned with finite representations of the coverage formation. It appears that factors of 10^{-5} and 10^{4} are adequate lower and upper bounds for these progressions because those frequency responses match well with Figures 3.17 and 3.18.

Order shifts are obvious in both Figures 3.19 and 3.20, and they are analogous and

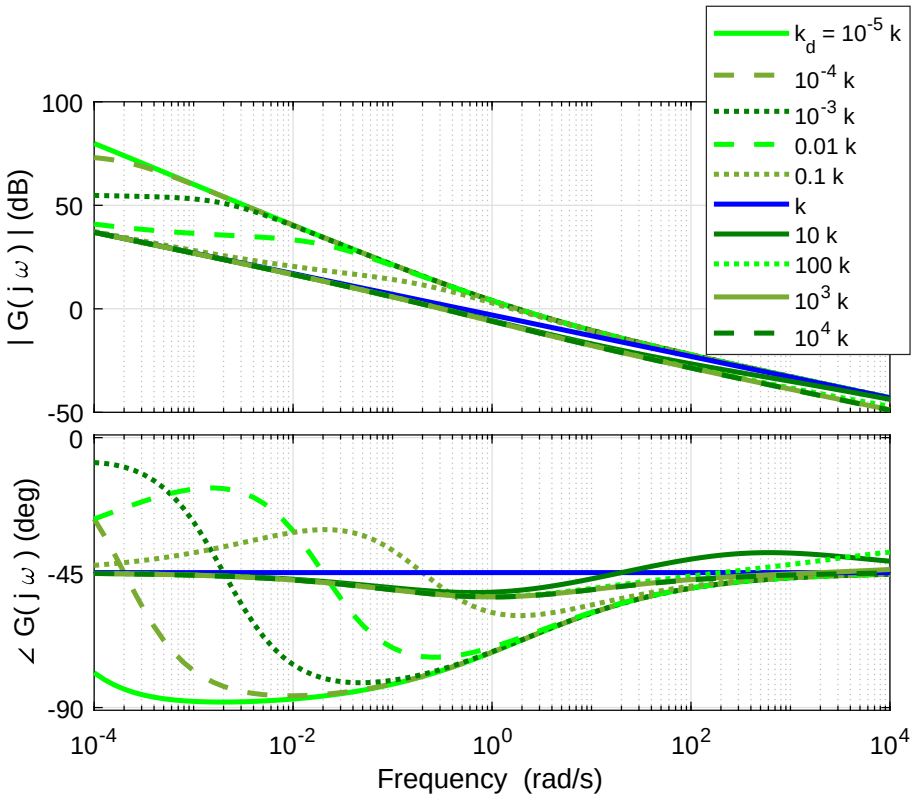

Figure 3.19. Frequency responses for various spring damage cases showing decreasing magnitude for increased stiffness.

opposite. However, in many cases, the phase difference changes significantly over the frequency window shown. Since these versions of the system do not display specific fractional orders over wide frequency bands, a computational system identification method is imperative in quantifying order.

3.3 Monitoring Insights

This section contains findings from other instances of damage in the robot formation example. These illustrate the most promising ways in which fractional order measurement might be applied for monitoring. Apparent limitations of the approach and ideas for its implementation in experimental settings are also included.

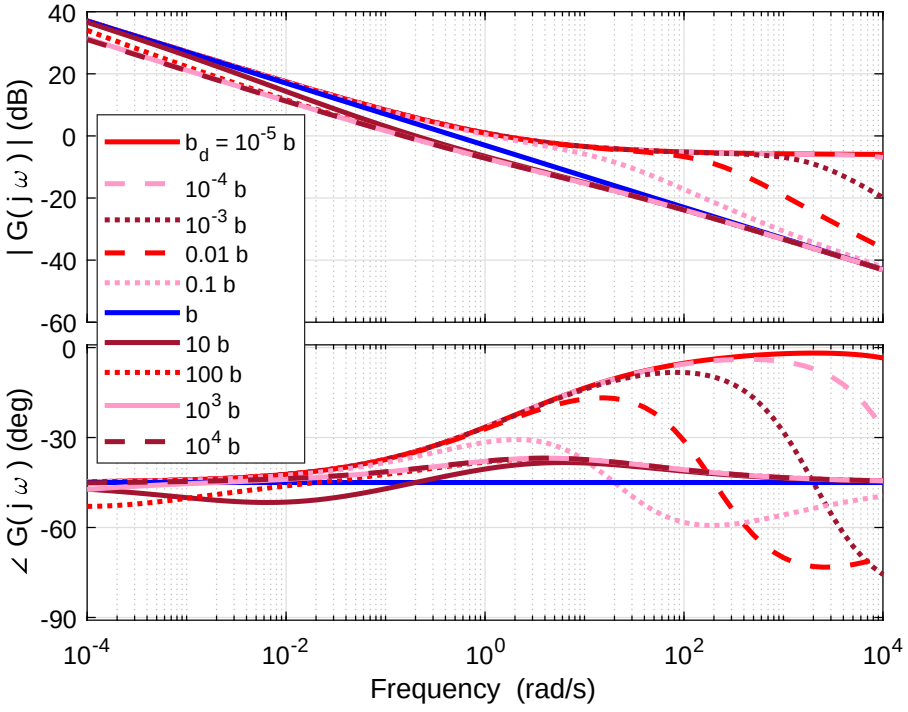

Figure 3.20. Frequency responses for various damper damage cases showing decreasing magnitude for increased damping.

3.3.1 Damage Detection

While the spring and damper of the first layer are the most influential components, the others show varied effects on the frequency response as well. The components serially connected with exclusively like elements contribute the most to the overall effective stiffness and effective damping of the tree; these are the springs along the upper edge of the tree diagram and the dampers along the lower edge. As such, effects of damage to these components are greater than those resulting from damage to others, so they are collectively called the critical components.

Perhaps naturally, there is a qualitatively tangible progression in the frequency response from damage to the most critical component to that of the least and, in turn, of no damage. In the case of the springs, for the damage case of $k_{i,1} = 0.1k$ as before (with $i \in [1, \ldots, n]$ for n layers of springs and dampers), the differences occur for medium and high frequencies. There is a medium-frequency band showing a phase difference of approximately -60 degrees, but this band contracts as the damage is given to less critical springs. High-frequency behavior similar to that of the undamaged system encroaches upon that territory. Thus, for medium-high frequencies, the phase difference is closer to the -45 degrees of the undamaged system. This damage progression for critical springs (CSs) is shown for a formation having eight layers of robots (seven layers of springs and dampers) in Figure 3.21.

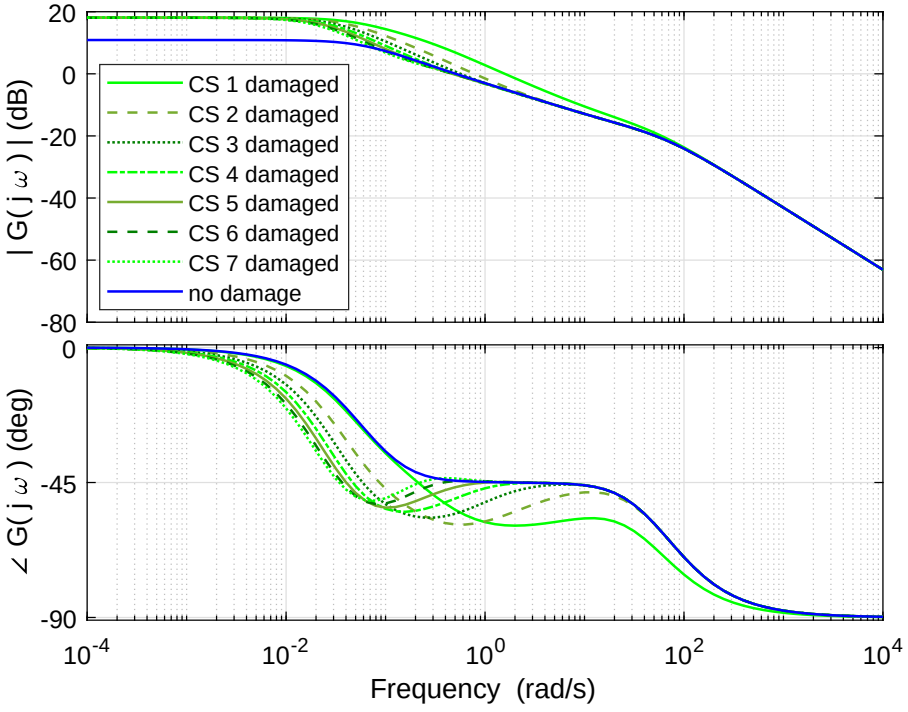

Figure 3.21. Damage progression for critical springs compared to undamaged frequency response.

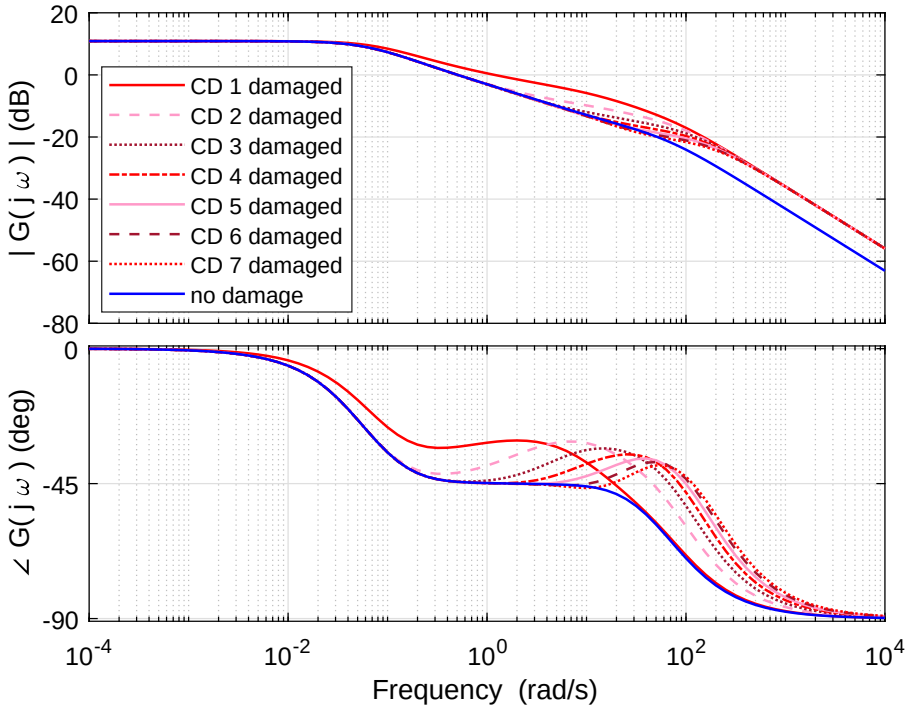

Figure 3.22. Damage progression for critical dampers compared to undamaged frequency response.

Results for the dampers are opposite. The damage case of $b_{i,\text{last}} = 0.1b$ causes a progression of varying frequency response behavior in the low- and medium-frequency areas on the Bode plot. The medium frequencies show a phase difference near -30 degrees, while the low frequencies cause responses similar to that of the undamaged system. The effect for decreasingly critical damage is that medium-low frequencies give a phase difference near -45 degrees. The frequency responses for these cases of damage to critical dampers (CDs), for a formation having seven layers of springs and dampers, are plotted together in Figure 3.22. In all of these cases, for springs and dampers alike, the phase difference as a function of frequency acquires inflection points; the decrease from 0 to -90 degrees is clearly not monotonic.

These progressions imply that the components on the left of the tree are more

important to the functioning of the formation than those on the right. This may be the case because the robots on the left are highly connected to their right. However, the truncation of the tree at, in this case, seven layers of springs and dampers means that the approximation of the transfer function as half-order is imperfect in some contexts. If the formation is extended to the theoretical ideal of infinitely many layers, rendering the half-order transfer function a perfect description, then every robot has the same connectedness. It is unclear how the frequency responses of such trees undergoing equivalent damages in different locations might differ, but series and parallel combinations along the lines of the computations for Figures 3.19 and 3.20 would yield those results.

3.3.2 Limitations

Damages of this nature are also considered for the components in the middle of the tree, that is, the components that are not critical. In these cases the nature of the "critical" label is made clear because there is little to no effect on the system's frequency response. While it is necessary that some coefficient in the high-order governing equation must change under this type of damage, the resulting dynamics are not visibly different from those of the undamaged system.

There are scenarios in which damages to these intermediate components may combine with one another to produce a more tangible effect. For example, reducing *all* of these constants by a factor of 1/10 results in a frequency response with no band of frequencies to suggest fractional-order dynamics. That is to be expected because this instance of the tree is essentially two elements: a series of springs in parallel with a series of dampers, with all effects from the damaged components in between considered negligible by comparison. The governing equation of this damped harmonic oscillator is well known to be of integer order.

In light of the overall transfer function of $(kbs)^{-1/2}$ for the undamaged system, it

is evident that the quantity kb has importance for this approach to damage detection. Hence, any sort of alteration to the system that might preserve kb would be difficult to detect. The nature of a physical example of damage that would bring about this result is not clear.

3.3.3 Implementation

Implementation of order measurement as a system monitoring method is hereby established in principle. One must collect frequency response data from operational and damaged versions of the same system, noting the orders of behavior that appear in these frequency responses. An order higher than expected implies damage to a spring, and lower, a damper, or the corresponding physical relationship modeled by either of these components.

The frequency band in which the response is abnormal can serve as an indicator of the severity of the damage. In the case of a multi-robot or other network system, damage near locations with high connectedness is implied by noticeable response changes over wide frequency bands. Effects contained within narrower frequency bands suggest less critical damage. These interpretations can translate to other types of similarly modeled systems if one assumes that the damage is localized, as in the scenarios detailed here.

This chapter has explained the use of fractional-order differential equations as a monitoring tool for systems such as formations of cooperating robots. The damage of interest may be detected by measuring the fractional order of dynamics present in the system's governing equation. Considering the broad space of systems that can be modeled with spring and damper elements, the principles outlined here may inform a new systemic health monitoring approach that is widely applicable.

CHAPTER 4

FRACTIONAL-ORDER SYSTEM IDENTIFICATION TO DETECT CHANGES IN ORDER

The previous chapter establishes fractional order as a status indicator. Measurement of changes in order may provide a foundation for health monitoring of high-order engineering systems such as the robot formation example. This chapter explains a computational method of system identification that lends itself to general applicability for measuring order changes. The method presented here can serve as the centerpiece of a new set of tools for system monitoring through the lens of fractional-order modeling. Much of this content appears in [39].

4.1 Identification Procedure

The method developed in this research was inspired by [54]. It is therefore prudent to outline that method for clarity so that the modifications made for generality can be conveyed most clearly. The starting point is a set of data containing a frequency response, denoted $G(s)$, to be matched, or identified. The end result, a transfer function that matches $G(s)$ as well as possible, is of the form

$$F(s) = \frac{K_0}{s^{d_0}} \frac{B(s)}{A(s)} = \frac{K_0 \sum_{k=0}^{n} b_k s^{\beta_k}}{s^{d_0} \sum_{k=0}^{d} a_k s^{\alpha_k}}$$

where $a_0 = b_0 = 1$, $\alpha_0 = \beta_0 = 0$, and $\alpha_k, \beta_k \in \mathbb{R}$. For illustration of the effects of these latter choices on the procedure, an equivalent representation of this form is

$$F(s) = \frac{K_0}{s^{d_0}} \frac{b_n s^{\beta_n} + \cdots + b_1 s^{\beta_1} + 1}{a_d s^{\alpha_d} + \cdots + a_1 s^{\alpha_1} + 1}, \tag{4.1}$$

ensuring that there is a constant, K_0, in the numerator. A proper transfer function can always be manipulated to satisfy that condition, but in general, it may not be possible to have a constant in the denominator as well. For this reason, s to the power d_0 is factored out of the denominator, and d_0 can take a nonzero value if needed.

These measures provide some flexibility, but not in a way that is integrated into the identification. One must choose the gain K_0 and the origin pole multiplicity d_0 at the beginning, along with α_k and β_k. A workaround for this limitation is revealed later in the discussion.

For the sake of solution by the simplex method, the result is posed as a state vector:

$$w = \begin{bmatrix} b_1 & \cdots & b_n & a_1 & \cdots & a_d & w_{n+d+1} \end{bmatrix}^{\mathrm{T}},$$

where all entries of $w \geq 0$. The entry w_{n+d+1} is expressly for inclusion in the linear constraints, which set a bound on the error metric

$$R(j\omega) = \frac{(j\omega)^{d_0}}{K_0} A(j\omega)(F(j\omega) - G(j\omega)), \tag{4.2}$$

specifically its L^∞-norm,

$$\|R(j\omega_i)\| = \max(|\mathrm{Re}(R(j\omega_i))|, |\mathrm{Im}(R(j\omega_i))|).$$

In Equation (4.2), the denominator $A(j\omega)$ of the identified transfer function $F(j\omega)$ is factored out so as to highlight the subtraction of the true frequency response G from F. The number of frequencies comprising $G(j\omega)$ is denoted n_{f}, so there are

n_f real and n_f imaginary parts of $R(j\omega)$. The method of [54] iteratively drives the largest absolute value of these $2n_\mathrm{f}$ numbers to a minimum. The formulation casts this problem as the minimization of one variable, a linear objective function, so the simplex method may be employed.

While convenient, that objective function considers only one frequency at a time, neglecting all other frequencies of $G(j\omega)$ until a different real or imaginary part of $R(j\omega)$ becomes the largest in magnitude. The approach developed here diverges from [54] by asserting that it is desired to treat all frequencies with equal weight at every step. The objective function chosen for this system identification method is

$$J = \sum_{i=1}^{n_\mathrm{f}} \left| \frac{\left(\sum_{k=0}^{n} b_k (j\omega_i)^{\beta_k} \right) - \frac{(j\omega_i)^{d_0}}{K_0} \left(\sum_{k=0}^{d} a_k (j\omega_i)^{\alpha_k} \right) G(j\omega_i)}{\frac{(j\omega_i)^{d_0}}{K_0} \left(\sum_{k=0}^{d} a_k (j\omega_i)^{\alpha_k} \right) G(j\omega_i)} \right|,$$

or equivalently,

$$J = \sum_{i=1}^{n_\mathrm{f}} \left| \frac{B(j\omega_i) - \frac{(j\omega_i)^{d_0}}{K_0} A(j\omega_i) G(j\omega_i)}{\frac{(j\omega_i)^{d_0}}{K_0} A(j\omega_i) G(j\omega_i)} \right|$$

and, in turn,

$$J = \sum_{i=1}^{n_\mathrm{f}} \left| \frac{\frac{(j\omega_i)^{d_0}}{K_0} A(j\omega_i) (F(j\omega_i) - G(j\omega_i))}{\frac{(j\omega_i)^{d_0}}{K_0} A(j\omega_i) G(j\omega_i)} \right|.$$

Therefore, the quantity being minimized in this procedure is

$$J = \sum_{i=1}^{n_\mathrm{f}} \left| \frac{F(j\omega_i) - G(j\omega_i)}{G(j\omega_i)} \right|.$$

This is a nonlinear objective function, so the simplex method is no longer able to solve the problem. The coefficients

$$v = \begin{bmatrix} b_1 & \cdots & b_n & a_1 & \cdots & a_d \end{bmatrix}^\mathrm{T}$$

are determined by nonlinear optimization in MATLAB. The interior-point and sequential quadratic programming (SQP) algorithms of the MATLAB function `fmincon` are considered, along with the pattern-search algorithm (function `patternsearch`). When the interior-point algorithm is employed, every entry in the state vector is nonzero, so the result for $F(s)$ has terms for every order in α and β. This demonstrates the relative dominance of each order. In contrast, the other two algorithms are capable of returning some coefficients of zero in the state vector, declaring that certain orders are not present in the optimal transfer function.

The function `fmincon` is a tool for constrained optimization, so an adaptation of this problem to serve as input to the function requires constraints. One may intuitively suggest that all entries in the solution vector v be greater than or equal to zero based on stability theory, and indeed, that is an appropriate line of reasoning. However, the set of constraints chosen here, for both `fmincon` and `patternsearch`, is slightly different: all entries of $v \geq 0$, except $a_1, b_1 \geq -1$. These two coefficients correspond to constants (exponents $\alpha_1 = \beta_1 = 0$) that, by virtue of these constraints, are able to cancel the built-in 1's in the numerator and denominator of Equation (4.1); this generalizes the form of the transfer function returned by the optimization.

4.2 Introduction of Driving Formation

Later in this chapter, the identification procedure is demonstrated on two mechanical models of systems. One is the coverage system of Chapter 3 resembling a tree diagram. The other is a group of autonomous robotic vehicles traveling together. This formation has two priorities, specifically preserving a desired spacing and velocity. The driving formation is shown in Figure 4.1, from [39].

In a manner similar to the example of the coverage formation, the driving formation can be cast as a mechanical system, as shown in Figure 4.2, from [39]. Spring elements with constant k enforce a specified distance between vehicles. Damping

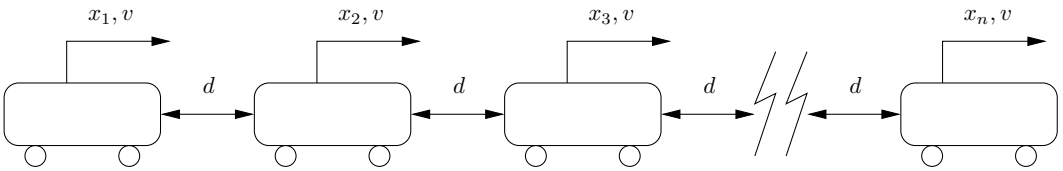

Figure 4.1. Diagram of mobile robots traveling in a line.

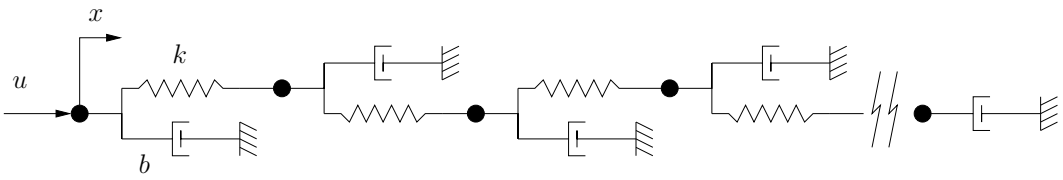

Figure 4.2. Schematic showing springs and dampers in driving formation.

elements with constant b are connected from each mobile robot to a moving ground having the desired velocity relative to the road. These are meant to ensure that the robots maintain that velocity as well.

The mechanical arrangement in Figure 4.2 is analogous to a ladder circuit of resistors and capacitors having behavior of order 1/2 in its relationship between current and voltage, as shown in [50]. A corresponding result is evident in the relationship between input force and displacement of the leftmost vehicle in the driving formation. The frequency response has a phase difference of $-45°$ over a wide band of frequencies, as shown in Figure 4.3 for the case of 1000 vehicles with $k = 1$ and $b = 1$ throughout the formation.

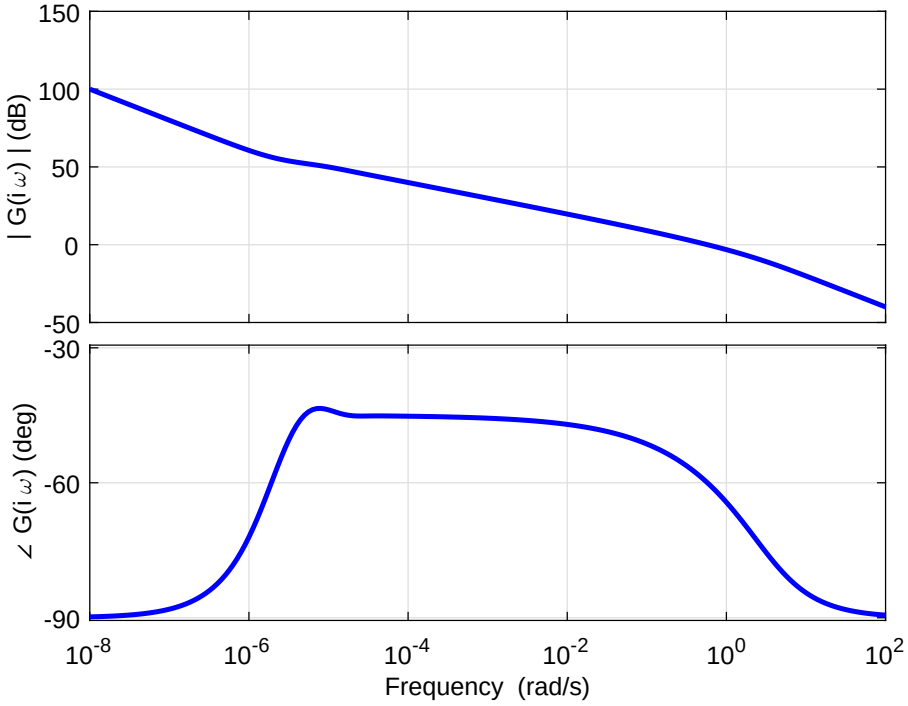

Figure 4.3. Bode plot for driving formation.

4.3 Results for Example Cases

With the identification procedure in hand, the tree system example of Chapter 3 and line of driving vehicles, both representing robot formations, can be extended. Recall that the transfer function of the undamaged tree system is derived to be some constant multiplied by $s^{-1/2}$. Damage to the first spring causes a shift toward $s^{-2/3}$; damage to the first damper, toward $s^{-1/3}$. These relationships are evident upon examination of the frequency responses for these versions of the system, shown in Figures 3.13 and 3.15, where respective phase differences of $-45°$, $-60°$, and $-30°$ are prominent over some frequency band. Transfer functions of the same orders are sought as identification results from running the procedure on the corresponding tree system data sampled over a representative frequency band.

In a manner similar to [54], α_k (with k starting at 1) is set to $0, 1/6, \ldots, 13/6$ so that over two integer orders of dynamics may be identified. Incrementing by $1/6$ is especially suitable for the coverage formation example because the results are expected to affirm the presence of orders that are integer multiples of $1/6$: $1/3$, $1/2$, and $2/3$. However, β_k is set to 0 only, ensuring that the numerator is a constant. Following from this choice, the computationally obtained results may transparently show the dominance of individual orders with respect to the others; these orders may be read directly from the denominators of the identified transfer functions.

The system identification procedure is expected to agree with the theoretical results, and the system is expected to be undamaged. Therefore, the starting point chosen for the optimization is

$$\begin{aligned} v_0 &= \begin{bmatrix} b_1 & a_1 & a_2 & \cdots & a_{14} \end{bmatrix} \\ &= \begin{bmatrix} 0 & -1 & 0 & 0 & 1 & 0 & \cdots & 0 \end{bmatrix}^{\mathrm{T}}, \end{aligned}$$

where the 1 is assigned to a_4 to yield $s^{-1/2}$. In general, if the 1 is assigned to a_k with $k > 1$, the transfer function represented by this starting point is $s^{-(k-1)/6}$. A detailed expression of the starting transfer function corresponding to such a choice of v_0 is

$$F_0(s) = \frac{0s^0 + 1}{s^{(k-1)/6} - s^0 + 1} = \frac{1}{s^{(k-1)/6}}.$$

The identification results are as follows. In presenting the transfer functions, both fraction components are scaled so that the highest-order coefficient in the denominator is 1.

4.3.1 Driving Formation

For the vehicles traveling in a line, the frequency band of interest for 1000 vehicles is from $10^{-5.4}$ to $10^{-1.4}$ rad/s, so logarithmic spacing with a step size of 0.1 powers of 10 leads to 41 frequencies ($n_\mathrm{f} = 41$). With the interior-point algorithm employed, $F(s)$ is given by

$$F(s) = \frac{4.5}{s^{13/6} + \cdots + 1.1s + \cdots + 4.5s^{1/2} + \cdots + 2\mathrm{e}{-4}}$$

and has error $J = 0.3583$. The SQP algorithm gives

$$F(s) = \frac{3.5}{s^{13/6} + s + 0.1s^{2/3} + 3.4s^{1/2} + 1\mathrm{e}{-4}}$$

with error $J = 0.3495$. The pattern-search algorithm gives

$$F(s) = \frac{38}{s^{13/6} + \cdots + 13s + \cdots + 37s^{1/2} + 4\mathrm{e}{-4}}$$

with error $J = 0.3557$. In each case, considering the relative magnitudes of the coefficients, order 1/2 is prominent. Here, the SQP algorithm performs best, but all

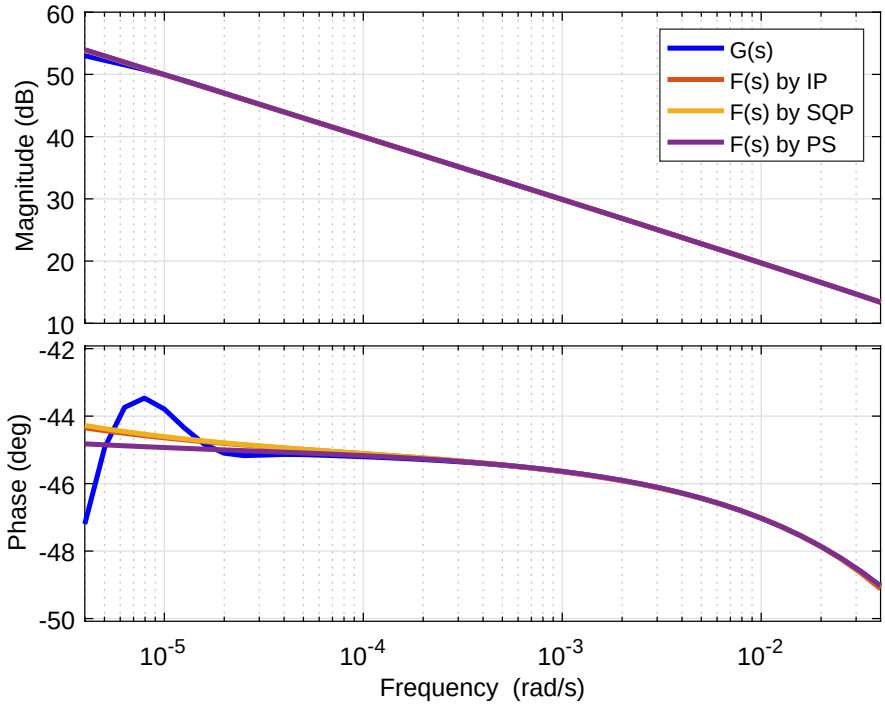

Figure 4.4. Bode plot of actual and identified transfer functions for the driving formation.

are similarly successful. Figure 4.5 shows the favorable comparison between $G(s)$ and the three results for $F(s)$. The results from the interior-point and SQP algorithms nearly overlap in the figure.

For the ladder arrangement with 1000 robots, $k = 100$, $b = 1$, and 41 frequencies ($n_{\mathrm{f}} = 41$) logarithmically spaced from $10^{-3.4}$ to $10^{0.6}$ rad/s (experimental boundaries on the dynamics of interest), the transfer functions are computed by the method of [54] and both integer- and fractional-order versions of the procedure developed here (with the SQP algorithm). The last of these is the best, given by

$$F(s) = \frac{7}{s^{7/6} + 2s + s^{2/3} + 74s^{1/2} + 0.03}$$

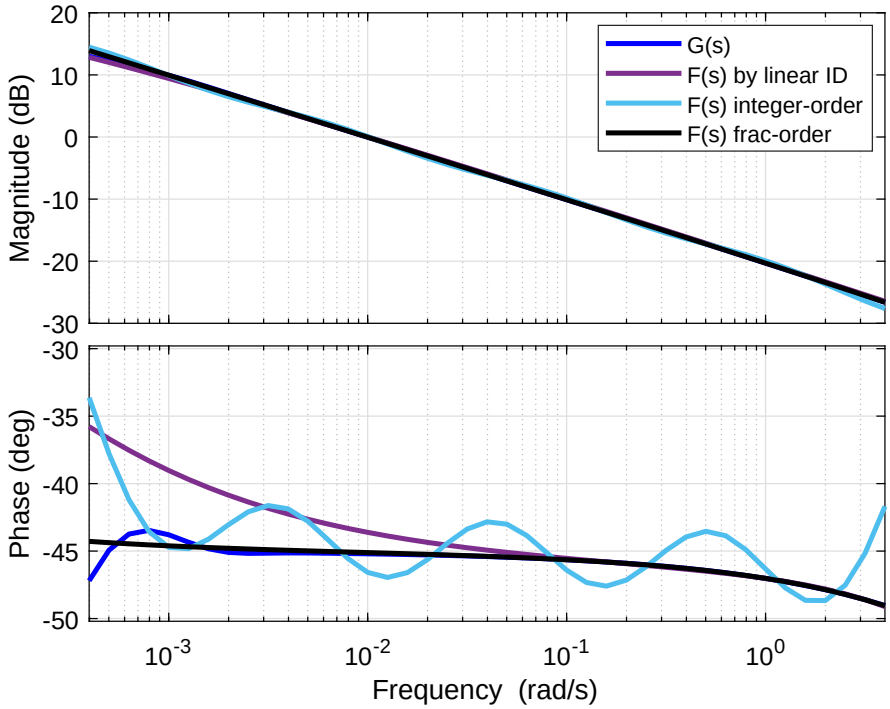

Figure 4.5. Actual and identified frequency responses for undamaged driving formation.

with error $J = 0.3495$. Note that the frequency window is shifted by two powers of 10 to match the shift in k/b (from 1 to 100) and that the error is the same. The comparison of each resulting $F(s)$ to $G(s)$ is shown in Figure 4.5; the same results are shown in [39]. It is clear that order $1/2$ is prominent.

Figure 4.5 shows the advantage of a fractional-order model relative to an integer-order one in accuracy; the optimization is allowed to explore as high as fourth order but returns a relatively poor phase difference match. The figure also shows that the nonlinear objective function of the method developed here ("F(s) frac-order") performs better than the linear one of [54] ("F(s) by linear ID") on the same fractional-order system identification problem.

4.3.2 Coverage Formation

This discussion concerns the undamaged tree system with eight generations of robots, stiffness $k = 2$, and damping $b = 1$. The frequency band of interest is from $10^{-0.8}$ to $10^{1.6}$ rad/s, so with logarithmic spacing by 0.1 powers of 10, $n_{\mathrm{f}} = 25$. With the interior-point algorithm, $F(s)$ is given by

$$F(s) = \frac{8.9 \times 10^8}{s^{13/6} + \cdots + 1.2 \times 10^9 s^{1/2} + 4.1 \times 10^7 s^{1/3} + \cdots + 1.1 \times 10^6}$$

and has error $J = 0.4144$. The SQP algorithm gives

$$F(s) = \frac{562}{s^{11/6} + 11s^{2/3} + 776s^{1/2} + 10}$$

with error $J = 0.3951$. The result from the pattern-search algorithm is identical. Order 1/2 is declared dominant by all three algorithms; this result agrees with the visual interpretation of the frequency response from [38]. However, the degree of prominence bears closer examination. The coefficient of $s^{1/2}$ is over 70 times the next largest before rounding, whereas for the driving formation, that multiplier is about 34. This suggests that the order dynamics are distributed slightly more evenly for the driving formation. In contrast, the coverage formation possesses order 1/2 more exclusively and, as a result, promises to be easier to monitor. The transfer functions $F(s)$ and $G(s)$ are compared in Figure 4.6. The three identified results essentially overlap.

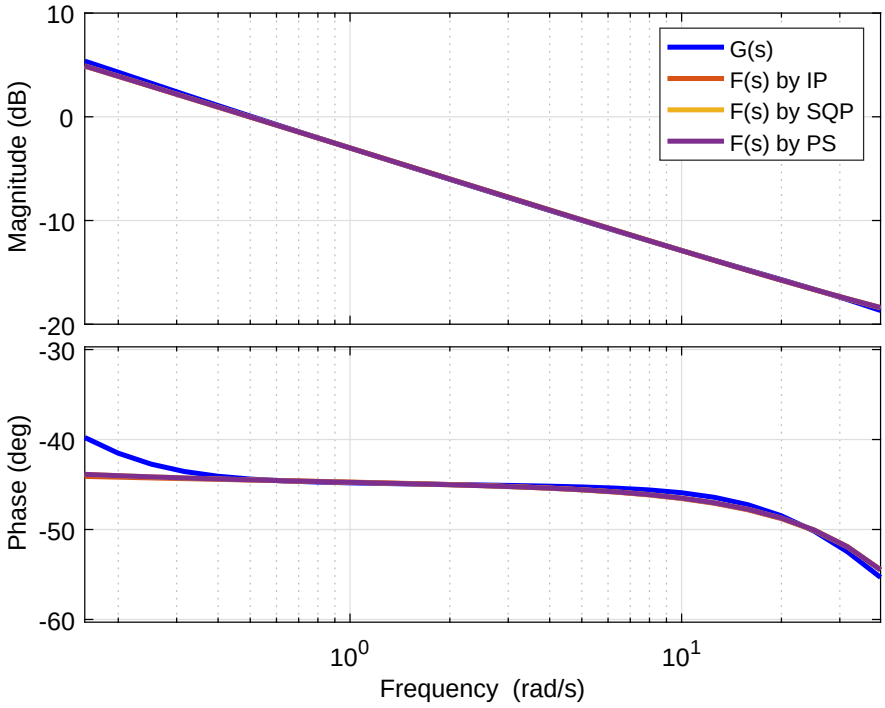

Figure 4.6. Bode plot of actual and identified transfer functions for the undamaged system.

For the system with damage to the first spring ($k_{11} = 0.1k$), and keeping the frequency band of $10^{-0.8}$ to $10^{1.6}$ rad/s, the identified transfer function returned by the interior-point algorithm is

$$F(s) = \frac{3944}{s^{13/6} + \cdots + 2733s^{2/3} + 32s^{1/2} + \cdots + 213}$$

and has error $J = 1.3353$. The SQP algorithm gives

$$F(s) = \frac{3905}{s^{13/6} + 2741s^{2/3} + 225}$$

with error $J = 1.3219$. Here, again, the pattern-search algorithm matches the SQP result. In these results, order 2/3 has the largest coefficient. The frequency responses of $F(s)$ each match the data well and are almost identical to one another, as illustrated in Figure 4.7.

In the case of damage to the first damper ($b_{11} = 0.1b$), with the same frequency band of $10^{-0.8}$ to $10^{1.6}$ rad/s, the optimization result given by the interior-point algorithm is

$$F(s) = \frac{1.4 \times 10^{10}}{s^{13/6} + \cdots + 1.7 \times 10^{8}s^{1/2} + 1.2 \times 10^{10}s^{1/3} + \cdots + 8.3 \times 10^{7}}$$

and has error $J = 0.9541$. The SQP algorithm gives

$$F(s) = \frac{143}{s^{4/3} + s^{7/6} + 130s^{1/3}}$$

with error $J = 0.9120$. To the given precision, the pattern-search result is identical and has the same error. Here, order 1/3 is dominant in each result. The comparison between these frequency responses and the tree formation's is shown in Figure 4.8. As in the previous cases, the three identified results all virtually overlap.

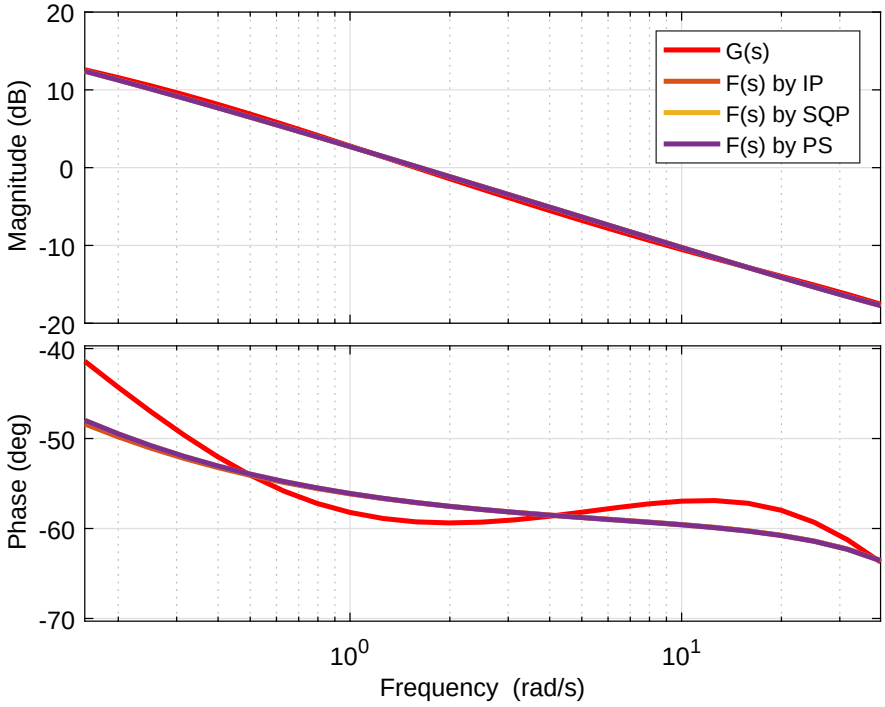

Figure 4.7. Bode plot of actual and identified transfer functions for the spring damage case.

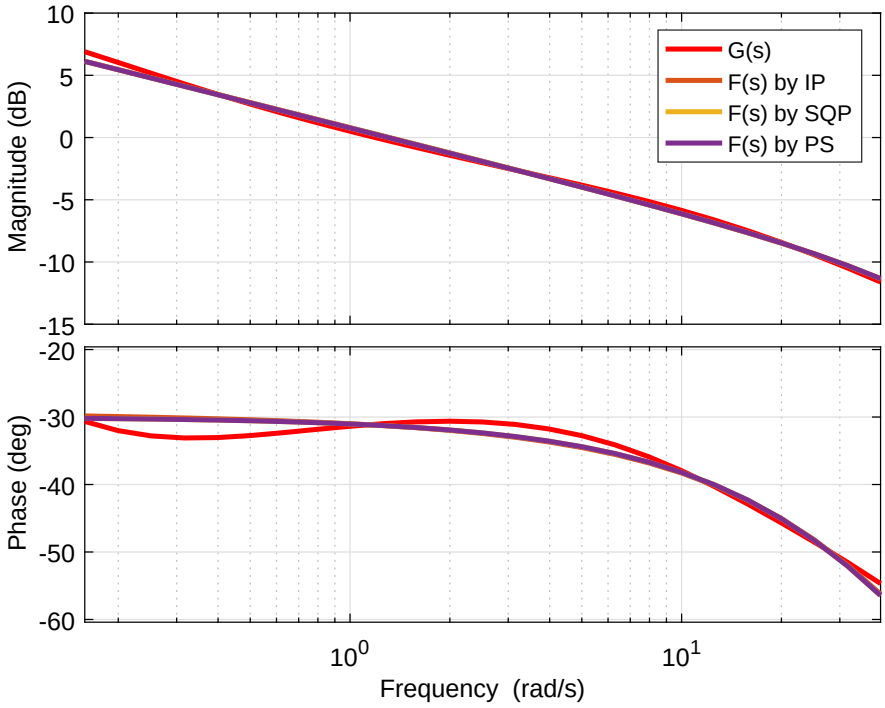

Figure 4.8. Bode plot of actual and identified transfer functions for the damper damage case.

The frequency band used in the identification was chosen experimentally for the purpose of best capturing the dynamics of interest. However, the results are strong enough to suggest robustness to this choice of frequency band; one might choose somewhat different boundaries or alter the frequency resolution and still obtain convincing results.

As can be seen in the Bode plots, the transfer functions $F(j\omega)$ match in magnitude almost exactly with $G(j\omega)$, but the two occasionally disagree by a few degrees in phase. This error may be attributed to the fact that, since the numerator is forced to be constant so as to show the dominant orders, $F(s)$ has no zeros. It follows that nonminimum phase dynamics cannot occur in the results, so the phase curves can only decrease as frequency increases.

The results presented to this point, for both the driving and coverage formations, expose the relative merits of the three algorithms under consideration. The interior-point algorithm is, in theory, the most informative; it gives a coefficient for every order included in the optimization. Consequently, though, the interior-point algorithm performs worse than the others, and upon further examination, the reason is clear. Forcing every order to have a nonzero coefficient constrains the appearance of the resulting frequency response. For example, a perfect match with a theoretical fractional integrator possessing only one order and, in turn, a constant phase difference (e.g. -45 degrees for order $1/2$), is not possible; the other powers of s present in the identified result must manifest themselves, at least at low or high frequencies. The value of comparing the relative prominence of irrelevant orders does not justify proceeding with an inferior algorithm for the identification problem.

In many cases, the SQP and pattern-search algorithms give identical results to a precision several orders of magnitude below the highest coefficient. At times, however, the SQP algorithm performs better and sets itself apart (only one of these cases has appeared so far, but there are others). Therefore, despite the profoundly intuitive

nature and generally effective performance of pattern search, SQP is the algorithm employed for the remainder of the results presented. The possibility of linking the two by choosing the solution from pattern search as the input to SQP has been explored, but this has not provided any additional reduction in the error metric compared to SQP on its own.

4.4 Varied Damage Cases

The value of the proposed monitoring technique depends on the notion that the severity of the damage influences the response of the system. This section demonstrates such a trend for both example systems.

4.4.1 Driving Formation

Consider the dynamics when the driving formation system is damaged; specifically, consider the version of the system with the leftmost spring having a stiffness different from its nominal value. Such a damage case causes a shift in phase difference from -45° toward 0° over a progressively narrower frequency band. This is illustrated in Figure 4.9, from [39], for $k_\mathrm{d} = 10$ and 1 instead of 100.

Another example of interest is the case of a spring-damper pair for which the stiffness and damping change in opposite directions. The challenge posed by a damage case of this nature is that the change in magnitude is nonuniform, but the phase curve is different enough to suggest a dynamical change. This dilemma gives rise to a need for sensitivity in health monitoring. Figure 4.10, from [39], shows the frequency responses when the component constants are changed from $k = 100$ and $b = 1$ to $k_\mathrm{d} = 1$ and $b_\mathrm{d} = 5$ for different spring-damper pairs. The examples of Figures 4.9 and 4.10 demonstrate that the severity and location of damage influence the frequency response in distinct ways.

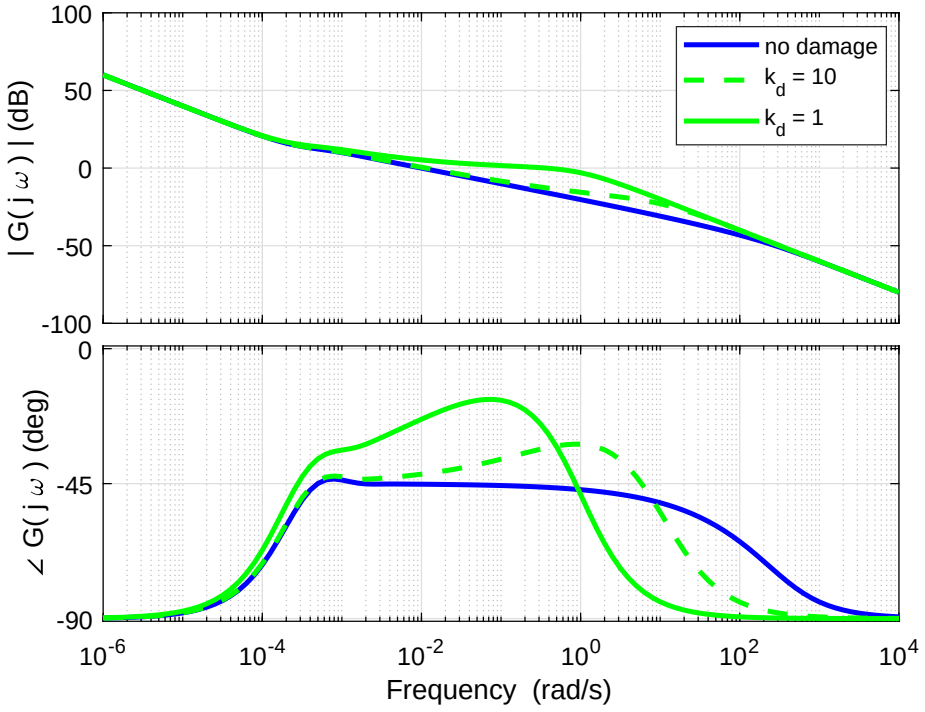

Figure 4.9. Frequency responses for driving formation, including damage cases.

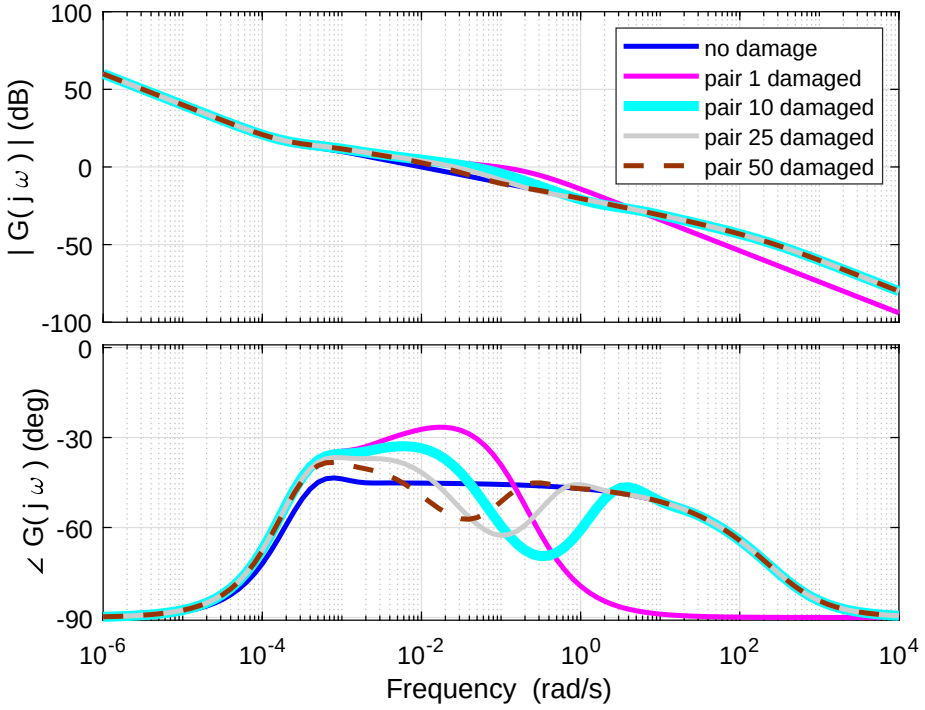

Figure 4.10. Frequency responses for driving formation with reduced stiffness and increased damping applied to different component pairs.

When the first spring is damaged to stiffness $k_{\mathrm{d}} = 10$, the procedure developed in this research gives

$$F(s) = \frac{5}{s^{13/6} + 28s^{1/2} + 8s^{1/3}}$$

with error $J = 5.0464$. This is informative in that it indicates a shift away from order $1/2$, i.e., the coefficient is only a few times greater than that of any other order. However, certainty about the extent of that shift is lacking; the optimization yielding that result examines only orders that are multiples of $1/6$. It is possible to isolate the true order of the system by refining the order resolution, for instance to multiples of 0.01. That result is

$$F(s) = \frac{7}{s^{2.01} + 25s^{0.44} + 19s^{0.43}}$$

with error $J = 4.0609$. It is therefore clear that this version of the system has a dynamical order of about 0.44. Both of these results are displayed in Figure 4.11, from [39].

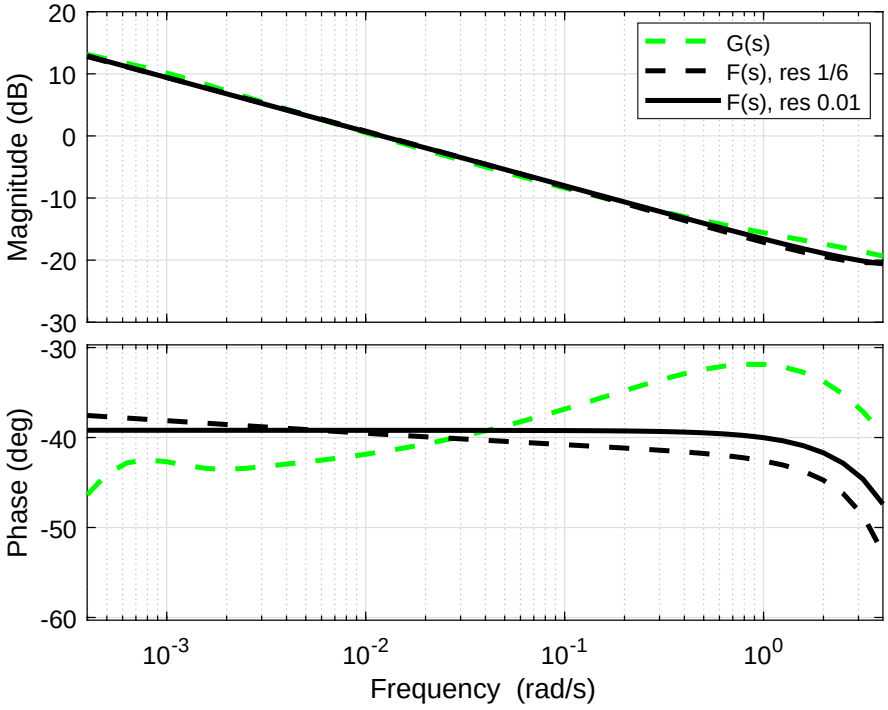

Figure 4.11. Actual and identified frequency responses for driving formation with moderately damaged first spring.

The more severe damage case, with stiffness reduced to $k_{\mathrm{d}} = 1$, initially leads to a transfer function of

$$F(s) = \frac{9.6}{s^{4/3} + 5.7s^{7/6} + 3.2s^{1/3} + 9.3s^{1/6}}$$

with error $J = 6.1085$. These coefficients are relatively close, so while order 1/6 is suggested, the interpretation of this model is not obvious. Refining the order resolution gives

$$F(s) = \frac{3.9}{s^{1.25} + 1.6s^{1.24} + 5.5s^{0.22}}$$

with error $J = 5.6145$. This result offers more clarity by showing the most prominent order to be 0.22. If the potential control strategy permits, recognizing some dynamics of approximate order 1.24 may be beneficial; however, this identification is primarily meant to determine one order. The frequency responses for these two transfer functions are plotted in Figure 4.12, from [39].

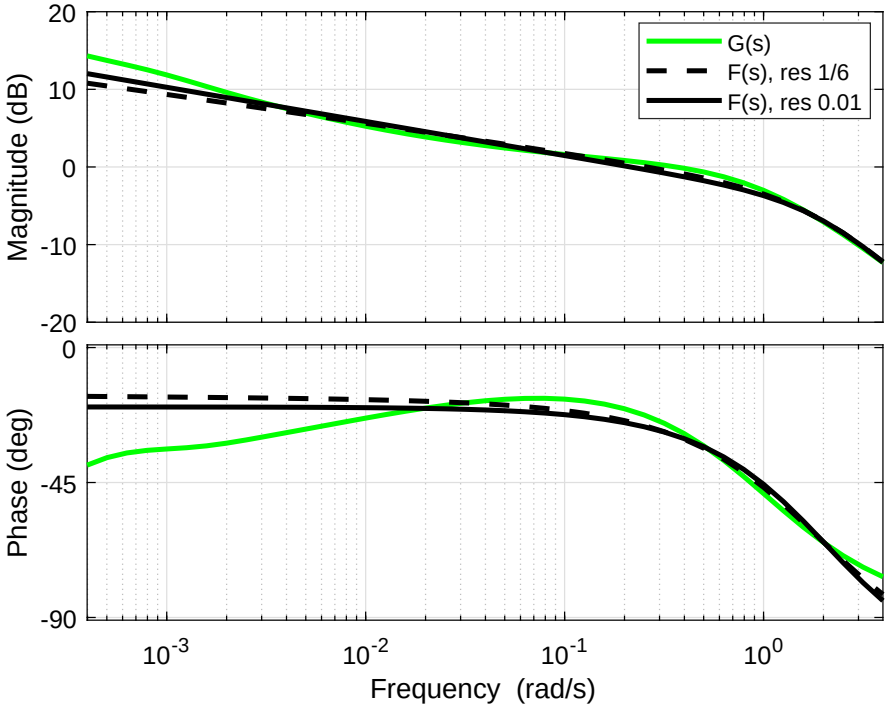

Figure 4.12. Actual and identified frequency responses for driving formation with severely damaged first spring.

The case of magnitude-invariant damage to the leftmost spring-damper pair, as shown in Figure 4.10, returns a transfer function of

$$F(s) = \frac{0.2}{s^{7/6} + 0.5s^{1/3} + 0.06s^{1/6}}$$

with error $J = 4.2034$. Damage to the 10th spring-damper pair yields

$$F(s) = \frac{0.2}{s + 0.8s^{5/6} + 0.4s^{1/3} + 0.03s^{1/6}}$$

with error $J = 6.6344$. Damage to the 25th spring-damper pair yields

$$F(s) = \frac{0.1}{s^{2/3} + 0.2s^{1/2} + 0.05s^{1/6}}$$

with error $J = 5.9051$. Damage to the 50th pair yields

$$F(s) = \frac{0.2}{s^{2/3} + 1.4s^{1/2} + 0.01}$$

with error $J = 4.4924$. Even with an order resolution of 1/6, an order shift based on damage location is clear. At first there are identified dynamics of approximate orders 7/6 and 1/3, but as damage locations farther from the force application point are considered, the higher order tends toward 1/2, while the lower one vanishes. This trend is seen more clearly with order resolution 0.01. In the four cases discussed here, the prominent orders are 1.12 and 0.28 ($J = 3.7987$), 0.90 and 0.29 ($J = 6.3637$), 0.62 only ($J = 5.8139$), and 0.56 only ($J = 4.0329$).

The presence of a measurable order shift reveals the potential utility of the foregoing identification procedure in system monitoring. The damage cases of Figure 4.10 are exactly alike, and they have only small effects on the magnitude of the response. The only unique characteristic among them is the damage location, so it is promising

that the identification procedure of this research is able to conclude that they have distinct fractional orders. These results suggest that it is possible to locate damage, a valuable feature in a monitoring tool for complex systems.

4.4.2 Coverage Formation

This subsection examines the effects of variations in the damage introduced into the coverage formation system and the resulting set of system identification results. These studies aid in understanding the manner in which the order shifts from 1/2 to 1/3 or 2/3 as the damage becomes greater, as well as what happens when it is more severe than the heretofore assumed reduction by a factor of 10 in stiffness or damping.

For consistency with the preceding discussions, the formation has eight layers of robots and constants $k = 2$ and $b = 1$. Damage to the leftmost spring is considered first. Figure 4.13 shows the effects of two moderate damages alongside the two reference curves from Chapter 3, specifically Figure 3.13. As is perhaps to be expected, the curves for 50 and 25 percent stiffness generally fall between those of the original case and that of 10 percent stiffness. However, the phase curves do not settle at one phase over the medium-frequency band to the obvious extent that the others do.

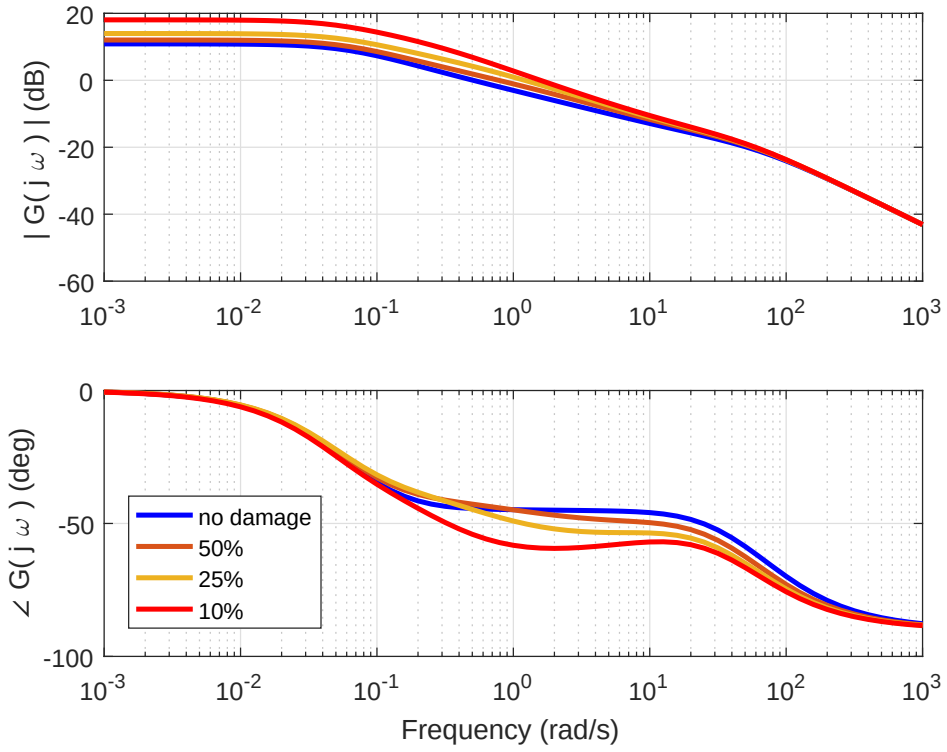

Figure 4.13. Effects of somewhat reduced stiffness labeled by percentage retained in leftmost spring.

Recall that the identification result for the undamaged system over the window of $10^{-0.8}$ to $10^{1.6}$ rad/s is

$$F(s) = \frac{562}{s^{11/6} + 11s^{2/3} + 776s^{1/2} + 10}$$

with error $J = 0.3951$. The case of 50 percent stiffness returns

$$F(s) = \frac{1664}{s^2 + 0.5s^{11/6} + 524s^{2/3} + 1245s^{1/2} + 189}$$

with error $J = 0.2143$. The case of 25 percent stiffness returns

$$F(s) = \frac{2852}{s^{13/6} + 1717s^{2/3} + 618s^{1/2} + 400}$$

with error $J = 0.4752$. The case of 10 percent stiffness returns the result from the last section:

$$F(s) = \frac{3905}{s^{13/6} + 2741s^{2/3} + 225}$$

with error $J = 1.3219$. Taken together, these transfer functions resulting from the identification procedure show the gradual shift in order from 1/2 to 2/3. The identification results are shown alongside the original curves over the frequency window of interest in Figure 4.14.

Frequency responses with more severe damage to the spring are shown in Figure 4.15. The original and 10-percent cases are shown as well, for comparison. The lower-frequency behavior changes drastically with the order of magnitude of the damage; however, the phase difference resurfaces to roughly -60 degrees in each case. These responses lend some support to the notion that the order shifts from 1/2 to 2/3 as a result of sufficiently severe damage.

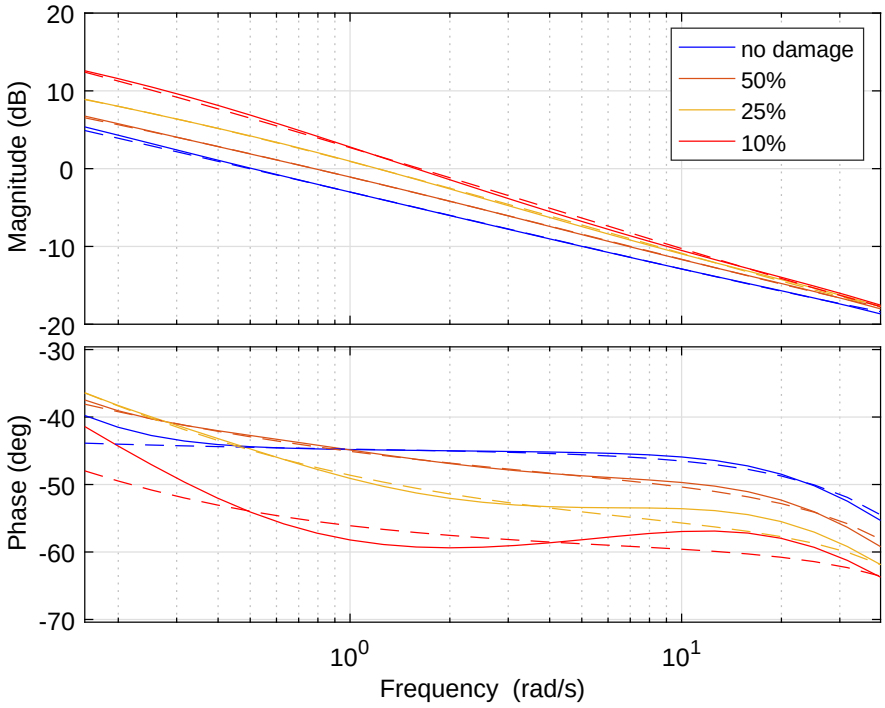

Figure 4.14. Identification results for somewhat reduced stiffness shown by dashed lines and compared with full system results.

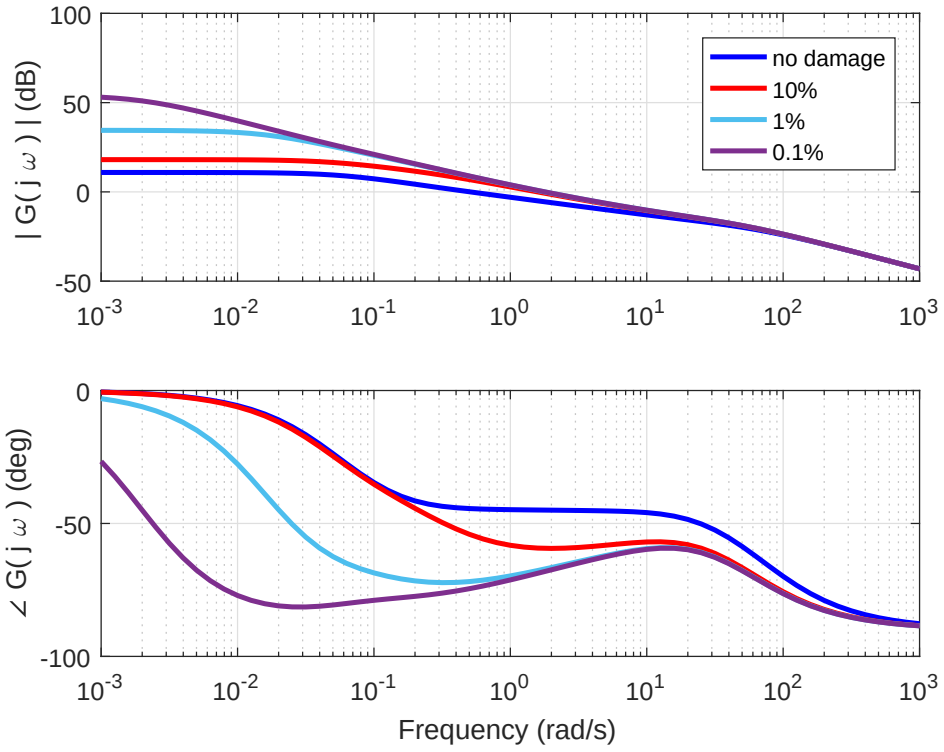

Figure 4.15. Effects of greatly reduced stiffness labeled by percentage retained in leftmost spring.

For purposes of following the progression, it bears repeating that the undamaged system has

$$F(s) = \frac{562}{s^{11/6} + 11s^{2/3} + 776s^{1/2} + 10}$$

with error $J = 0.3951$, while the system with 10 percent stiffness in the leftmost spring has

$$F(s) = \frac{3905}{s^{13/6} + 2741s^{2/3} + 225}$$

with error $J = 1.3219$. Reducing the stiffness to 1 percent gives

$$F(s) = \frac{25799}{s^{13/6} + 4015s^{5/6} + 12409s^{2/3}}$$

with error $J = 3.1295$. Reducing it further, to 0.1 percent, gives

$$F(s) = \frac{19564}{s^{13/6} + 3180s^{5/6} + 9251s^{2/3}}$$

with error $J = 3.6128$. The last two of these are similar. The ratio of dominance for order 2/3 in the case of 1 percent stiffness is 3.1 (12409/4015), while the same ratio in the case of 0.1 percent stiffness is 2.9 (9251/3180). This means that, while the trend of increasing order diminishes substantially, it does continue; the case of 0.1 percent stiffness exhibits more 5/6-order behavior than the other, though the overall behavior still more strongly suggests order 2/3. The limiting case of $k = 0$ also has its largest coefficient corresponding to order 2/3 and is nearly identical to the case of 0.1 percent stiffness. The identification results are shown in Figure 4.16; for visual clarity, the case of $k = 0$ is omitted.

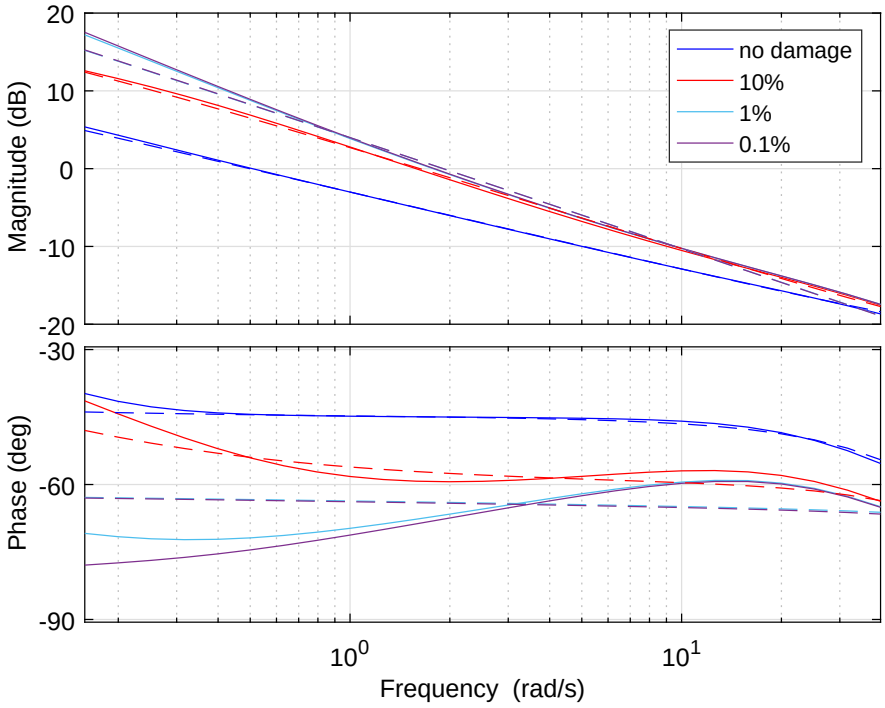

Figure 4.16. Identification results for greatly reduced stiffness shown by dashed lines and compared with full system results.

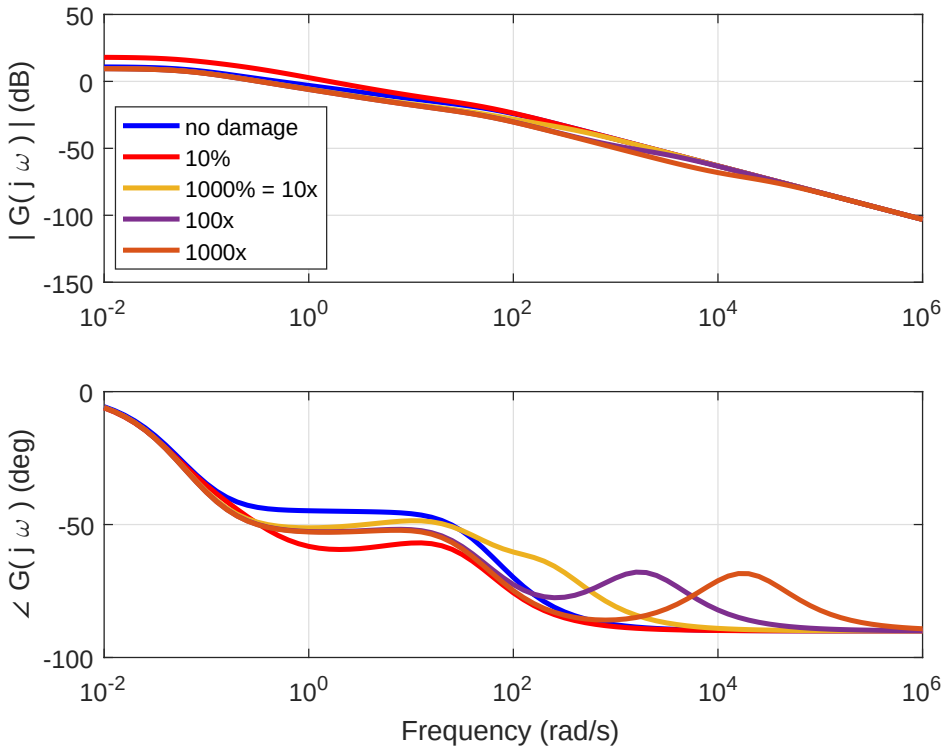

Figure 4.17. Effects of increased stiffness in leftmost spring.

One may also consider a damage case that is opposite to the preceding ones, that is, with k increasing instead of decreasing. Perhaps surprisingly, there is still an order shift upward, though not all the way to 2/3; this is illustrated in Figure 4.17. The frequency window is different from those in the other figures so that the high-frequency trend may be shown. The nature of this result is explained by the magnitude plot; there is less transmission of force through the system than in the original and weakened (k reduced by a factor of 10) cases. In other words, this may be likened to a different damage case in which all springs *except* the leftmost are reduced by a factor of 10 or more. From that perspective, a result different in appearance from the others is to be expected.

The undamaged system remains a worthwhile point of comparison; its identified

transfer function is

$$F(s) = \frac{562}{s^{11/6} + 11s^{2/3} + 776s^{1/2} + 10}$$

with error $J = 0.3951$. The case of k increased by a factor of 10 returns

$$F(s) = \frac{2667}{s^{13/6} + 1515s^{2/3} + 3616s^{1/2}}$$

with error $J = 1.1187$. The case of k increased by a factor of 100 returns

$$F(s) = \frac{1149}{s^{13/6} + 1067s^{2/3} + 1234s^{1/2}}$$

with error $J = 0.8466$. The case of k increased by a factor of 1000 returns

$$F(s) = \frac{1051}{s^{13/6} + 1031s^{2/3} + 1077s^{1/2} + 7}$$

with error $J = 0.8260$. These are shown alongside the full system results in Figure 4.18. In the cases of 100 and 1000 times the original stiffness, the resulting coefficients for orders 1/2 and 2/3 are close. The only interpretation permissible by the given order resolution, sixths of orders, is that both orders are present in the system. However, it is possible that the system has behavior suggestive of one specific order between 1/2 and 2/3. Varying the optimization settings could confirm this.

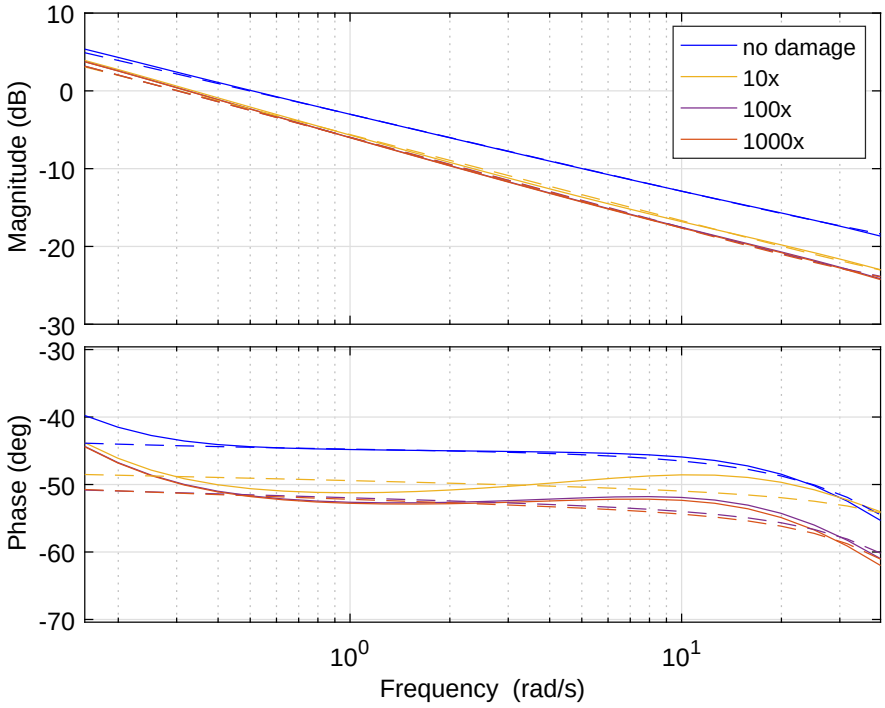

Figure 4.18. Identification results for increased stiffness shown by dashed lines and compared with full system results.

Following are the analogous cases for the leftmost damper. The effects of less severe damage than by a factor of 10 are shown in Figure 4.19. In a sense, this mirrors Figure 4.13, and that is consistent with intuition as it relates to order shifting. The progression of transfer functions begins again with the undamaged system:

$$F(s) = \frac{562}{s^{11/6} + 11s^{2/3} + 776s^{1/2} + 10}$$

with error $J = 0.3951$. In the case of 50 percent damping,

$$F(s) = \frac{13694}{s^2 + 7s^{11/6} + 149s^{7/6} + 236s + 13550s^{1/2} + 1516s^{1/3} + 1023}$$

with error $J = 0.2376$. In the case of 25 percent damping,

$$F(s) = \frac{60}{s^{7/6} + 2s + 19s^{1/2} + 41s^{1/3}}$$

with error $J = 0.4159$. In the case of 10 percent damping, the identified transfer function is as previously given:

$$F(s) = \frac{143}{s^{4/3} + s^{7/6} + 130s^{1/3}}$$

with error $J = 0.9120$. Figure 4.20 shows these identification results and the computed frequency responses over the window of interest. The order shift from 1/2 to 1/3 is evident by examining the coefficients.

Conversely, the frequency responses corresponding to more severe damage are displayed in Figure 4.21. It is previously demonstrated that each phase curve reflecting greatly reduced stiffness tends toward the characteristic -60 degrees for medium-high frequencies in Figure 4.15. Correspondingly, each phase curve reflecting greatly reduced damping tends toward -30 degrees for medium-low frequencies.

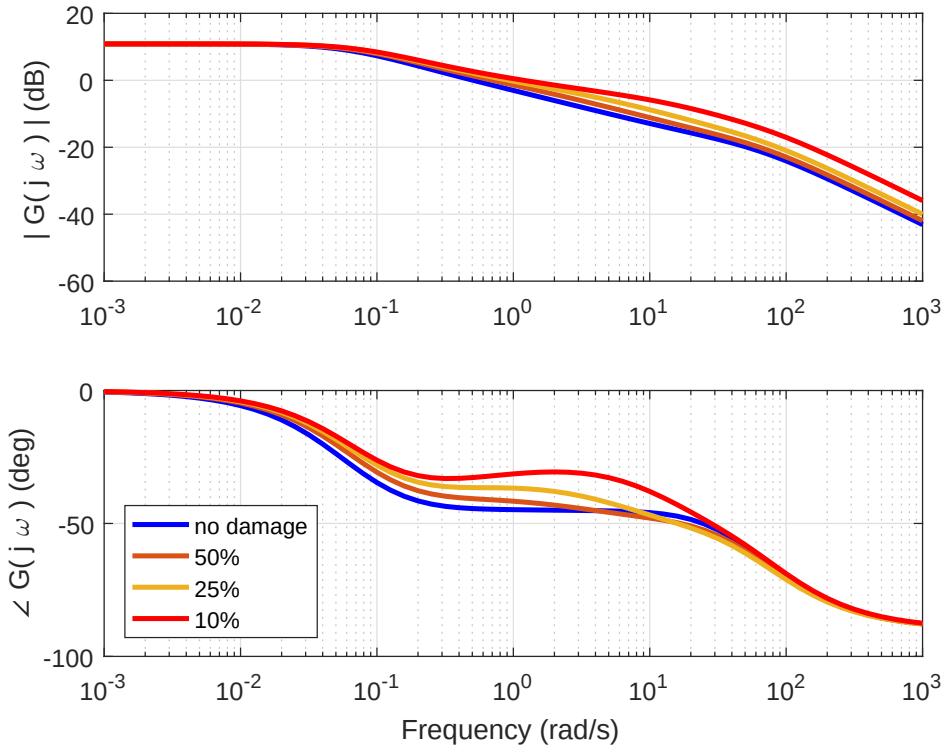

Figure 4.19. Effects of somewhat reduced damping labeled by percentage retained in leftmost damper.

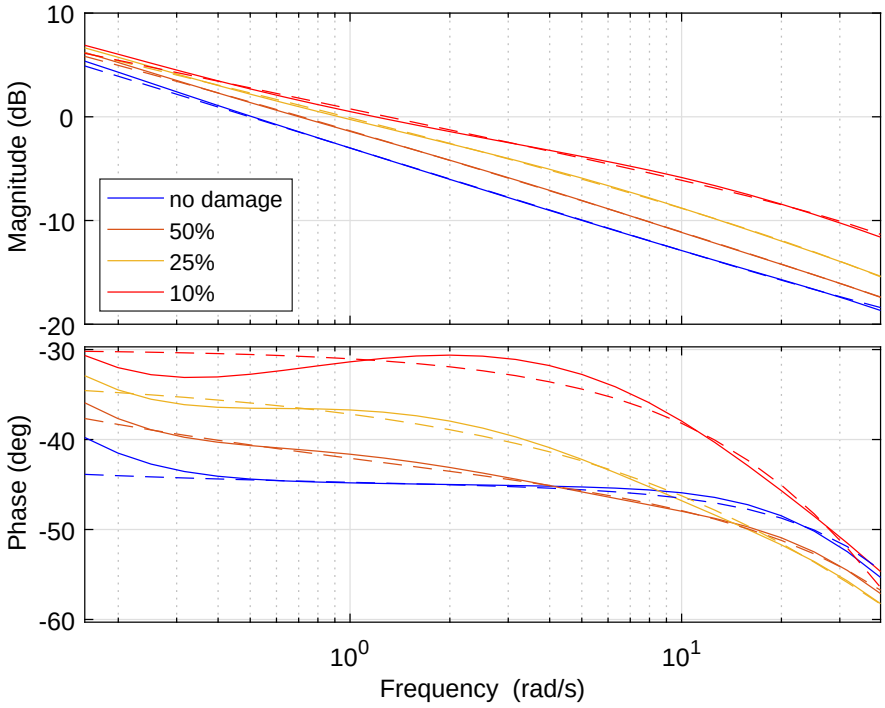

Figure 4.20. Identification results for somewhat reduced damping shown by dashed lines and compared with full system results.

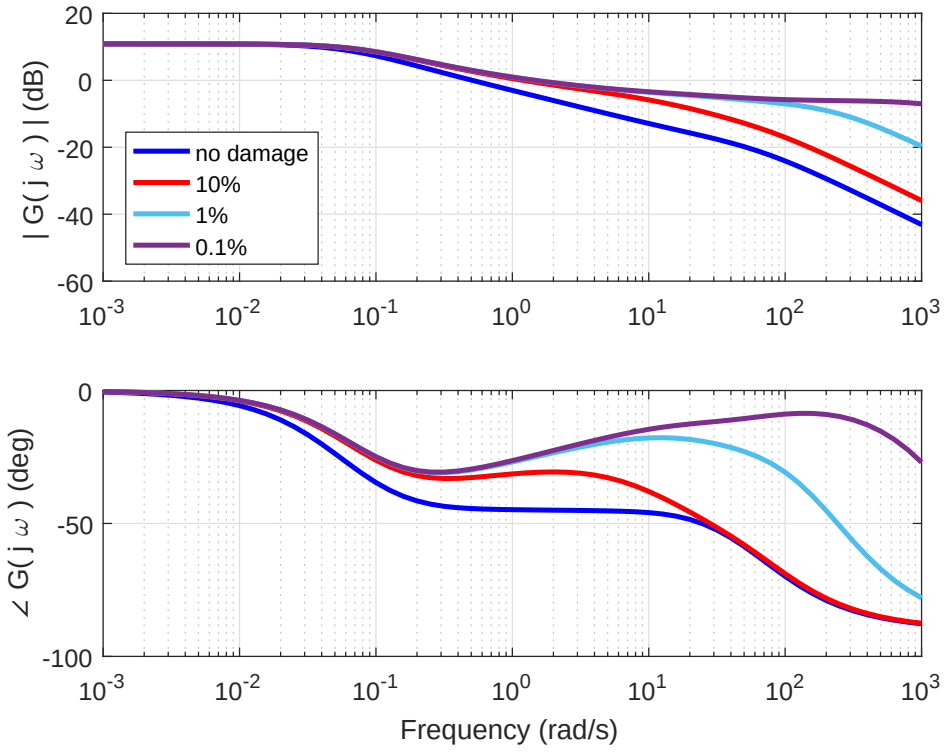

Figure 4.21. Effects of greatly reduced damping labeled by percentage retained in leftmost damper.

The identified transfer functions for the undamaged system,

$$F(s) = \frac{562}{s^{11/6} + 11s^{2/3} + 776s^{1/2} + 10}$$

with error $J = 0.3951$, and that with 10 percent damping in the leftmost damper,

$$F(s) = \frac{143}{s^{4/3} + s^{7/6} + 130s^{1/3}}$$

with error $J = 0.9120$, are as before. The result for 1 percent damping is

$$F(s) = \frac{7497}{s^{13/6} + 2914s^{1/3} + 3800s^{1/6}}$$

with error $J = 2.8539$. The result for 0.1 percent damping is

$$F(s) = \frac{8932}{s^{13/6} + 2974s^{1/3} + 5070s^{1/6}}$$

with error $J = 3.6457$. The result for $b_d = 0$ is similar in substance and is omitted. As in the other damage examples, a progression is apparent. The fact that the two cases of greatest damage yield 1/6-order, instead of 1/3-order, behavior is not consistent with the stiffness example, which possesses order 2/3 in the limiting case. Admittedly, these cases with increasing phase difference are challenging for the optimization in its current configuration, by which it is constrained to prevent nonminimum phase in its results for the sake of clear interpretation. This challenge is evident in the differences between the original and identified frequency responses in Figure 4.22.

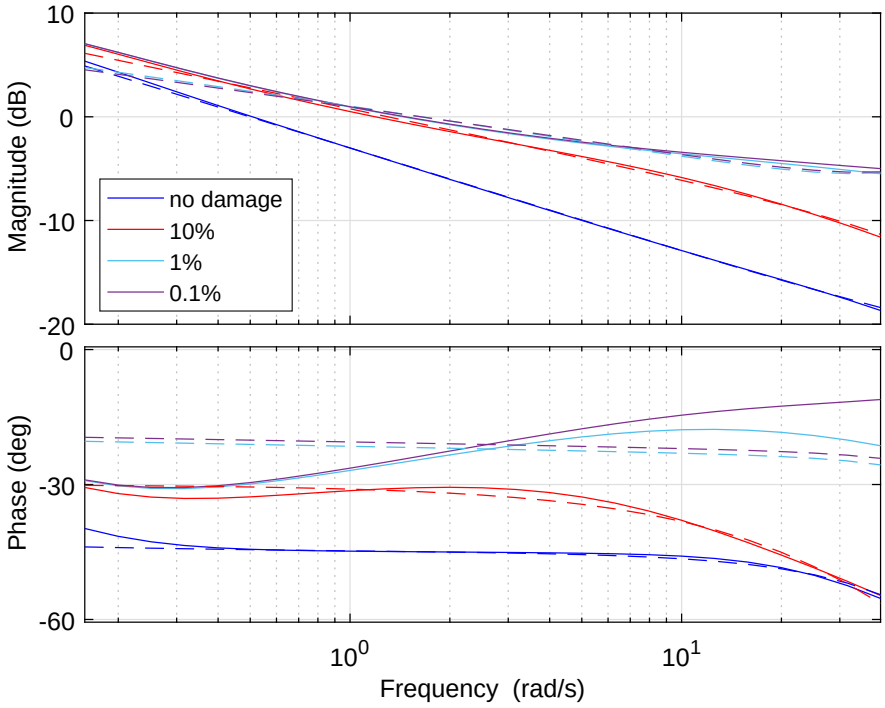

Figure 4.22. Identification results for greatly reduced damping shown by dashed lines and compared with full system results.

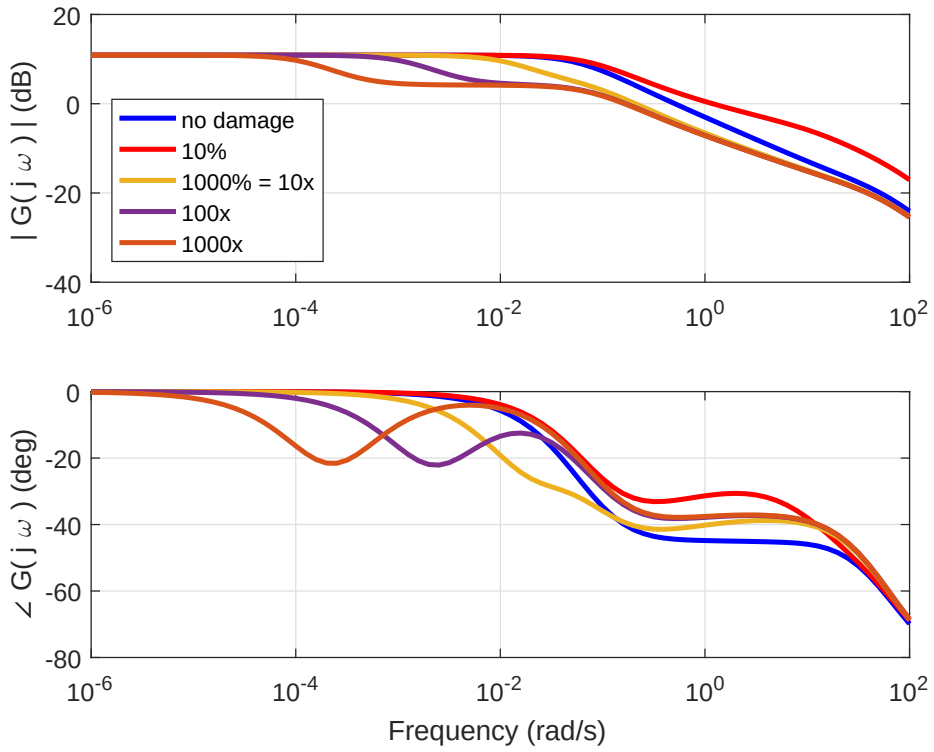

Figure 4.23. Effects of increased damping in leftmost damper.

Increasing the damping in the leftmost damper yields the responses shown in Figure 4.23. For purposes of visibility, the frequency window differs from those in the other figures. The phase difference behavior is analogous to that shown in Figure 4.17. The magnitude curves are certainly more distinct from one another than those resulting from increased stiffness, but there is no conceptual difference to be noted; the magnitude and phase curves are inextricably linked, and the magnitudes are simply following the trajectories they must as functions of frequency in order to possess the appropriate slopes.

Naturally, this progression of transfer functions begins with that for the undamaged system:

$$F(s) = \frac{562}{s^{11/6} + 11s^{2/3} + 776s^{1/2} + 10}$$

with error $J = 0.3951$. Increasing the damping by a factor of 10 gives

$$F(s) = \frac{1717}{s^2 + 3s^{11/6} + 2232s^{1/2} + 1376s^{1/3}}$$

with error $J = 0.9501$. Increasing it instead by a factor of 100 gives

$$F(s) = \frac{447}{s^{11/6} + 0.5s^{5/3} + 481s^{1/2} + 523s^{1/3}}$$

with error $J = 0.7184$. Increasing it instead by a factor of 1000 gives

$$F(s) = \frac{553}{s^{11/6} + s^{5/3} + 578s^{1/2} + 676s^{1/3}}$$

with error $J = 0.6984$. The last two cases are similar in coefficient ratio of orders $1/3$ and $1/2$, and those frequency responses follow each other closely in the comparison plot, Figure 4.24. Within the chosen frequency window, there is little to distinguish those two damage cases from each other. The value of this response as a monitoring result, then, is to say that the new damping exceeds some threshold close to 100 times the original damping. The drop in magnitude distinguishes such a case from a decrease in damping that might produce a similar phase difference curve.

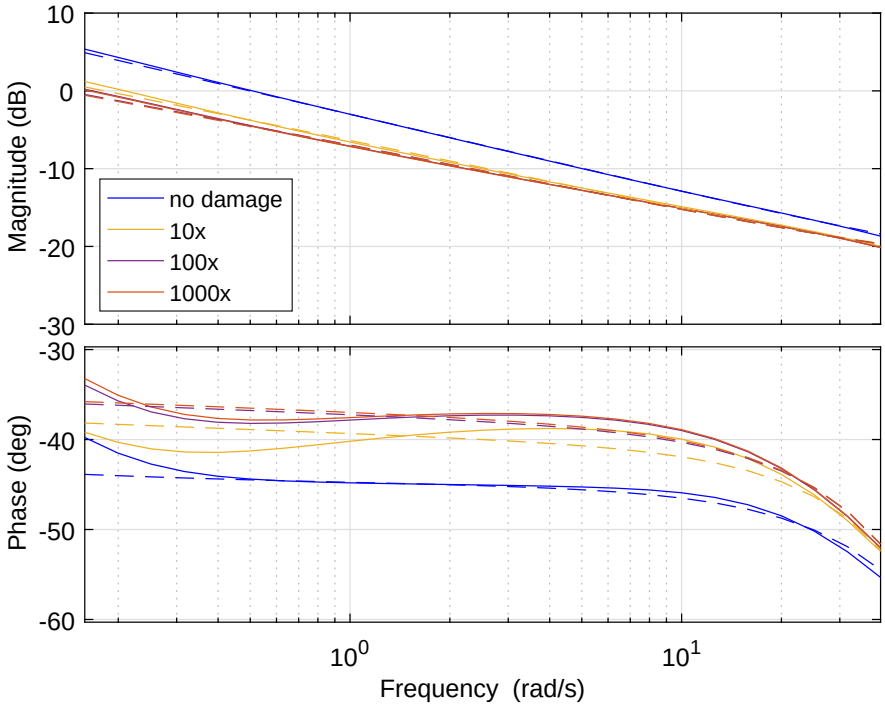

Figure 4.24. Identification results for increased damping shown by dashed lines and compared with full system results.

In the remainder of this section, to promote the idea that this identification procedure can be used in conjunction with physical data collection, the frequency resolution is cut roughly in half. The constants are still $k = 2$ and $b = 1$, but the frequency window contains $n_{\mathrm{f}} = 13$ frequencies from 10^{-2} to 10^{2} rad/s, a deliberately generic choice. Figure 4.25, from [39], shows a comparison between the frequency responses of a damaged system ($k_1 = k_{\mathrm{d}} = 0.1k$) and its identified model. Orders corresponding to other damage cases are discussed later in this section, but in this case, the identified model is

$$F(s) = \frac{5972}{s^{13/6} + 833s^{5/6} + 3044s^{2/3} + 613}$$

with error $J = 0.9888$.

Figure 4.26, from [39], is analogous for $b_1 = b_{\mathrm{d}} = 0.1b$. The identified model is

$$F(s) = \frac{175}{s^{4/3} + s^{7/6} + 47s^{1/2} + 83s^{1/3} + 27}$$

with error $J = 1.2686$. In both Figures 4.25 and 4.26, it is seen that the identified transfer functions match well with the true transfer functions of the damaged systems.

Figures 4.27 and 4.28, both from [39], display the most comprehensive results. The ratio of each denominator coefficient to the sum of those for all orders, called the coefficient share, is shown for all cases examined in this study representing varied stiffness from $k_{\mathrm{d}} = 2 \times 10^{-5}$ to 2×10^{4} (Figure 4.27) and varied damping from $b_{\mathrm{d}} = 10^{-5}$ to 10^{4} (Figure 4.28). The quantities k_{d}/k and b_{d}/b represent the severity of damage. For each choice of k_{d}/k or b_{d}/b, the coefficient share across all orders has a sum of 1.

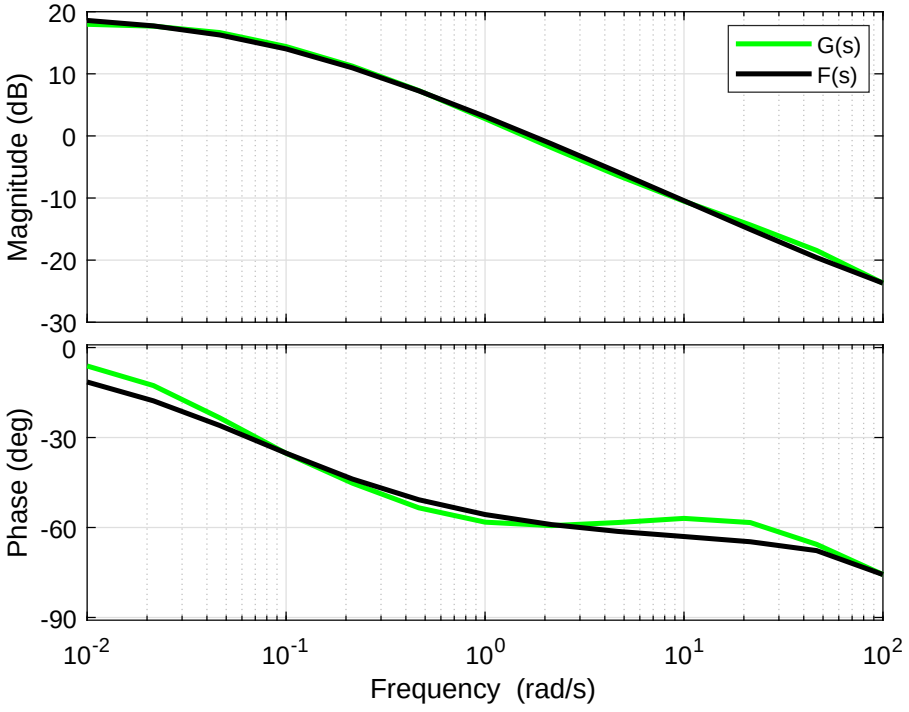

Figure 4.25. Low-density frequency responses for coverage formation with damaged first spring.

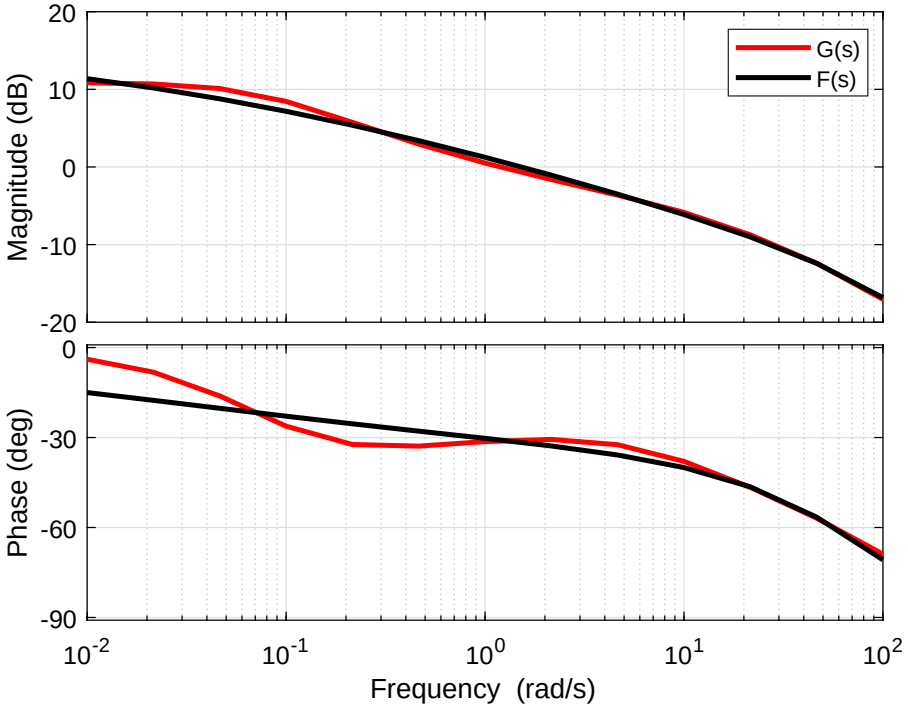

Figure 4.26. Low-density frequency responses for coverage formation with damaged first damper.

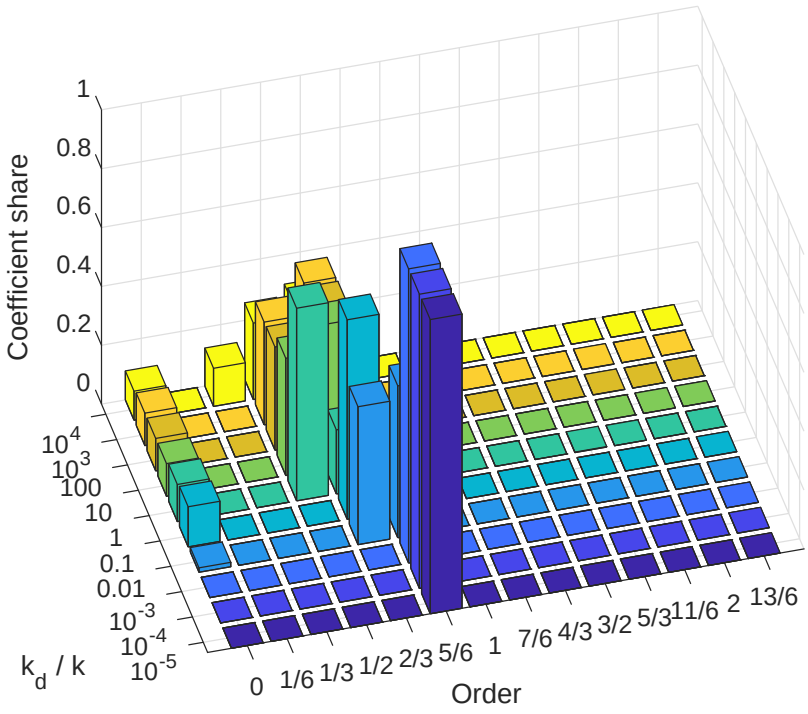

Figure 4.27. Identified orders for coverage formation with damaged spring.

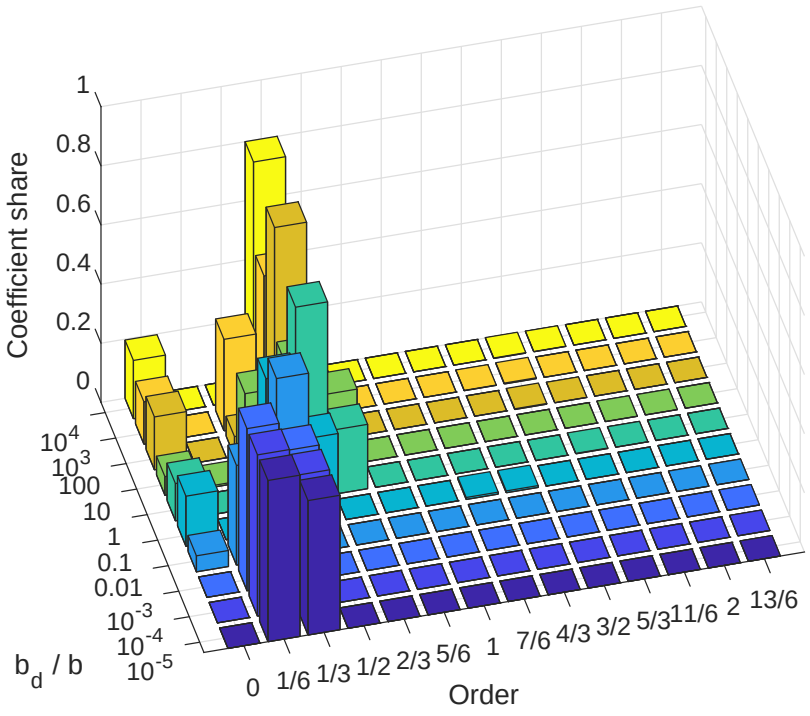

Figure 4.28. Identified orders for coverage formation with damaged damper.

The results of Figures 4.27 and 4.28 show that dynamical order follows a clear trend with respect to the severity of damage that has occurred. In the case of the damaged spring (Figure 4.27), the most severe damage case, i.e., the smallest value of k_1, suggests an order of 5/6. An order of 5/6 implies a magnitude slope of -16.7 dB/dec and phase difference of $-75°$, so that result aligns well with expectation from the analogous infinite systems with responses shown in Figure 3.19. For $k_1 = 0.1k$, the system is identified as 2/3-order; the undamaged system having $k_1 = k$ is seen to possess order 1/2. These results are consistent with Figures 4.6 and 4.7 despite different frequency window boundaries. In cases where k_1 increases, the system is best modeled with terms of orders 1/2 and 2/3. This is a reasonable result; increasing stiffness is not the same as changing the degree of reduced stiffness, so the pattern seen with reduced stiffness is not necessarily supposed to continue.

When damage is instead applied to the damper (Figure 4.28), the most severe damage case, i.e., the smallest value of b_1, suggests an order of 1/6 with some 1/3-order behavior as well. The corresponding magnitude slope of -3.3 dB/dec and phase difference of $-15°$ make sense with respect to the infinite systems of Figure 3.20. For $b_1 = 0.1b$ and $b_1 = b$, the system is respectively 1/3-order and 1/2-order. The former is consistent with Figure 4.8 despite the frequency window change; the latter is the same system as $k_1 = k$ in Figure 4.27, so the bars are the same. When b_1 increases, the identified model features both 1/2-order and 1/3-order terms prominently. As in the discussion of varying stiffness, those results are not expected to be part of the order trend from the reduced damping cases.

It is clear that, from the undamaged system of order 1/2, reduced stiffness in the leftmost spring drives the overall order toward 5/6, while reduced damping in the leftmost damper drives it toward 1/6. From these results, it can be asserted that a monitoring method that tracks the fractional order of some relationship of interest within a complex system has potential utility *in diagnosing the mechanical*

or operational change the system has experienced.

While the order trends clearly evolve in opposite directions for reduced stiffness and damping, they do not quite evolve at the same rate. Severely reduced stiffness implies that the system's order clearly shifts to 5/6, but severely reduced damping does not bring about order 1/6 to the same extent; a notable term of order 1/3 is still present. This asymmetry is a topic of interest for future inquiries.

This study has only introduced stiffness and damping variations in the first layer of the coverage formation. While the results presented here are not exhaustive, their applicability is extended when the analogy to an infinite formation is recalled. In that context, as mentioned previously, there is self-similarity; each node has a replica of the overall formation attached to it. It can also be recalled from, e.g., Figure 3.10, that as layers are added to the finite formation, the convergence of its behavior to that suggested by the fractional-order model of the infinite formation occurs in five to ten generations (for the foregoing parameter choices). Therefore, the findings presented in this discussion can fit neatly into analysis of damage cases within the first layer or any after roughly the fifth. This is because, in the latter case, it is possible to view the damaged system as an arrangement of series and parallel combinations of subsystems, i.e., replicas of the undamaged formation having order 1/2 (or of damaged formations having other orders) connected by other components. With regard to layers two to five, the same treatment is viable, though there may be no simplifying model for the first few layers ahead of the damage location.

Each of the instances of varied damage produces the expected trend. The identification procedure is able to capture this trend in computational terms, indicating the relative dominance of each of the dynamical orders considered in the optimization. However, the effects of different choices of those orders, though subtle, can influence the interpretation suggested by the optimization results.

4.5 Order Resolution Study

In the discussion of the damage case of increasing stiffness, it is hinted that the conclusion that the coverage formation system has behavior reflecting two orders roughly equally may not be the best description. Rather, after optimizing with order steps of 1/6, the possibility remains that a different resolution may return one prominent order, presumably between 1/2 and 2/3 in the case of increasing stiffness. This section considers variation of the choices of order in the optimization and the ensuing changes in the resulting transfer functions.

The preceding section shows results containing the orders $0, 1/6, \ldots, 13/6$. For consistency, it is not feasible to preserve 13/6 as the upper bound; 13/6 is not an integer multiple of any convenient order increment except 1/12, 1/18, and so on, for a strained definition of "convenient." To display a more reasonable set of resolutions, then, the upper bound is set at 2.

These results pertain to the system with 100 times the original stiffness in the leftmost spring. This scenario is introduced in the discussion containing Figure 4.17; there are eight layers of robots, $k = 2$, $b = 1$, and the frequency window contains 25 frequencies evenly spaced on a logarithmic scale from $10^{-0.8}$ to $10^{1.6}$ rad/s. When the order resolution is 1/4, the identified transfer function is

$$F(s) = \frac{902}{s^2 + 468s^{3/4} + 1342s^{1/2}},$$

and the error $J = 1.1331$. When the resolution is 1/6,

$$F(s) = \frac{711}{s^2 + 636s^{2/3} + 787s^{1/2}}$$

with error $J = 0.8844$. When the resolution is $1/8$,

$$F(s) = \frac{662}{s^2 + 837s^{5/8} + 479s^{1/2} + 6}$$

with error $J = 0.8061$. When the resolution is $1/10$,

$$F(s) = \frac{710}{s^2 + 363s^{7/10} + 478s^{3/5} + 399s^{1/2} + 180s^{2/5}}$$

with error $J = 0.9505$. When the resolution is $1/12$,

$$F(s) = \frac{618}{s^2 + 37s^{2/3} + 1181s^{7/12} + 19}$$

with error $J = 0.7489$. When the resolution is 0.01,

$$F(s) = \frac{617}{s^2 + 897s^{0.59} + 315s^{0.58} + 22}$$

with error $J = 0.7444$. Some of these curves are shown in Figure 4.29. Resolutions $1/6$, $1/8$, and $1/12$ are omitted from the figure for visual clarity; those three follow the curve for resolution 0.01 almost perfectly. Resolutions $1/4$ and $1/10$ give slightly less accurate results, and that additional error is sufficient to render those curves visible in the plot.

The observations emerging from these results are diverse and, as such, indicative of the inconclusiveness of a single choice of order resolution for this optimization problem. There is only a loose error trend downward as the order is resolved more finely; for example, resolutions $1/14$ and $1/16$ have more error than $1/12$, though less than $1/8$. Furthermore, isolating the prevailing order does not necessarily become easier as the number of orders in the computation increases. Here, orders 0.58 and 0.59 both appear prominent when the resolution is 0.01. It is reasonable to declare

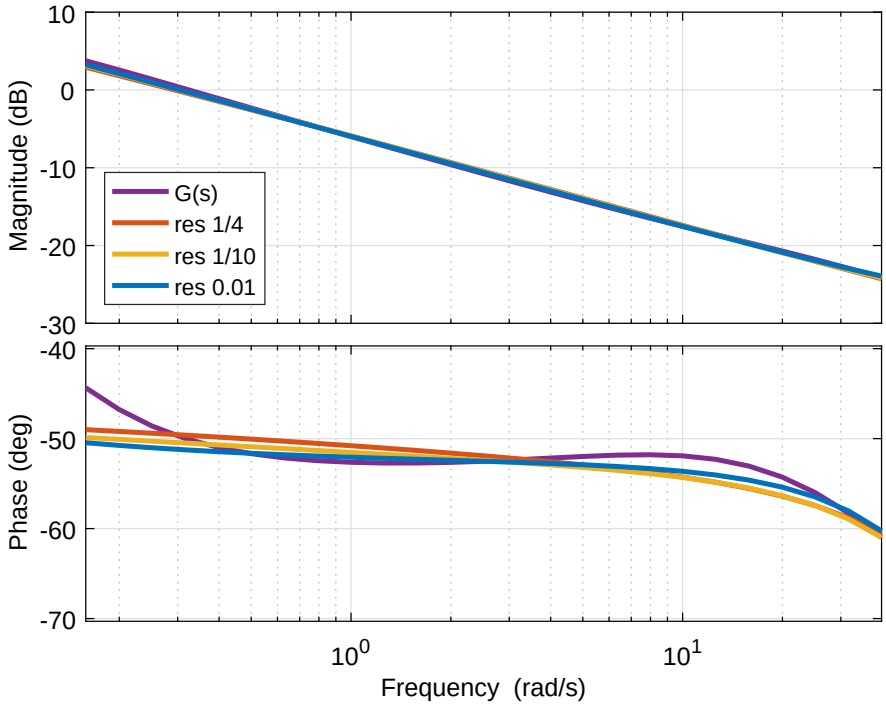

Figure 4.29. Identification results for one case of increased stiffness with varied order resolution.

the true order to be 0.59, but the most dominant order in this set of trials is 7/12, or 0.5833. Overall, though, every error is small enough to make the corresponding magnitude curve nearly interchangeable with the full system's frequency response.

This chapter has presented an identification method for fractional-order systems. The results of the method indicate the real orders of dynamics that are most prominent in a system's frequency response. For the previously developed example of a robot formation that can be subjected to damage, this chapter has demonstrated that the identification procedure is able to compute transfer functions of fractional order that match the results from the high-order model. These transfer functions can be found both before and after the introduction of damage, and these computational results are in agreement with the expected order changes. As a monitoring

tool for general mechanically modeled systems of high order, this procedure may be a valuable source of information about the nature and extent of damage that may have occurred.

CHAPTER 5

MODELING LARGE AND INFINITE MASS-SPRING-DAMPER NETWORKS WITH FRACTIONAL AND IMPLICIT OPERATORS

Complex mechanical systems are susceptible to vibration because excitations can spread easily among many interacting components. This behavior is commonly quantified with numerical routines, but the complexity is an ostensible deterrent to mathematical analysis. This chapter presents a general and intuitive mathematical framework to relate applied force and displacement in mechanical systems with models called mechanical networks. Establishing these dynamics in a modular way pushes toward the goal of efficient modeling of these systems, their components and subsystems, and all combinations thereof. Much of this content appears in [40].

The systems examined in this chapter resemble those considered previously in this dissertation. However, the preceding chapters are primarily concerned with numerical results. This chapter is a more analytical thrust in pursuit of the operators that can be used to describe these systems. The operators presented in this chapter are, in general, implicit; the use of fractional differential operators as proxies for their implicit counterparts is discussed as well.

The concept of mechanical networks is inspired by the well-established theory of electrical networks and takes advantage of Ohm's and Kirchhoff's current laws by analogy. Two common analogies similar to the one presented here are used to relate current and voltage to force and velocity, where the difference between analogies lies in which electrical quantity is connected to which mechanical one. However, this research gives displacement a key role in the analogy instead of velocity. The

modifications stemming from that decision are the preferred way to account for the mechanical dynamics of interest.

The dynamics of these systems consist of inertia, damping, and elasticity, so the systems can be modeled with masses, dampers, and springs, respectively. No parallels are drawn to electrical circuits, so inerters are not needed; for a discussion of inerters and equivalent circuits, see [66]. The motion resulting from a periodic input suggestive of vibration is considered unidirectional and the springs and dampers linear. In discussing models of systems with many components, it is assumed unless otherwise noted that the stiffness and damping constants are uniform.

In the remainder of the chapter, the principles of this view of mechanical networks are presented, followed by component-level equations that govern these networks on a physical level. The utility of this approach is demonstrated on two types of example systems: the ladder and the tree, both analogous to applications of interest. The potential of this modeling framework in system design is outlined at the conclusion of the chapter.

5.1 Mechanical Networks

This section connects the mechanical systems of interest in this chapter to the language of networks. A network is comprised of nodes and the connections between them, called branches. The concept of mechanical networks flows from the idea that network branches can resemble mechanical components. Mechanical systems can be translated into networks by taking mass to be located exclusively at the nodes, with springs and dampers likewise in the branches. This treatment is perhaps gratuitous for simple systems, but those with more degrees of freedom map to intricate networks that may not resemble their mechanical geometry, thus revealing a new perspective on their dynamics.

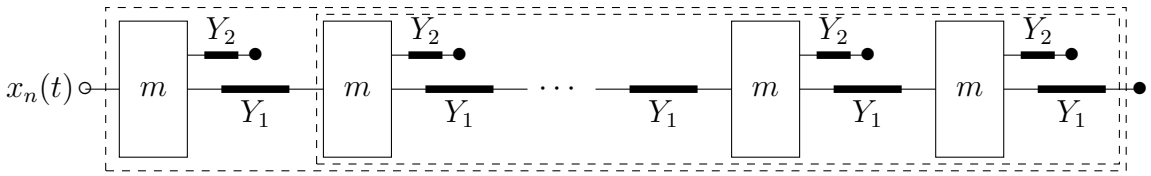

Figure 5.1. Form of two-component ladder network.

5.1.1 Finite and Infinite Networks

Real systems, obviously, are finite. Even a fine-mesh continuum analysis does not contend that the system of interest is comprised of infinitely many elements. However, the idea of an infinite system is useful when thinking of mechanical systems as networks. When the pattern of components used to model the system is repetitive, it is often the case that the dynamics are similar with or without the last layer of components. In other words, there is some sort of limit to which the dynamics converge once there are sufficiently many layers of components in the model. Approximating a complex system as an infinite version of itself can give rise to the desired mathematical simplicity in a governing equation while preserving the requisite accuracy. More details about this can be found in [22] and [38].

This chapter considers two repeating patterns of components as examples of mechanical networks. A *ladder* is a linear arrangement of masses, as shown in Figure 5.1, from [40]. Each mass is connected to three components: two in the forward direction (right in the figure), with one connected to the next mass and the other grounded, and one in the backward direction (left in the figure) that connects to the previous mass. When the system is sufficiently large, the dynamics of the two dashed boxes are approximately the same. The driving formation of Section 4.2 qualifies as a ladder.

A *tree* is a bifurcating arrangement, as illustrated in Figure 5.2. Each mass is connected to three others: two in front (right in the figure) and one behind (left). In both geometries, the first mass has no component behind it, while the last mass

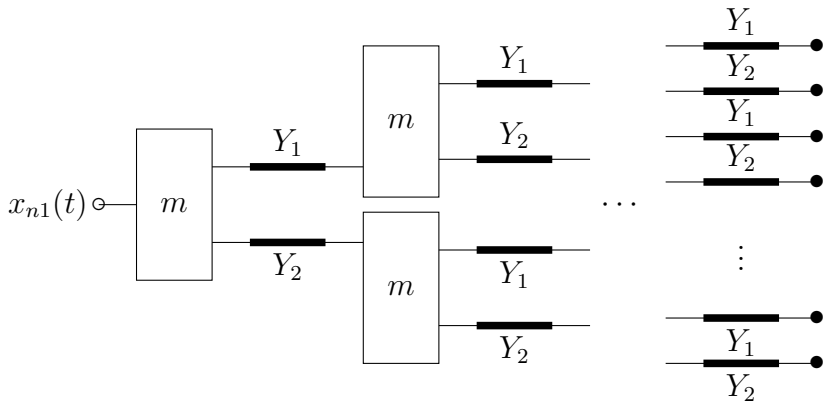

Figure 5.2. Form of two-component tree network.

(or, in the tree, each of the last masses) has two components going to ground in the absence of a next mass to which to connect. The coverage formation of Section 3.1 is an example of a tree.

Both of these arrangements suggest analogies to physical applications. Both can be considered plausible models for groups of simple vehicles traveling in a coordinated manner, with the connecting components representing low-level control relationships between each vehicle and its neighbors. The ladder suggests a long, flexible surface possessing inertia, damping, and elasticity everywhere. The tree might represent a similar surface with an amorphous shape; even with the structure defined, the orientation is not assumed, and the masses need not all connect to one another in the same direction.

Capturing the dynamics of these systems in a concise manner requires some mathematical tools not commonly seen in engineering. These methods and their utility to this modeling framework are outlined next.

5.1.2 Fractional and Implicit Operators

In determining differential equation models for systems, the amount of added flexibility provided by fractional derivatives cannot be overstated. They are especially useful in quantifying a relationship between two sides of a complex system, such as the networks discussed in this chapter, when the intermediate dynamics must be considered but need not be captured. Knowing the order representing the overall dynamics has potential benefits in control as well as modeling. For the purposes of this chapter, the choice of fractional derivative definition is not important.

It may be the case that a network is governed only by an *implicit operator*. This is a generalization of the typical concept of operators. For example, in the equation

$$\left(L^2 + E_1 L - E_0\right) f(t) = 0,$$

assuming that the function $f(t)$ is arbitrary, the operator L is the solution of the quadratic equation $L^2 + E_1 L - E_0 = 0$, with E_0 and E_1 representing any operators. In the special case of E_0 being the first derivative D and E_1 the zero operator, L is the derivative of order $1/2$. Implicit operators are not necessarily intended to reduce complexity but rather to provide a concise language of sorts with which to describe the relationships of interest. All linear systems, in theory, can be described by implicit operators.

5.2 Basic Equations

Branches and nodes are the building blocks of all networks, including the mechanical networks presented here. This section relates the mathematical notions arising from basic network structure to the physics of the systems of interest. It also places admittance into context as an operator, one that appears throughout the remainder of the chapter.

Figure 5.3. Network branch consisting of a mechanical component of admittance Y.

As previously mentioned, the springs and dampers in these networks are linear and are found in the branches. Figure 5.3 is a schematic of a network branch with an arbitrary component representing a spring-damper combination. The amount of compression is $\Delta x(t) = x_i(t) - x_{i-1}(t)$, where x_i and x_{i-1} are the respective displacements of nodes i and $i-1$ from their initial positions. The relationship between compression and force, $F(t)$, is

$$Y\Delta x = F; \tag{5.1}$$

they are linked by the admittance Y. An introductory example is a spring and a damper in parallel, with stiffness and damping constants k and b, respectively. In this case, Equation (5.1) becomes

$$(bD + k)\Delta x = F,$$

where D is the time derivative. The admittance is $Y = bD + k$. This is an example of combining admittances for components in parallel; the equivalent admittance is the sum of the individual admittances.

The branches are the connections between the nodes, where mass is located. Newton's law applied to the mass shown in Figure 5.4 gives the force balance

$$\sum_j F_j = m\frac{\mathrm{d}^2x}{\mathrm{d}t^2} = mD^2x,$$

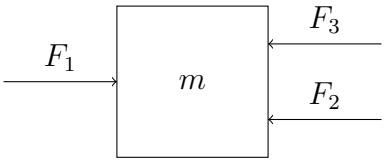

Figure 5.4. Network node consisting of a mass m subject to forces F_1, F_2, and F_3.

where mD^2 is the inertia operator. The masses are treated as points, an interpretation consistent with the aim of treating complex systems as networks with many nodes. Continuous mass distributions would have to be discretized as in commonplace finite-element methods.

5.3 Ladders

The ladder arrangement described in Section 5.1.1 is shown in Figure 5.1. The components have arbitrary admittances Y_1 and Y_2. The relationship of interest is that between the force applied on the left of the figure and the displacement x_0. This is of value in two ways: one can express an unknown vibration input or disturbance if the displacement is measured or, alternatively, predict the displacement for a known input in a simulation setting.

For each example, it is desirable to state the relationship between force and displacement with differential operators only. Following from this choice, the dynamics of the system are clear and can be calculated from any initial conditions. The differential relationships presented here are reasonable starting points from which to implement a simulation of the dynamics if either the force or the displacement is prescribed.

5.3.1 Finite Ladders

The ladder dynamics are presented here, first for smaller systems having few equations. The number of layers in each ladder is n. For each ladder, a relationship of the form $F = Y_{\text{eq}} x_n$ is sought, where Y_{eq} is the ladder's equivalent overall admittance. Mechanical admittance for an individual component is considered to satisfy Equation (5.1).

5.3.1.1 Base Cases

One-Layer Ladder: For $n = 1$, the ladder is shown in Figure 5.5, from [40]. A force balance leads to the governing equation

$$m\ddot{x}_1 = F - (Y_1 + Y_2)\, x_1$$

for the one mass. Algebraic manipulation gives

$$m\ddot{x}_1 + (Y_1 + Y_2)\, x_1 = \left(mD^2 + Y_1 + Y_2\right) x_1 = F,$$

so the admittance is

$$Y_{\text{eq}} = \frac{F}{x_1} = mD^2 + Y_1 + Y_2.$$

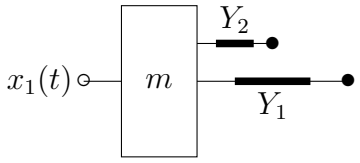

Figure 5.5. One-layer ladder network.

Two-Layer Ladder: For $n = 2$, the ladder is illustrated in Figure 5.6, from [40]. The equations of motion are

$$mD^2 \begin{bmatrix} x_1 \\ x_2 \end{bmatrix} = \begin{bmatrix} 0 \\ F \end{bmatrix} + \begin{bmatrix} -2Y_1 - Y_2 & Y_1 \\ Y_1 & -Y_1 - Y_2 \end{bmatrix} \begin{bmatrix} x_1 \\ x_2 \end{bmatrix}, \tag{5.2}$$

where x_1 is the displacement of the mass on the right and x_2 that on the left. Starting from the second line,

$$mD^2 x_2 = F + Y_1 x_1 - (Y_1 + Y_2)x_2.$$

Equivalently,

$$\begin{aligned} mD^2 \left(mD^2 + 2Y_1 + Y_2\right) x_2 = \left(mD^2 + 2Y_1 + Y_2\right) F + \left(mD^2 + 2Y_1 + Y_2\right) Y_1 x_1 \\ - \left(mD^2 + 2Y_1 + Y_2\right) (Y_1 + Y_2)x_2. \end{aligned}$$

From Equation (5.2), $\left(mD^2 + 2Y_1 + Y_2\right) x_1 = Y_1 x_2$, and that substitution gives

$$\begin{aligned} mD^2 \left(mD^2 + 2Y_1 + Y_2\right) x_2 = \left(mD^2 + 2Y_1 + Y_2\right) F + Y_1^2 x_2 \\ - \left(mD^2 + 2Y_1 + Y_2\right) (Y_1 + Y_2)x_2; \end{aligned}$$

when rearranged, it becomes

$$\left(\left(mD^2 + Y_1 + Y_2\right) \left(mD^2 + 2Y_1 + Y_2\right) - Y_1^2\right) x_2 = \left(mD^2 + 2Y_1 + Y_2\right) F,$$

an equation describing the relationship only in terms of differential operators.

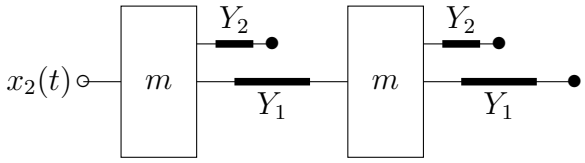

Figure 5.6. Two-layer ladder network.

Three-Layer Ladder: For $n = 3$, the ladder is depicted in Figure 5.7, from [40]. The equations are

$$mD^2 \begin{bmatrix} x_1 \\ x_2 \\ x_3 \end{bmatrix} = \begin{bmatrix} 0 \\ 0 \\ F \end{bmatrix} + \begin{bmatrix} -2Y_1 - Y_2 & Y_1 & 0 \\ Y_1 & -2Y_1 - Y_2 & Y_1 \\ 0 & Y_1 & -Y_1 - Y_2 \end{bmatrix} \begin{bmatrix} x_1 \\ x_2 \\ x_3 \end{bmatrix}. \tag{5.3}$$

One can apply $(mD^2 + 2Y_1 + Y_2)$ to the second line of Equation (5.3), at which point one may substitute the first line: $(mD^2 + 2Y_1 + Y_2)\, x_1 = Y_1 x_2$. It follows that

$$\left(\left(mD^2 + 2Y_1 + Y_2 \right)^2 - Y_1^2 \right) x_2 = \left(mD^2 + 2Y_1 + Y_2 \right) Y_1 x_3. \tag{5.4}$$

Applying $\left(\left(mD^2 + 2Y_1 + Y_2 \right)^2 - Y_1^2 \right)$ to the third line of Equation (5.3) enables the substitution given in Equation (5.4), so the relationship is

$$\begin{aligned} \Big[\left(mD^2 + Y_1 + Y_2 \right) \left(\left(mD^2 + 2Y_1 + Y_2 \right)^2 - Y_1^2 \right) - \left(mD^2 + 2Y_1 + Y_2 \right) Y_1^2 \Big] x_3 \\ = \left(\left(mD^2 + 2Y_1 + Y_2 \right)^2 - Y_1^2 \right) F. \end{aligned}$$

n-Layer Ladder: The equations presented for one, two, and three layers can be generalized to n layers. The matrix equation of motion for a ladder system with n

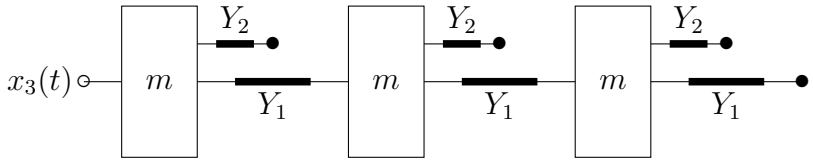

Figure 5.7. Three-layer ladder network.

layers is

$$mD^2 \begin{bmatrix} x_1 \\ x_2 \\ \vdots \\ \vdots \\ x_n \end{bmatrix} = \begin{bmatrix} 0 \\ \vdots \\ \vdots \\ 0 \\ F \end{bmatrix} + \begin{bmatrix} -2Y_1 - Y_2 & Y_1 & 0 & \cdots & 0 \\ Y_1 & \ddots & \ddots & \ddots & \vdots \\ 0 & \ddots & \ddots & \ddots & 0 \\ \vdots & \ddots & \ddots & -2Y_1 - Y_2 & Y_1 \\ 0 & \cdots & 0 & Y_1 & -Y_1 - Y_2 \end{bmatrix} \begin{bmatrix} x_1 \\ x_2 \\ \vdots \\ \vdots \\ x_n \end{bmatrix}. \quad (5.5)$$

The differential relationship between x_n and F can be derived as for the smaller ladders.

5.3.1.2 Extension to Large Ladders

Even with as few as three layers, the exact governing equation is somewhat cumbersome. Self-similarity can be exploited in writing the differential relationship for an arbitrarily large number of masses n in a much more concise form than would be determined from Equation (5.5). If the leftmost Y_1 has twice the admittance of the others ($Y_{1,n} = 2Y_1$), that relationship has the form

$$E_n x_n = E_{n-1} F; \quad (5.6)$$

$$E_i = \left(mD^2 + 2Y_1 + Y_2\right) E_{i-1} - Y_1^2 E_{i-2}, \quad (5.7)$$

where $E_0 = I$ and $E_{-1} = 0$ for purposes of recursion. The operators E_i are differential operators; they are computed by Equation (5.7) and govern the ladder network according to Equation (5.6). The admittance Y_{eq} is sought such that $Y_{\text{eq}} x_n = F$. The introduction of self-similarity is manifested in the approximation $E_{n-1} x_n \approx E_{n-2} F$; in other words, the displacement $x_n(t)$ corresponds to the force $F(t)$ whether there are n or $n-1$ layers because the system is large. Starting with a substitution for E_n,

$$\left(mD^2 + 2Y_1 + Y_2\right) \underbrace{E_{n-1} x_n}_{\approx E_{n-2} F} - Y_1^2 E_{n-2} x_n = E_{n-1} F = \underbrace{E_{n-1} Y_{\text{eq}} x_n}_{\approx Y_{\text{eq}} E_{n-2} F}.$$

By definition, $Y_{\text{eq}} x_n$ can be substituted for F to yield

$$\left(mD^2 + 2Y_1 + Y_2\right) E_{n-2} Y_{\text{eq}} x_n - Y_1^2 E_{n-2} x_n = Y_{\text{eq}}^2 E_{n-2} x_n;$$

rearranging gives

$$\left(Y_{\text{eq}}^2 - \left(mD^2 + 2Y_1 + Y_2\right) Y_{\text{eq}} + Y_1^2\right) E_{n-2} x_n = 0.$$

The displacement x_n is arbitrary, and the operator E_{n-2} cannot be the zero operator if $n > 1$. Therefore, it is valid to express Y_{eq} as the solution of a quadratic equation:

$$Y_{\text{eq}} = \frac{1}{2}\left(mD^2 + 2Y_1 + Y_2 \pm \left(\left(mD^2 + 2Y_1 + Y_2\right)^2 - 4Y_1^2\right)^{1/2}\right). \tag{5.8}$$

Admittances $Y_1 = k$ and $Y_2 = bD$ would create a spring-damper ladder. For neatness, suppose the leftmost Y_1, called $Y_{1,n}$, has twice the stiffness of the others. Therefore, $Y_{1,n} = 2k$, and the equivalent admittance is

$$Y_{\text{eq}} = \frac{1}{2}\left(mD^2 + bD + 2k \pm \left(\left(mD^2 + bD + 2k\right)^2 - 4k^2\right)^{1/2}\right).$$

If the leftmost Y_1 is the same as the others, that is, $Y_{1,n} = k$, then Equation (5.8) still holds for the first $n-1$ layers, counting from the right. The last is included by combining admittances in series:

$$\frac{1}{Y_{\text{eq}}} = \frac{1}{mD^2 + bD + k} + \frac{2}{mD^2 + bD + 2k \pm \left((mD^2 + bD + 2k)^2 - 4k^2\right)^{1/2}}.$$

Numerical evaluations of ladder dynamics enforce the notion of self-similarity. That is, the ladder can become large enough that additional layers make little difference in a time-domain response. This result shows that the dynamics to which the ladder arrangement converges are captured by an implicit operator. Furthermore, the frequency response shows that fractional-order behavior such as the operator raised to the power 1/2 in Equation (5.8) must be included for a concise, accurate differential equation relationship.

5.3.2 Infinite Ladders

Implicitly defined dynamics are also evident by considering the network system as infinite from the start. Specifically, the approximation of the system as an infinite version of itself allows for analogous neighboring positional relationships to be considered equal. The results of this section, combined with the previous section, show that the overall dynamics and those at the component level are connected when the ladder is taken to be infinite.

The equation of motion for mass i is

$$mD^2 x_i = -Y_2 x_i + Y_1(x_{i+1} - x_i) - Y_1(x_i - x_{i-1}).$$

The neighbors' displacements are related according to

$$Y_1 x_{i+1} = Y_{\text{eq}} x_i; \tag{5.9}$$

that is, for a large ladder, the force propagating to the right through a node ($F = Y_{\text{eq}} x_i$) is equal to that coming in from the left. Defining a displacement ratio, a transfer function of sorts, called G and substituting $G = x_{i+1}/x_i \approx x_i/x_{i-1}$ yields

$$mD^2 x_i = \left(-Y_2 + Y_1(G - I) - Y_1\left(I - G^{-1}\right)\right) x_i;$$

it follows that

$$\left(Y_1 G^2 - \left(mD^2 + 2Y_1 + Y_2\right) G + Y_1\right) x_i = 0.$$

The formal solution is

$$G = \frac{1}{2Y_1}\left(mD^2 + 2Y_1 + Y_2 \pm \left(\left(mD^2 + 2Y_1 + Y_2\right)^2 - 4Y_1^2\right)^{1/2}\right).$$

From Equation (5.9), it can be inferred that $G = Y_{\text{eq}}/Y_1$; that substitution gives an expression for Y_{eq} that is consistent with Equation (5.8). The "plus" solution is the relevant one because its frequency response has nonpositive phase difference, indicating the intended property of causality. Furthermore, it matches the finite systems' frequency responses at least partially with mass neglected, as shown in Figure 5.8, from [40] ("large approx"). The "minus" solution is reflected about zero on both y-axes from the "plus" solution and is not shown.

The approximation of the system as infinite is valuable in light of the frequency responses of the corresponding finite arrangements of these components. The implicit operator that appears to be governing the system suggests fractional-order behavior of the type seen over a wide band of frequencies, as depicted in Figure 5.8. The dominant slope in magnitude of -10 dB/dec and phase difference of $-45°$ are suggestive of order 1/2; this is consistent with the result from a similar system in Figure 4.3. In Figure 5.8, that behavior is progressively more evident as more layers are added to the ladder. Therefore, it is accurate to model a system with sufficiently many layers

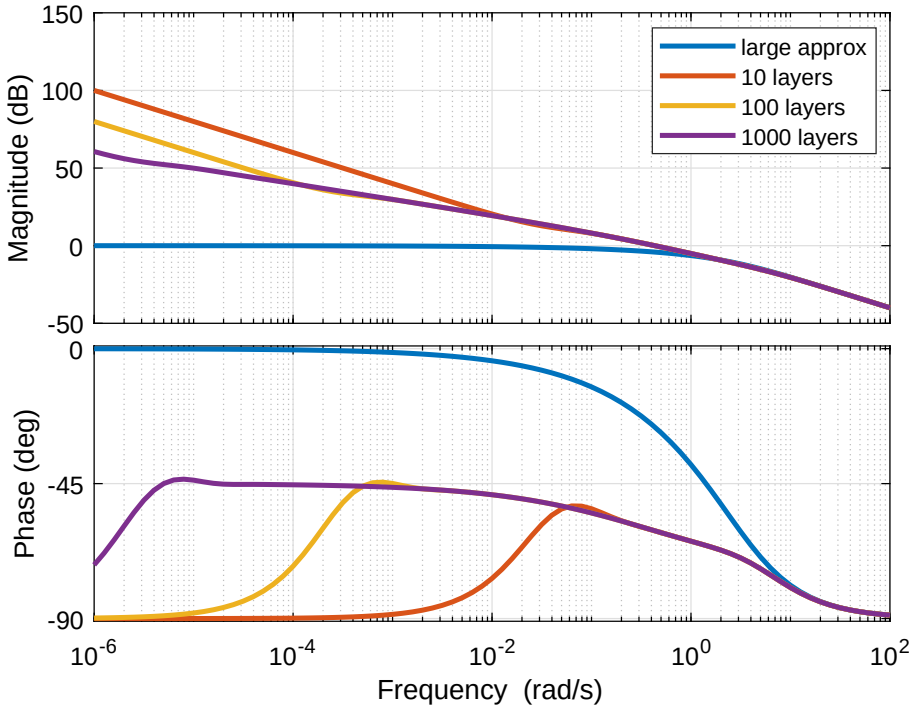

Figure 5.8. Large ladder approximation and elongation of frequency band suggesting fractional-order behavior for finite ladders.

as fractional.

Figure 5.9, from [40], is a high-frequency comparison between the simulated response of a ladder with 1000 layers and the solution of the governing equation for a fractional-order system having the same input, except that it is attenuated in magnitude, as suggested by comparing the two frequency responses. The fractional-order model is not exactly the large approximation of Equation (5.8); that model's implicit operator cannot be applied directly. Rather, Figure 5.8 shows a phase difference slightly less than $-90°$ for high frequencies, with magnitude slope to match, and therefore suggests that the model has order slightly less than 1. The order chosen in the computations of Figure 5.9 is 0.85.

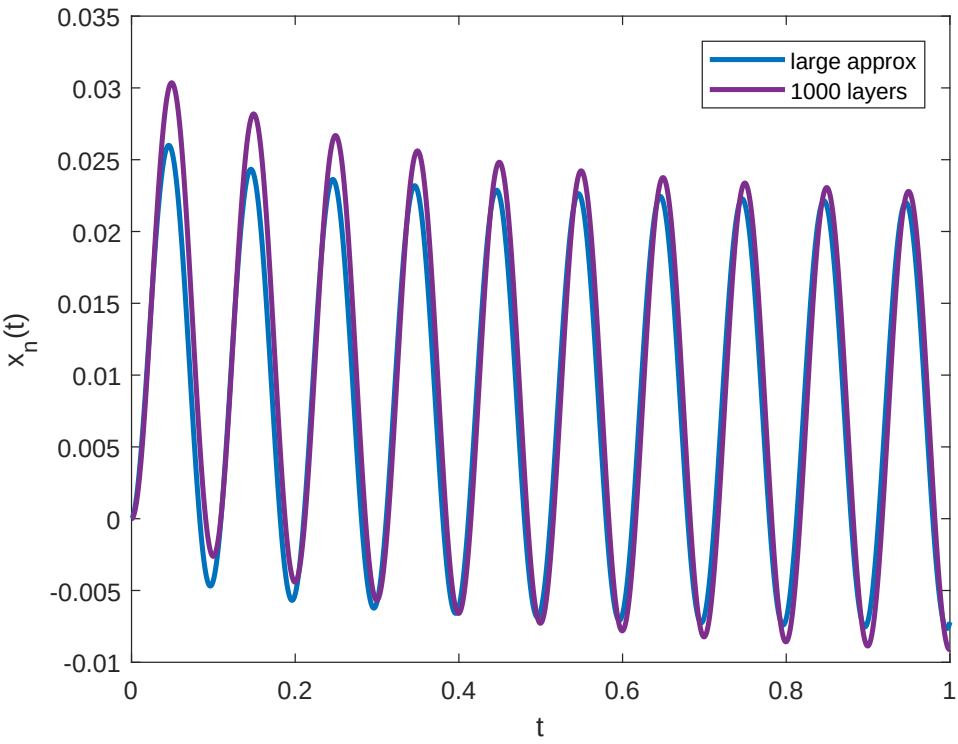

Figure 5.9. Time-domain excitation at frequency 20π rad/s showing agreement between ladder and approximation.

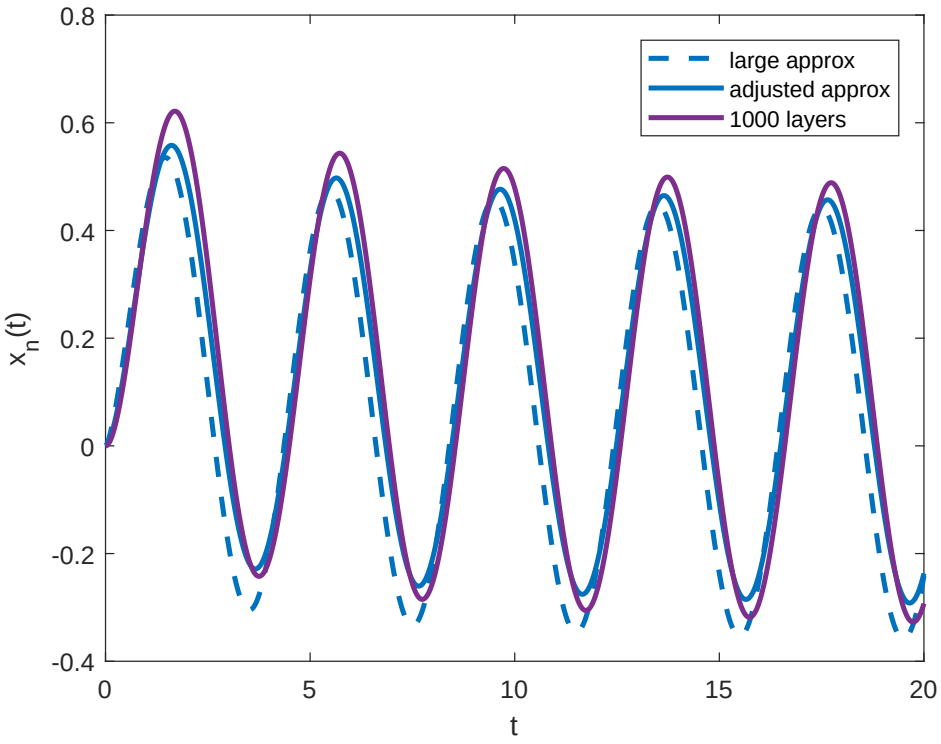

Figure 5.10. Time-domain excitation at frequency $\pi/2$ rad/s showing mismatch between ladder and approximation.

At low frequencies, however, it may not be accurate to model the system with the large approximation. As shown in Figure 5.8, the frequency response of $1/Y_{\text{eq}}$ for the infinite system deviates substantially from those of the finite systems for frequencies below roughly 1 rad/s. Figure 5.10, from [40], confirms that the large approximation breaks down for low frequencies. At $\pi/2$ rad/s, the magnitude slope and phase difference of the large approximation suggest an order of roughly 0.5. However, a better match is seen from an equation of order 0.65 ("adjusted approx"), more in line with the 1000-layer ladder system's frequency response curves in Figure 5.8. In both cases, the force magnitude is attenuated in the same manner as in the high-frequency case to yield an informative comparison.

In Figure 5.8, the peaks of the phase curves become gradually less negative for

longer systems. However, considering how slowly that trend evolves despite being on a logarithmic scale, it appears that a physically unrealistic number of layers would be needed to see convergence to the large approximation for low frequencies. There is a clear match for high frequencies, though, so the large approximation is appropriate in that case.

5.4 Trees

The tree arrangement is illustrated in Figure 5.2. As with the ladder, the relationship of interest is between the force applied at left and the displacement x_0. The right components are attached to ground. The component admittances are Y_1 and Y_2. The special case of no mass is considered later in the discussion, but at the outset, the masses m are included.

As with the ladder examples, each relationship between force and displacement is written with differential operators only. This mitigates any possible concerns about initial conditions or, put another way, unknown constants of integration. If either the force or the displacement is a known function of time, the other can be computed easily.

5.4.1 Finite Trees

This discussion seeks to determine each tree's equivalent admittance Y_{eq}. Mechanical admittance is considered to satisfy Equation (5.1). The number of layers in each tree is n.

5.4.1.1 Base Cases

One-Layer Tree: For $n = 1$, the tree and ladder are the same (Figure 5.5). A force balance leads to the governing equation

$$m\ddot{x}_{11} = F - (Y_1 + Y_2)\, x_{11}$$

for the one mass. The subscript is changed to 11 for ease of expansion to larger trees. Algebraic manipulation gives

$$m\ddot{x}_{11} + (Y_1 + Y_2)\, x_{11} = \left(mD^2 + Y_1 + Y_2\right) x_{11} = F.$$

Two-Layer Tree: For $n = 2$, the tree is shown in Figure 5.11. The equations of motion are

$$mD^2 \begin{bmatrix} x_{11} \\ x_{12} \\ x_{21} \end{bmatrix} = \begin{bmatrix} 0 \\ 0 \\ F \end{bmatrix} + \begin{bmatrix} -2Y_1 - Y_2 & 0 & Y_1 \\ 0 & -Y_1 - 2Y_2 & Y_2 \\ Y_1 & Y_2 & -Y_1 - Y_2 \end{bmatrix} \begin{bmatrix} x_{11} \\ x_{12} \\ x_{21} \end{bmatrix}.$$

In an analogous fashion to the case of the ladder, a purely differential relationship between x_{21} and F can be determined. Starting from the third line,

$$mD^2 x_{21} = F + Y_1 x_{11} + Y_2 x_{12} - (Y_1 + Y_2) x_{21};$$

$$\left(mD^2 + 2Y_1 + Y_2\right)\left(mD^2 + Y_1 + 2Y_2\right)\left(mD^2 x_{21} = F + Y_1 x_{11} + Y_2 x_{12} - (Y_1 + Y_2) x_{21}\right).$$

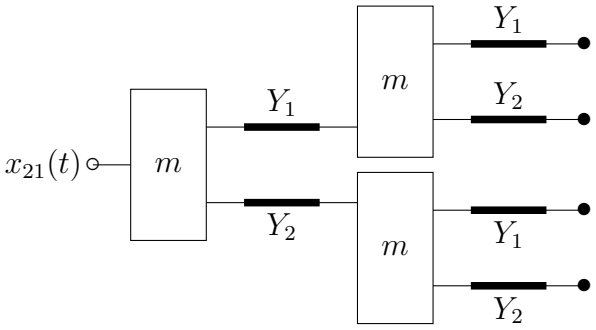

Figure 5.11. Two-layer tree network.

From the substitutions $(mD^2 + 2Y_1 + Y_2)\, x_{11} = Y_1 x_{21}$ and $(mD^2 + Y_1 + 2Y_2)\, x_{12} = Y_2 x_{21}$,

$$\begin{aligned}
&\left(mD^2 + 2Y_1 + Y_2\right)\left(mD^2 + Y_1 + 2Y_2\right) mD^2 x_{21} \\
&\quad = \left(mD^2 + 2Y_1 + Y_2\right)\left(mD^2 + Y_1 + 2Y_2\right) F + \left(mD^2 + Y_1 + 2Y_2\right) Y_1^2 x_{21} \\
&\qquad + \left(mD^2 + 2Y_1 + Y_2\right) Y_2^2 x_{21} \\
&\qquad - \left(mD^2 + 2Y_1 + Y_2\right)\left(mD^2 + Y_1 + 2Y_2\right)(Y_1 + Y_2) x_{21};
\end{aligned}$$

rearranging gives

$$\begin{aligned}
&\Big(\left(mD^2 + 2Y_1 + Y_2\right)\left(mD^2 + Y_1 + 2Y_2\right)\left(mD^2 + Y_1 + Y_2\right) \\
&\qquad - \left(mD^2 + Y_1 + 2Y_2\right) Y_1^2 - \left(mD^2 + 2Y_1 + Y_2\right) Y_2^2\Big)\, x_{21} \\
&\qquad = \left(mD^2 + 2Y_1 + Y_2\right)\left(mD^2 + Y_1 + 2Y_2\right) F.
\end{aligned}$$

Three-Layer Tree: For $n = 3$, the tree is illustrated in Figure 5.12. The equations are

$$mD^2x = F + \begin{bmatrix} Y_a = -2Y_1 - Y_2 & 0 & 0 & 0 & Y_1 & 0 & 0 \\ 0 & Y_b = -Y_1 - 2Y_2 & 0 & 0 & Y_2 & 0 & 0 \\ 0 & 0 & Y_a & 0 & 0 & Y_1 & 0 \\ 0 & 0 & 0 & Y_b & 0 & Y_2 & 0 \\ Y_1 & Y_2 & 0 & 0 & Y_a & 0 & Y_1 \\ 0 & 0 & Y_1 & Y_2 & 0 & Y_b & Y_2 \\ 0 & 0 & 0 & 0 & Y_1 & Y_2 & -Y_1 - Y_2 \end{bmatrix} x,$$

where

$$x = \begin{bmatrix} x_{11} & x_{12} & x_{13} & x_{14} & x_{21} & x_{22} & x_{31} \end{bmatrix}^{\mathrm{T}}$$

and

$$F = \begin{bmatrix} 0 & 0 & 0 & 0 & 0 & 0 & F \end{bmatrix}^{\mathrm{T}}$$

are abbreviated for reasons of space. Regarding the differential relationship, the details are omitted, but the procedure is the same as in the $n = 2$ case.

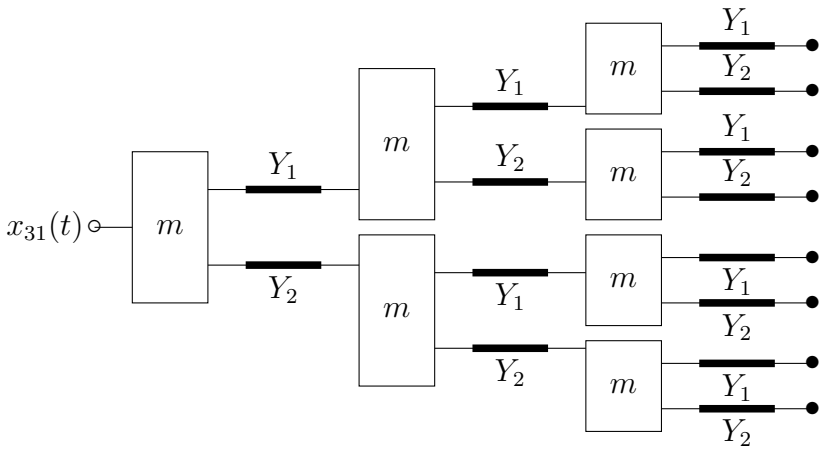

Figure 5.12. Three-layer tree network.

n-Layer Tree: The matrix governing equation for one, two, or three layers can be expanded for a tree of n layers:

$$mD^2x = \begin{bmatrix} 0 \\ \vdots \\ 0 \\ F \end{bmatrix} + \left(\begin{bmatrix} \begin{bmatrix} Y_a & 0 \\ 0 & Y_b \end{bmatrix} & 0 & \cdots & 0 \\ 0 & \ddots & \ddots & \vdots \\ \vdots & \ddots & \begin{bmatrix} Y_a & 0 \\ 0 & Y_b \end{bmatrix} & 0 \\ 0 & \cdots & 0 & -Y_1 - Y_2 \end{bmatrix} \right.$$
$$\left. + \begin{bmatrix} 0 & \begin{bmatrix} Y_1 \\ Y_2 \end{bmatrix} & 0 & \cdots & 0 \\ & & \ddots & \ddots & \vdots \\ \begin{bmatrix} Y_1 & Y_2 \end{bmatrix} & & \ddots & \ddots & 0 \\ 0 & \ddots & & & \begin{bmatrix} Y_1 \\ Y_2 \end{bmatrix} \\ \vdots & \ddots & \ddots & & \\ 0 & \cdots & 0 & \begin{bmatrix} Y_1 & Y_2 \end{bmatrix} & 0 \end{bmatrix} \right) x, \qquad (5.10)$$

where

$$x = \begin{bmatrix} x_{11} & x_{12} & \cdots & x_{1,2^{n-1}} & x_{21} & x_{22} & \cdots & x_{2,2^{n-2}} & \cdots & x_{n1} \end{bmatrix}^{\mathrm{T}}.$$

To clarify, the blocks containing Y_1 and Y_2 step to the left by one column sequentially in the upper triangle, and the matrix is symmetric. The blank space, aside from the progressions of blocks, contains only zeros. The matrix is decomposed for neatness, but it is also valid to consider the first matrix as the influence of each mass on its own position, while the second contains all contributions from neighbors. A differential equation relating F and x_{n1} can be determined by substituting rows into one another as with the ladder.

5.4.1.2 Extension to Large Trees

The exact governing equation for the tree can only be written neatly from the form of Equation (5.10) for one or two layers. As in the case of the ladder, substitutions informed by self-similarity may be made in the differential equation relationship for a large number of layers n. That relationship is

$$L_n x_{n1} = R_n F, \tag{5.11}$$

where

$$\begin{aligned} L_i = {} & L_1(L_{i-1} + Y_1 R_{i-1})(L_{i-1} + Y_2 R_{i-1}) \\ & - (L_{i-1} + Y_2 R_{i-1}) R_{i-1} Y_1^2 - (L_{i-1} + Y_1 R_{i-1}) R_{i-1} Y_2^2 \end{aligned}$$

and

$$R_i = (L_{i-1} + Y_1 R_{i-1})(L_{i-1} + Y_2 R_{i-1}).$$

The recursion begins with $L_1 = mD^2 + Y_1 + Y_2$ and $R_1 = I$. Therefore, L_i and R_i are differential operators, and they govern the tree network according to Equation (5.11).

After substituting the expressions for L_i and R_i, the equation simplifies to

$$\Big[mD^2\left(L_{n-1}^2 + (Y_1+Y_2)R_{n-1}L_{n-1} + Y_1Y_2R_{n-1}^2\right) + (Y_1+Y_2)L_{n-1}^2 + 2Y_1Y_2R_{n-1}L_{n-1}\Big]x_{n1} = (L_{n-1}+Y_1R_{n-1})(L_{n-1}+Y_2R_{n-1})F. \quad (5.12)$$

An expression for the admittance Y_{eq} is desired such that $Y_{\text{eq}}x_{n1} = F$. Self-similarity gives rise to the approximation $L_{n-1}x_{n1} \approx R_{n-1}F$, prescribing the system to have the same relationship between x_{n1} and F whether it has n or $n-1$ layers. The admittance is determined as follows: expanding Equation (5.12) on both sides gives

$$\begin{aligned} mD^2\left(L_{n-1}^2 + (Y_1+Y_2)R_{n-1}L_{n-1} + Y_1Y_2R_{n-1}^2\right)x_{n1} + (Y_1+Y_2)L_{n-1}^2x_{n1} \\ +2Y_1Y_2R_{n-1}L_{n-1}x_{n1} &= (L_{n-1}+Y_1R_{n-1})(L_{n-1}+Y_2R_{n-1})F \\ &= L_{n-1}^2F + (Y_1+Y_2)R_{n-1}L_{n-1}F + Y_1Y_2R_{n-1}^2F. \end{aligned}$$

Applying $L_{n-1}x_{n1} \approx R_{n-1}F$ followed by $F = Y_{\text{eq}}x_{n1}$ three times each yields an equation that can be rearranged to give

$$\left(Y_{\text{eq}}^3 - mD^2(Y_{\text{eq}}+Y_1)(Y_{\text{eq}}+Y_2) - Y_1Y_2Y_{\text{eq}}\right)R_{n-1}^2x_{n1} = 0.$$

The displacement x_{n1} is arbitrary, and the operator R_{n-1} cannot be the zero operator. Therefore, Y_{eq} is a root of the cubic expression given. There is only one real root; it is

$$Y_{\text{eq}} = \frac{1}{3}mD^2 + \frac{\sqrt[3]{2}Y_c}{3\left(Y_d + (-4Y_c^3 + Y_d^2)^{1/2}\right)^{1/3}} + \frac{1}{3\sqrt[3]{2}}\left(Y_d + \left(-4Y_c^3 + Y_d^2\right)^{1/2}\right)^{1/3},$$

where $Y_c = m^2D^4 + 3mD^2(Y_1+Y_2) + 3Y_1Y_2$ and $Y_d = 2m^3D^6 + 9m^2D^4(Y_1+Y_2) + 36mD^2Y_1Y_2$. Admittedly, an operator of this complexity is likely beyond the desired scope of most simulations in the absence of useful approximations.

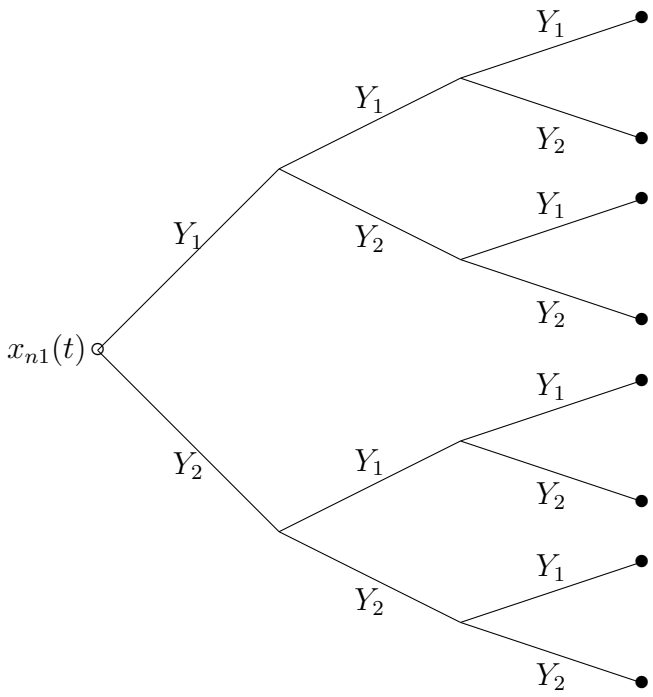

Figure 5.13. Massless three-layer tree network.

One such approximation is considering the mass to be negligible, as one may do for a system dominated by damping and elasticity. This version of the tree is drawn in Figure 5.13. This yields $Y_{\text{eq}}^2 - Y_1 Y_2 = 0$, assuming that $Y_{\text{eq}} \neq 0$. In turn,

$$Y_{\text{eq}} = \pm (Y_1 Y_2)^{1/2}. \tag{5.13}$$

Presumably the positive solution is of exclusive interest, considering that the negative solution is not physically realizable with springs and dampers having positive constants.

As with the ladder, numerical evaluations of tree dynamics suggest self-similarity. This result shows that the dynamics to which the tree arrangement converges are of an order that is a multiple of 1/2 (1/2 exactly for the previous choices of $Y_1 = k$ and $Y_2 = bD$). The frequency responses for large trees clearly suggest order 1/2 as well.

5.4.2 Infinite Trees

As in the case of the ladder, the system can be analyzed as infinite to yield concise relationships capturing the behavior of interest. One may begin by considering the node equations, but progress is expedited by considering series and parallel combinations to produce the 1/2-order conclusion rather quickly. Above all, this demonstrates that the modeling framework outlined here does not necessarily prescribe one way to examine a system; rather, the results will be consistent for all approaches, though ease of computation may vary.

The following developments are based on the branch equation,

$$Y_i \Delta x_i = F_i,$$

and the node equation,

$$\sum_j F_j = 0.$$

In the notation to follow, the first index refers to the network layer (counting from right to left in Figure 5.13), and the second refers to the branch (counting from top to bottom).

For $n = 1$, the three equations for the one node are

$$F_{11} = bD(0 - x_{11});$$
$$F_{12} = k(0 - x_{11});$$
$$F_{11} + F_{12} = -F_{\text{eq}}.$$

These can be combined, resulting in

$$bD(0 - x_{11}) + k(0 - x_{11}) = -F_{\text{eq}},$$

so in the definition

$$Y_{1,\text{eq}} x_{11} = F_{\text{eq}},$$

the equivalent admittance is

$$Y_{1,\text{eq}} = bD + k.$$

This approach takes $m = 0$ in order to portray dynamics dominated by stiffness and damping, so the term mD^2 does not appear. In this example, Y_{eq} can be applied to a known x_{n1} to compute the unique solution F_{eq}.

For $n = 2$, there are three nodes with three equations each:

$$\begin{aligned}
F_{21} &= bD(x_{11} - x_{21}); \\
F_{22} &= k(x_{12} - x_{21}); \\
F_{21} + F_{22} &= -F_{\text{eq}}; \\
F_{11} &= bD(0 - x_{11}); \\
F_{12} &= k(0 - x_{11}); \\
F_{11} + F_{12} &= -F_{21}; \\
F_{13} &= bD(0 - x_{12}); \\
F_{14} &= k(0 - x_{12}); \\
F_{13} + F_{14} &= -F_{22}.
\end{aligned}$$

After solving the above as a linear system, it is seen that the solution is

$$F_{\text{eq}} = (bD + k)\left(\frac{b}{k}D + \frac{k}{b}D^{-1}\right) x_{21} = Y_{2,\text{eq}} x_{21}. \tag{5.14}$$

It should be noted that this equivalent admittance contains an integral operator, so Equation (5.14) is not strictly a differential equation. Even with only two layers in the tree, the exact modeling approach introduces undesired complexity.

For $n \to \infty$, the equations for series and parallel combinations imply that

$$Y_{\infty,\text{eq}} = \frac{Y_1 Y_{\infty,\text{eq}}}{Y_1 + Y_{\infty,\text{eq}}} + \frac{Y_2 Y_{\infty,\text{eq}}}{Y_2 + Y_{\infty,\text{eq}}}.$$

It is possible to start here because it is clear that the subtrees attached to the first Y_1 and Y_2 are exact copies of the large tree. Disregarding the possibility that $Y_{\infty,\text{eq}} = 0$, the solution is

$$Y_{\text{eq}} = (Y_1 Y_2)^{1/2},$$

which for $Y_1 = bD$ and $Y_2 = k$ gives

$$Y_{\text{eq}} = (kbD)^{1/2}.$$

This is consistent with the analysis of the finite tree that culminated in Equation (5.13). The tree system as described is clearly of order 1/2. In keeping with the discussion of Figure 3.4, it is no surprise that finite instances of the tree exhibit 1/2-order behavior over a window of frequencies that becomes wider as more layers of components are added to the system. These results are compared to the large approximation in Figure 5.14, with larger trees' $1/Y_{\text{eq}}$ curves having a magnitude slope of -10 dB/dec and a phase difference of $-45°$ at progressively more frequencies.

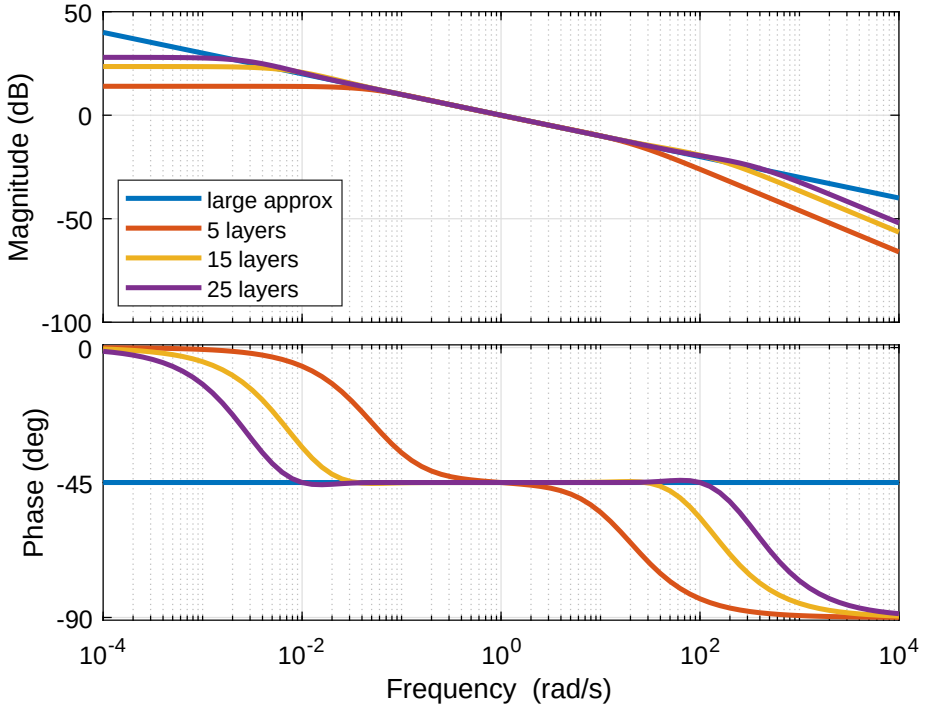

Figure 5.14. Large tree approximation and elongation of frequency band suggesting half-order behavior for finite trees.

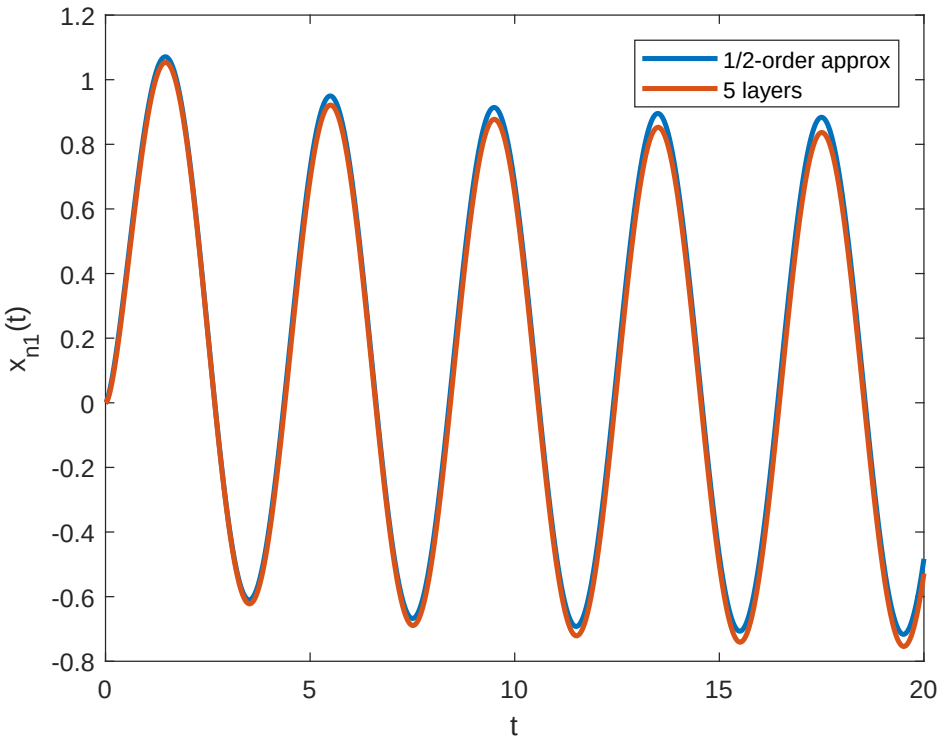

Figure 5.15. Time-domain excitation at frequency $\pi/2$ rad/s showing agreement between tree and approximation.

Figure 5.15 compares the response of a five-layer tree to a sinusoidal input with the solution of the governing equation for a purely 1/2-order system having the same input. A higher-frequency input creates a mismatch between the tree system and the same 1/2-order approximation, as shown in Figure 5.16. The magnitude slope and phase difference shown in the frequency response of Figure 5.14 suggest that the order approaches 1 for high frequencies. A better match, computed with order 8/9, is shown in Figure 5.16 as "shifted-order approx." In this approximation, the input force magnitude is amplified to correspond to the full system at the input frequency, as suggested by Figure 5.14. Such a step is not needed in the 1/2-order approximation, for which the magnitudes agree at the lower input frequency.

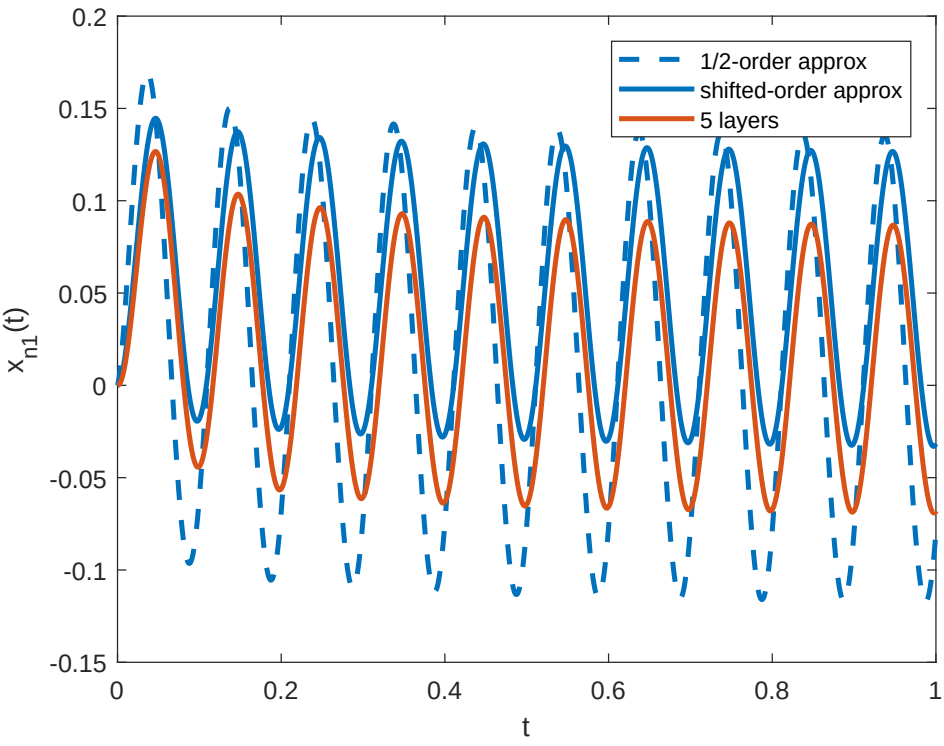

Figure 5.16. Time-domain excitation at frequency 20π rad/s showing agreement between tree and adjusted approximation.

As shown in Figures 5.15 and 5.16, the tree systems introduce transient behavior that is not captured well by the approximations. However, considering that vibration analysis is typically concerned with steady-state dynamics, these approximations are still accurate in the sense that the vibration amplitudes and phases are consistent with those of the system simulations. This method of approximation is therefore promising for simplifying models of complex mechanical systems.

This chapter has presented a descriptive framework for mechanical networks. It is intended primarily to enhance understanding of these systems, which are representative of a wide range of complex mechanical systems in applications of interest. The research presented in this chapter is an extension of Chapters 3 and 4 to systems with arbitrary linear connections; it is a pursuit of as yet unexplored analytical tools for the purpose of modeling such systems. These tools open possibilities for related but distinct endeavors, including quantifying the effects of component constants that are varied, perhaps in a random distribution. The reverse problem of constructing systems of arbitrary order from known components is also of interest.

Naturally, the potential exists to explore other network arrangements that may correspond to still more systems. The intention of this chapter is to assert that such a procedure can be informative in general. It is possible that simulations containing the systems of interest can be made more computationally efficient, in development time as well as runtime, when a physically exact model is replaced with a more concise relationship while preserving sufficient accuracy.

The systems studied in this research are characterized by interconnected dynamics that complicate attempts to model all of the influential behavior exactly. This framework contributes concise and accurate descriptions of such dynamics. Relationships of interest can be captured without having to preserve a large state space of other quantities. Models of the nature produced by this framework, generally of fractional order, give a clear picture of the dynamical nature of the important behavior; this

can be a valuable asset when designing a control strategy. Overall, these findings are presented with the aim of filling the theoretical foundation to exist alongside the numerical one for analysis of complex mechanical systems.

CHAPTER 6

FRACTIONAL-ORDER TRAJECTORY-FOLLOWING CONTROL FOR TWO-LEGGED DYNAMIC WALKING

The preceding chapters demonstrate that fractional order is a parameter that can be used to track dynamical changes within a system. One effort that can be aided by knowledge of these dynamical changes is control. Relating fractional-order dynamics to a suitable corresponding fractional-order controller is documented in studies such as [75]. This chapter presents an example of the utility of fractional order in control for a system that is not suspected to have fractional-order behavior, in turn reinforcing the notion that integer-order systems can be treated as special cases within the class of fractional-order systems.

Two-legged dynamic walking is arguably the most useful kind of walking. Static walkers are focused on balance and require constant control effort to execute movements, resisting inertia and gravity, so their application space is limited. In contrast, dynamic walkers take advantage of inertia and gravity, so their movements are more energetically efficient. They also allow for more freedom of movement at the expense of instantaneous balance, and this expands the variety of terrain that can be traversed. Walkers with more than two legs can be similarly versatile, but space considerations favor two legs.

This chapter presents a new path toward improvement in performance and energy efficiency for a two-legged dynamic walker. The equations of motion for such a walker suggest that feedback linearization is desirable for the purpose of implementing classical control methods. The contribution of this research is to show that fractional-

order control has possible benefits over proportional-derivative (PD) control in a robot's trajectory-following ability and energy consumption.

The premise of fractional-order control is to alter the order of a linear controller, not merely its gains. Rather than controlling from an error quantity and its first derivative, one may instead use a derivative having a different order q that is not necessarily an integer. Thus, the concept of fractional-order control is guaranteed to do at least as well as PD control; $q = 1$ restores it. Less intuitive is the potential of other controller orders. This chapter demonstrates the merits of changing the order and suggests that fractional-order control is a straightforward way to improve a two-legged dynamic walker's response relative to that resulting from PD control.

6.1 Walker Dynamics

This section presents the dynamics of the two-link walker model of interest in this research. A schematic of the walker is shown in Figure 6.1.

The angles are defined as follows. The angle of the swing leg relative to the stance leg is called θ_1. The angle of the stance leg relative to the vertical is called θ_2. For practical purposes, neither angle should have a value outside of the interval $[-\pi/2, \pi/2]$ rad.

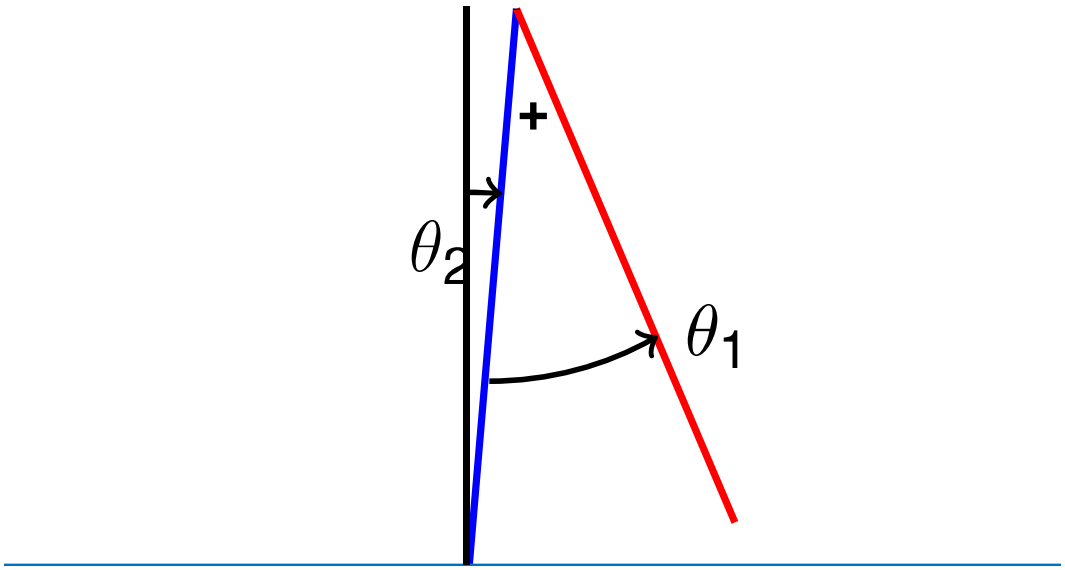

Figure 6.1. Walker with angle definitions.

The equations of motion for the two-legged walker take the form

$$D(\theta)\begin{bmatrix}\ddot{\theta}_1\\ \ddot{\theta}_2\end{bmatrix} + C(\theta,\dot{\theta})\begin{bmatrix}\dot{\theta}_1\\ \dot{\theta}_2\end{bmatrix} + G(\theta) = B(\theta)u(t), \tag{6.1}$$

where D, C, G, and B are the inertia, velocity, gravity, and control matrices respectively. A system of first-order differential equations equivalent to Equation (6.1) can be written:

$$\dot{x} = \begin{bmatrix} x_3 \\ x_4 \\ D^{-1}\left(-C\begin{bmatrix}x_3\\ x_4\end{bmatrix} - G + Bu(t)\right)_{2\text{x}1} \end{bmatrix}, \tag{6.2}$$

where $x_1 = \theta_1$, $x_2 = \theta_2$, $x_3 = \dot{\theta}_1$, and $x_4 = \dot{\theta}_2$. The physical parameters influencing D, C, and G are l, the leg length (1 m for this walker); l_c, the position of the leg's center of mass measured from the base of the leg (0.8 m); m, the leg mass (0.3 kg); and J, the leg's moment of inertia about its center of mass (0.03 kg m^2). These parameters originate from previous research in the author's department on the same simulated walker. Also referenced is g, the acceleration due to gravity.

The inertia matrix D is given by

$$\begin{aligned}
D_{11} &= J + m(l - l_c)^2;\\
D_{12} &= -J - m(l - l_c)\left(l - l_c - l\cos(\theta_1)\right);\\
D_{21} &= D_{12};\\
D_{22} &= 2J + ml_c^2 + m\left(l^2 + (l - l_c)^2 - 2l(l - l_c)\cos(\theta_1)\right).
\end{aligned}$$

The velocity matrix C is given by

$$C = \begin{bmatrix} 0 & -ml(l-l_c)\sin(\theta_1)\dot{\theta}_2 \\ -ml(l-l_c)\sin(\theta_1)(\dot{\theta}_1 - \dot{\theta}_2) & ml(l-l_c)\sin(\theta_1)\dot{\theta}_1 \end{bmatrix}.$$

The gravity matrix G is given by

$$G = \begin{bmatrix} mg(l-l_c)\sin(\theta_1 - \theta_2) \\ -mg\left(l\sin(\theta_2) + l_c\sin(\theta_2) + (l-l_c)\sin(\theta_1 - \theta_2)\right) \end{bmatrix}.$$

The control matrix B is simply

$$B = \begin{bmatrix} 1 \\ 0 \end{bmatrix}$$

because the torque input $u(t)$ only drives the swing leg, changing its angular velocity.

The specifics of the error metric h are discussed further in the next section, but for now it is important to note that it depends only on θ_1 and θ_2. For control purposes, it is desirable to compute the time derivative of h:

$$\begin{aligned} \frac{dh}{dt} &= \frac{\partial h}{\partial x}\frac{dx}{dt} \\ &= \begin{bmatrix} \frac{\partial h}{\partial x_1} & \frac{\partial h}{\partial x_2} & 0 & 0 \end{bmatrix} \frac{dx}{dt} \\ &= \frac{\partial h}{\partial x_1}x_3 + \frac{\partial h}{\partial x_2}x_4. \end{aligned}$$

In contrast with higher derivatives of h, this does not depend on the input $u(t)$. Therefore, the first derivative of h can be used in a straightforward way in *computing* $u(t)$ as the walker progresses through time.

6.2 Angle-Following Algorithm

Leg angles are compared to the desired trajectory. During a step, the swing leg angle relative to the stance leg, θ_1, should follow a specific function of the stance leg angle from vertical, θ_2. That function, $z(\theta_2(t))$, is a Bézier polynomial chosen for dynamic stability. Trajectory-following error is given by

$$h(x) = x_1 - z(x_2) = \theta_1 - z(\theta_2). \tag{6.3}$$

The desired trajectory prescribed by the Bézier polynomial is illustrated in Figure 6.2. The error function of Equation (6.3) enforces the desired trajectory by giving large negative penalties when the stance leg angle θ_2 deviates too much from zero. In those situations, a corresponding θ_1 of larger than 1 rad, as plotted in Figure 6.2, is unattainable in practice during an attempt to continue walking, so the error $h(t)$ is certain to be large and negative.

In this case, $z(\theta_2)$ is a fourth-order polynomial:

$$z(\theta_2) = z_0 + z_1\theta_2 + z_2\theta_2^2 + z_3\theta_2^3 + z_4\theta_2^4.$$

For the examples of this chapter, the coefficients are

$$z_0, \ldots, z_4 = \begin{bmatrix} 0.469 & 3.06 & -17.9 & -21.0 & 170. \end{bmatrix}.$$

These coefficients come from a set of five parameters chosen in previous research to establish a desired walking speed of 0.17 m/s. A detailed discussion on choosing the coefficients can be found in [71].

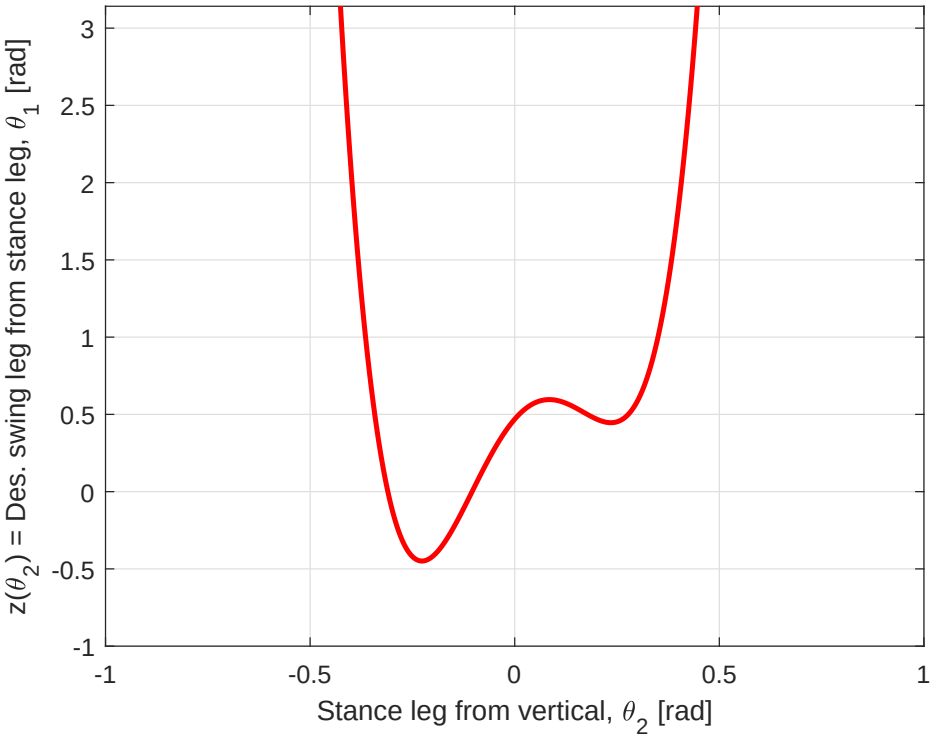

Figure 6.2. Desired correspondence between leg angles.

Given the state-space model of Equation (6.2), decomposed as

$$\dot{x} = f(x) + g(x)u(t),$$

an exponentially attractive periodic orbit can be achieved with the feedback linearization step

$$u(t) = \left(L_g L_f h(x)\right)^{-1} \left(v(t) - L_f^2 h(x)\right).$$

Here, the Lie derivatives L_f and L_g are equivalent to directional derivatives such that

$$\begin{aligned} L_f h(x) &= \frac{\partial h}{\partial x}(x) f(x), \\ L_f^2 h(x) &= \frac{\partial}{\partial x}\left(L_f h(x)\right) f(x), \end{aligned}$$

and so on. Along the lines of the discussion in [71], it follows that

$$\frac{d^2 h}{dt^2}(t) = v(t), \tag{6.4}$$

implying that an appropriate choice of $v(t)$ leads to stability.

The chosen algorithm is linear feedback. For any positive real numbers K_D and K_P, the solutions of the second-order differential equation

$$\frac{d^2 h}{dt^2}(t) + K_D \frac{dh}{dt}(t) + K_P h(t) = 0$$

drive $h(t)$ to zero. Therefore, keeping in mind Equation (6.4), the control signal

$$v(t) = -\left(K_D \frac{dh}{dt}(t) + K_P h(t)\right) \tag{6.5}$$

does the same. In this algorithm, the proportional-derivative control of Equation (6.5)

is generalized to

$$v(t) = -\left(K_D \frac{d^q h}{dt^q}(t) + K_P h(t)\right). \tag{6.6}$$

Compared to the shorthand PD, this type of control may be abbreviated PD^q. The execution of this control strategy based on a fractional derivative is discussed in the next section.

6.3 Fractional Derivative Control

Fractional derivatives are approximated in order to implement Equation (6.6). In the Laplace domain, the Padé approximant

$$s^q \approx \frac{b_0 + b_1 s + \cdots + b_n s^n}{a_0 + a_1 s + \cdots + a_n s^n}$$

is substituted for the fractional derivative of order q. Considering that powers of s correspond to derivatives, the Padé approximant is a way to improve accuracy relative to a Taylor series expansion of order n without needing to compute higher-order derivatives. An example of a first-order approximation is

$$s^{0.95} \approx \frac{1 + 39s}{39 + s}.$$

A comparison of this power of s and its approximation is given in Figure 6.3.

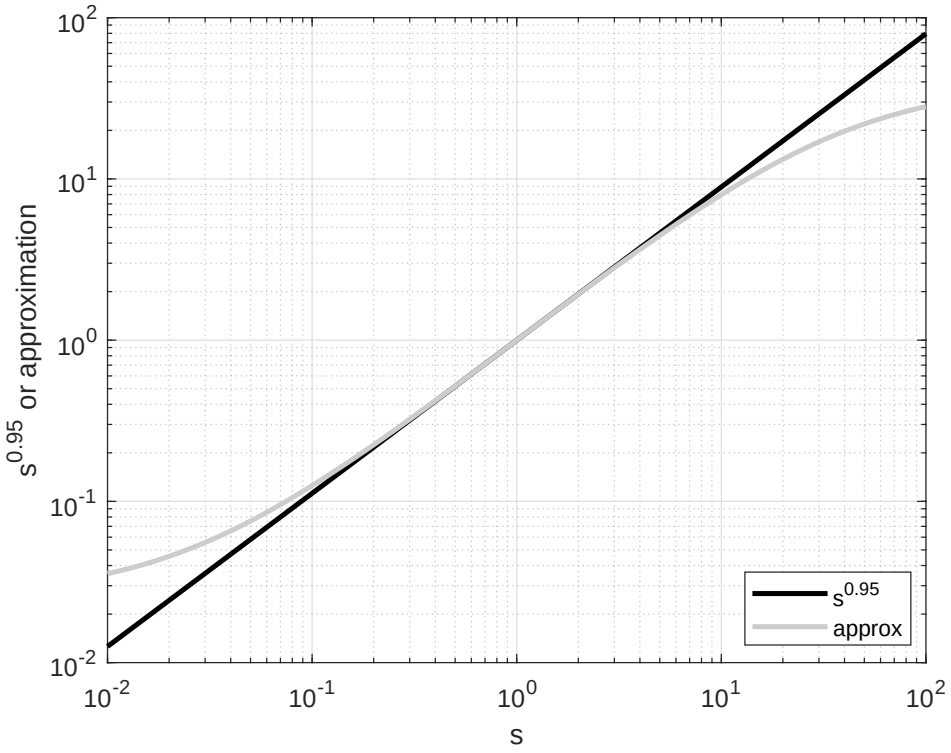

Figure 6.3. First-order Padé approximant about $s = 1$ for $s^{0.95}$.

The control and dynamics are computed together. The PD control equation, Equation (6.6), becomes

$$V(s) = -\left(K_D \frac{b_0 + b_1 s + \cdots + b_n s^n}{a_0 + a_1 s + \cdots + a_n s^n} H(s) + K_P H(s) \right).$$

After some manipulation,

$$\begin{aligned} &(a_0 + a_1 s + \cdots + a_n s^n) V(s) = \\ &\qquad - \left[K_D (b_0 + \cdots + b_n s^n) + K_P (a_0 + \cdots + a_n s^n) \right] H(s). \end{aligned}$$

In the time domain, this is a differential equation of order n to be solved for $v(t)$. The error $h(t)$ and its first derivative are known at each computation step; higher-order derivatives of $h(t)$ are not. However, recalling Equation (6.4), the substitution $s^2 H(s) = V(s)$ can be made as needed:

$$\begin{aligned} &\left[(a_0 + K_D b_2 + K_P a_2) + (a_1 + K_D b_3 + K_P a_3) s + \cdots \right. \\ &\qquad \left. + (a_{n-2} + K_D b_n + K_P a_n) s^{n-2} + a_{n-1} s^{n-1} + a_n s^n \right] V(s) \\ &\qquad = - \left[K_D (b_0 + b_1 s) + K_P (a_0 + a_1 s) \right] H(s). \end{aligned}$$

It follows that fractional derivative control is implemented by computing $v(t)$ from $h(t)$ and its first derivative. The time-domain differential equation is

$$\begin{aligned} &a_n v^{(n)}(t) + a_{n-1} v^{(n-1)}(t) \\ &\qquad + (a_{n-2} + K_D b_n + K_P a_n) v^{(n-2)}(t) \\ &\qquad + \cdots + (a_1 + K_D b_3 + K_P a_3) \dot{v}(t) \\ &\qquad + (a_0 + K_D b_2 + K_P a_2) v(t) \\ &\qquad = - \left((K_D b_0 + K_P a_0) h(t) + (K_D b_1 + K_P a_1) \frac{dh}{dt}(t) \right). \end{aligned}$$

In the examples that follow, $n = 1$, so the equation is

$$\begin{aligned} & a_1\dot{v}(t) + a_0 v(t) \\ & \qquad = -\left((K_D b_0 + K_P a_0) h(t) + (K_D b_1 + K_P a_1) \frac{dh}{dt}(t) \right). \end{aligned}$$

Computationally, the infrastructure of Equation (6.5) has to be expanded to accommodate $v(t)$ as the solution of a differential equation of order n. In the context of a numerical solver, this can be accomplished by adding n first-order equations alongside those defining the derivatives of $x_1, \ldots, x_4$. The new states represent $v, \ldots, v^{(n-1)}$, and all $n + 4$ equations can be solved simultaneously.

6.4 Error and Torque Results

Varying the controller order causes dynamical changes. This section presents the different types of beneficial results that are achievable by extending conventional PD to fractional-order control.

The first objective is to reduce error by changing the controller order q. In this scenario, the walker takes ten steps after a velocity disturbance. The walker's states before the disturbance are

$$x = \begin{bmatrix} -0.25 & -0.15 & 2.1 & 0.46 \end{bmatrix},$$

with the first two measured in rad and the others in rad/s. The disturbance raises x_4, the time derivative of $x_2 = \theta_2$, from 0.46 to 4.2 rad/s. Negative values of $x_1 = \theta_1$ and $x_2 = \theta_2$ mean that the walker has not yet crossed vertical and is thus early in its step; a greater x_4 pushes it forward unexpectedly fast. Controllers vary in order from 0.9 to 1, where 1 represents conventional PD. The error as a function of time, calculated by Equation (6.3), is plotted for selected values of q in Figure 6.4.

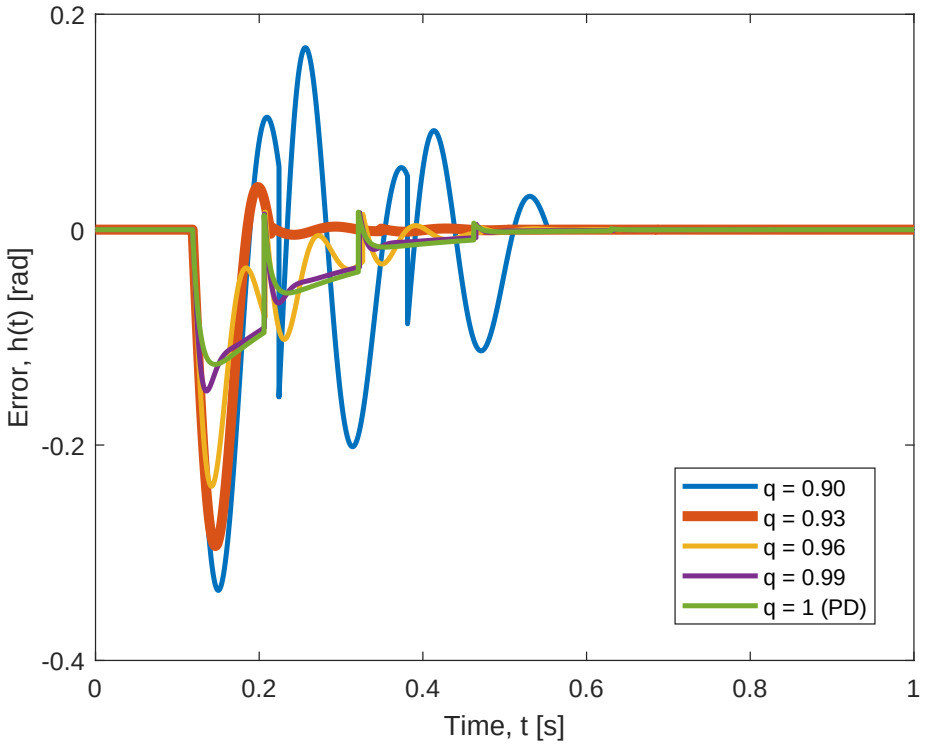

Figure 6.4. Error results for different control orders.

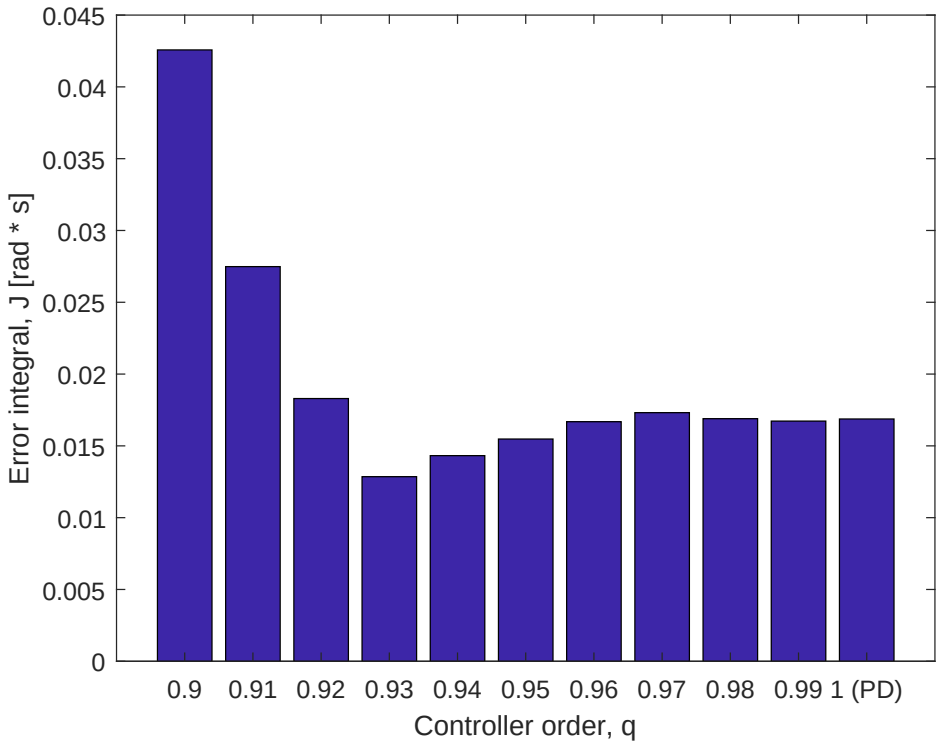

Figure 6.5. Performance results for different control orders.

Performance is measured by integrating the absolute value of the error $h(t)$ over the time taken for the PD-controlled walker to take ten steps. Order 0.93 performs best, as shown in Figure 6.5. The improvement is 24% less error compared to the case of PD control.

Order flexibility can also reduce the energy input required to execute the control strategy. The second objective is to recover similar performance to the PD controller, but with reduced gains. An example result that fulfills this objective is shown in Figure 6.6. With order 0.93, 32% less proportional gain, and 16% less derivative gain, the walker has the same integrated error (within a few percent) as it does with the original PD controller.

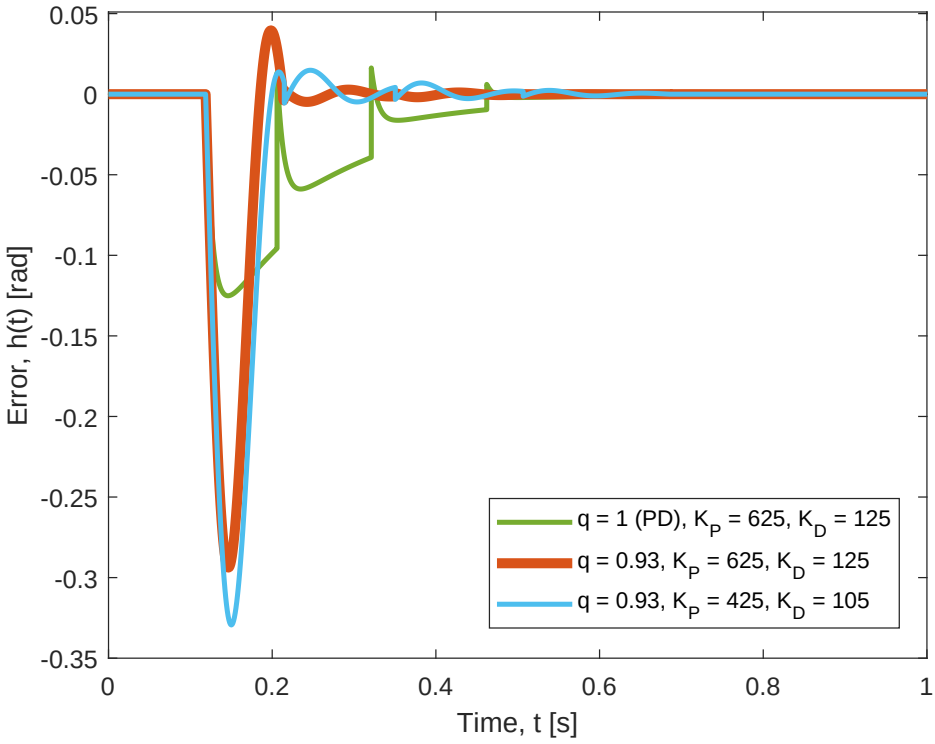

Figure 6.6. Evidence of fractional-order control with lower gains yielding the original level of performance.

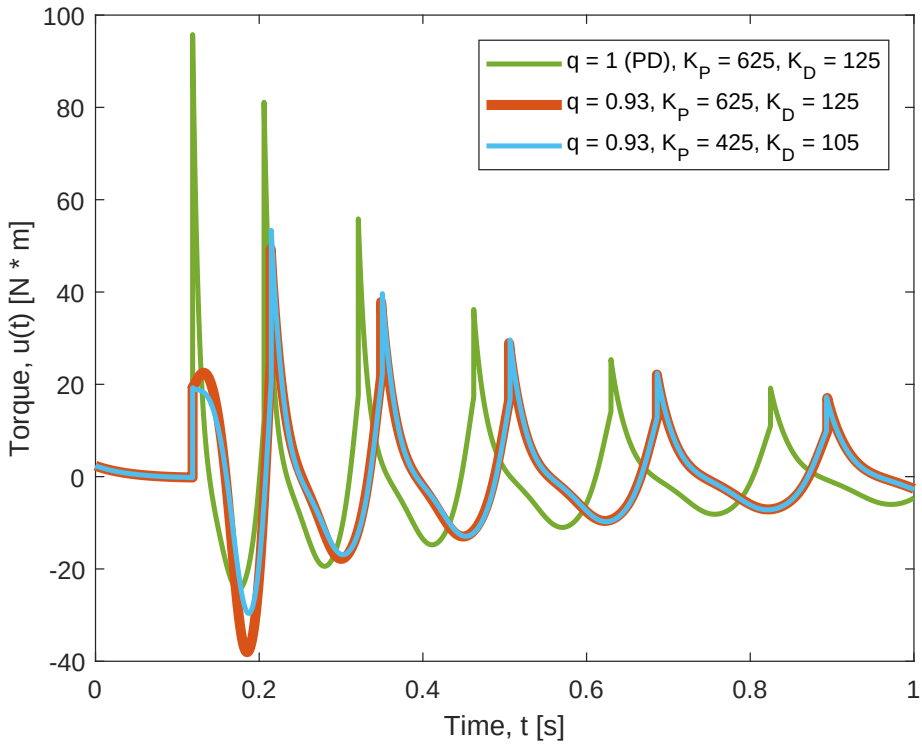

Figure 6.7. Evidence of fractional-order control with lower gains yielding reduced torque at the hip joint.

In the fractional-order controllers of Figure 6.6, the derivative gain is multiplying the time derivative of $h(t)$ having order 0.93 rather than order 1, and the function $h(t)$ itself evolves differently in each case. Therefore, that result does not conclusively demonstrate a reduced energy cost. To demonstrate those savings, the torque at the hip joint is examined; indeed the walker experiences less torque under fractional-order control. The controllers of order 0.93 bring about reduced torque magnitude, that is, smaller peaks, as shown in Figure 6.7. By inspection, the integral of the absolute value of torque with the reduced-gain controller is lower than that with the PD controller.

This chapter has taken the idea that fractional order can be varied in control and applied it to the setting of two-legged dynamic walking. The resulting improvements

are seen here in simulation; the walker can better follow a trajectory indicative of stability or replicate its previously established performance level with less applied torque.

Many lines of inquiry along which this research effort can continue are apparent. Broader searches and optimizations of several parameters would be informative. To this point, the problem has shown itself to be more numerically challenging for derivative orders outside the interval $[0.9, 1]$. Among control variables, the Padé approximant order stands out as a possible means to expand the solution space; however, increasing n has not been sufficient in isolation. Altering the gains is likely required to control the robot effectively with a wider range of controller orders. Incidentally, for test cases chosen among the successful examples presented here, increasing n adds computational complexity and does not change the resulting control signal.

The point s about which the Padé approximant is computed also influences the result. Considering that this control strategy uses s as an operator, it is not intuitive to associate s with a numerical value, and yet the expansion cannot be computed without doing so. Varying the expansion point and determining the mathematical ramifications of such a step would both be beneficial efforts.

The choices of controller order and gains in this chapter are experimental. Optimizing those would fall, respectively, within the categories of system identification and optimal control. While those pursuits are beyond the scope of this chapter, they would have the potential to expedite decisions about how to improve efficiency by expanding PD control to include fractional order.

Furthermore, the results of this research represent one example situation, not an exhaustive study. Making these results more comprehensive would involve varying the walker's initial leg angles and angular velocities. The parameters related to the disturbance can be varied as well, for purposes such as quantifying robustness.

Fractional-order control always has the potential to outperform PD and, in the

worst case, performs equally well when derivative order $q = 1$. This research has explored and demonstrated the potential of this added dimension of control design for a simulated two-legged dynamic walker. In separate trials, the robot's ability to follow a desired trajectory and its energy consumption are shown to improve. Therefore, fractional-order control is a possible pathway by which to develop more efficient walking robots.

CHAPTER 7

CONCLUSIONS AND SUGGESTED FUTURE ENDEAVORS

In complex systems cast as networks of mechanical components, order changes as a result of damage are evident. In Chapter 3, it is demonstrated that damage to a component causes a shift in frequency response that corresponds to an order change. Chapter 4 affirms these order changes by way of a computational system identification procedure. It is desired to incorporate fractional order measurement into a framework that transcends the context of the robot formation examples. To that end, the procedure of Chapter 4 can serve as a bridge from the observation of order changes within that context to monitoring of high-order systems in general. Chapter 5 expands the potential scope of application from systems containing springs and dampers to those having arbitrary linear connections. The link between dynamical changes and fractional-order models is promising for control of complex systems; Chapter 6 shows that fractional-order control can lead to marked improvement over integer-order control even in a setting not suggestive of fractional-order dynamics.

The main contributions of this dissertation are illustrations of principles underlying the proposed monitoring technique — tracking fractional order — and results asserting its value as an engineering tool. Some findings from the mechanically behaving robot formation systems presented in Chapters 3 and 4 that reveal the value of fractional order in system monitoring are:

- The order shifts resulting from damage among the interactions within these systems are linked with shifting frequency response characteristics that follow clear trends observable from data.

- Offsetting changes in mechanical properties of these systems' components, despite allowing roughly the same amount (magnitude) of force to be transmitted, can be diagnosed because they result in distinct fractional-order models.
- Damage to different components within these systems can be distinguished, and resulting dynamical effects quantified, merely by measuring the overall system's input-output relationship; exhaustive sensing is not necessary.

Findings such as these have the potential to shed new light on the practice of system monitoring. A comprehensive method built around fractional-order models would provide an efficient transition from data collection to damage detection and updating of models and control strategies. Inferences from these models could make the task of keeping a system operational after damage more viable.

This chapter proposes the remainder of the path leading to this comprehensive monitoring. The insights that have been presented so far can be buttressed mathematically; Chapter 5 is meant to light the way for those inquiries. They can be tested in environments that will assess practical applicability; Chapter 6, though limited to simulation, is meant to demonstrate the potential of fractional order in all modeling and control settings. Furthermore, they can be extended in the direction of an inverse problem of sorts: how to design a system with dynamics of a certain order that, in effect, is intentionally suitable for monitoring by fractional order. These discussions are followed by concluding remarks about the contributions of this dissertation.

7.1 Supporting Mathematical Framework

This branch of future work seeks further consolidation of the results presented so far with the theory of fractional calculus and differential equations. It is hypothesized that an explicit relationship can be found between the governing equation of a damaged system and that for an undamaged one, assuming that the damage is known in terms of the equation parameters. This extended mathematical analysis would strengthen the findings that suggest the presence of such a relationship.

In the coverage formation example, the duality between the damage results is compelling; the order change resulting from damage to the first spring is equal and opposite to that resulting from damage to the first damper. This occurs in spite of the fact that the operational constants for the stiffness and damping are different. The research effort proposed here would pursue the mathematical framework connecting damage to effects on a system's order and, in turn, its governing equation. The most obvious line of inquiry along which to proceed initially is perturbation analysis.

7.1.1 Perturbation Analysis

The fractional-order transfer function that is established as an accurate description for the undamaged coverage formation system comes from analysis of an infinite version of the system. It is plausible that further information about the causes of order changes may be found by probing the infinite system further.

If the new spring constant k_{d} is defined to be *any* deviation from expectation, $k_{\mathrm{d}} = k + \epsilon$, then the formulation of the transfer function for the infinite tree system is affected in the following way:

$$G_{\infty,\mathrm{damaged}}(s) = \frac{1}{\dfrac{1}{\dfrac{1}{k+\epsilon} + \dfrac{1}{\sqrt{kbs}}} + \dfrac{1}{\dfrac{1}{bs} + \dfrac{1}{\sqrt{kbs}}}}.$$

As explained in [38], the full self-similarity is lost. This inhibits one's ability to perform algebraic manipulations that might lead to a closed-form solution for $G_{\infty,\mathrm{damaged}}$, apart from condensing the fraction into

$$G_{\mathrm{damaged}}(s) = \frac{(k+\epsilon)\sqrt{bks} + bs\left(\sqrt{bks} + 2k + \epsilon\right)}{bs\left(k\left(2\sqrt{bks} + bs + \epsilon\right) + 2\epsilon\sqrt{bks} + k^2\right)}, \tag{7.1}$$

which raises no apparent interpretation of its own accord.

Perturbation analysis appears to be the most direct path by which the mathematical effects of damage to a high-order system may be discovered. Introducing a variable such as ϵ permits propagation of the damage throughout manipulation of any equation related to the system. In light of this mathematical advantage and the computational verification that damage can be detected in the infinite version of the example system, further insights can be pursued from perturbation.

7.1.2 Continued Fractions

At first glance, there is no order shift apparent in Equation (7.1). It is desired to reach a level of mathematical clarity that would lead to the analytical emergence of a transfer function of an order other than 1/2, or the expected order in general, after the introduction of damage to the model. In this regard, an avenue that presents a possible alternative to perturbation analysis is the study of continued fractions.

To be specific, one may express a transfer function of some noninteger power of s (or, in the robot formation example context, kbs) as a continued fraction. Two examples of these are

$$(kbs)^{1/2} = 1 + \cfrac{kbs-1}{2 + \cfrac{kbs-1}{2 + \cfrac{3(kbs-1)}{6 + \cfrac{3(kbs-1)}{2 + \ddots}}}}$$

and

$$(kbs)^{2/3} = 1 + \cfrac{2(kbs-1)}{3 + \cfrac{kbs-1}{2 + \cfrac{5(kbs-1)}{9 + \cfrac{4(kbs-1)}{2 + \ddots}}}}.$$

These particular continued fractions condense into ratios of polynomials where the numerator and denominator have the same order. This is problematic in a systems framework because, as transfer functions, they are improper; causality is lost, even keeping in mind that the specific link to the example system lies with the reciprocals of these fractions representing positive powers of kbs. However, these continued fraction representations are not unique. Future research could pursue alternative ways to obtain transfer functions for systems that contain fractional dynamics yet can be constructed from integer-order mechanical modeling components.

7.2 Robustness and Practical Examples

The shortest path of development from the principles presented in this work to their application in the physical world is likely to be their incorporation into system identification and structural health monitoring. The goal of applicability in the former suggests a need for assurance that the procedure is robust. For the latter, it should be shown that the method continues to reveal conclusive information across a variety of systems and damage cases.

7.2.1 Identification Refinement

Currently, with regard to the identification procedure that has been put forth, some sensitivity is present. Adjusting the boundaries of the frequency window chosen for the identification can have an effect on the dominance of the expected order in

the result. These effects, for the example systems of this dissertation, have not been sufficient to obscure the dominant order altogether; however, making a suboptimal choice of frequency boundaries can raise the question of whether there are actually several orders with noticeable impact on the response.

It is not always possible to know the best frequency window for sampling, so automating this decision is desirable. In light of the ease of computation of the transfer functions, an additional optimization loop that would iteratively select frequency boundaries and run the system identification procedure anew may be beneficial. In theory, this would extract the strongest possible result from the frequency response information, thus ensuring knowledge of the dynamical order of greatest importance.

However, considering the broad space of mechanical models, it is possible that some systems pose a situation in which multiple fractional-order terms are needed for faithful modeling. In such a case, it would be important to capture more than one dominant order. Multiple-term models are available from the identification procedure presented here, but their utility is less clear than that of their single-term counterparts. Perhaps there is a class of "multi-fractional-order" systems.

Systems with nonminimum phase cannot be perfectly modeled with the simplest version of the identification procedure of Chapter 4. One potential research direction could be to examine the effects of numerator terms on the identified transfer function accuracy and determine what conditions merit their inclusion and how many terms should be introduced. The order of the system becomes less clear with numerator terms, but monitoring from frequency response would still be possible.

7.2.2 Discussion of Applications

Throughout the procedure's evolution, it should be tested on data from multiple types of fractional-order systems. The choices of systems to examine may be inspired by the literature, but at least in part, this effort should incorporate physical data. A

priority of this research has been to lay a foundation for the engineering community to make use of these principles, so such uses should be forthcoming.

One potentially fruitful setting for this work is linear friction welding. This industrial application lends itself to fractional-order modeling because the types of forces on the oscillating part vary throughout the process. Initially, friction and elastic forces dominate, but the steady rise in temperature brings about effects suggestive of viscosity. The interpretation of this progression in a systems context is that the order of the forcing shifts from 0 to 1. Modeling of this process with a fractional-order differential equation is a pursuit motivated by the possibility of model simplification from a time-varying governing equation to a homogeneous one if the correct fractional order is chosen.

Solving equations relating parameters from proprietary data consisting of force (input) and part position (output) sinusoids from ten welds has yielded dozens of physically plausible governing equations with fractional-order terms. In other words, the coefficients of the second-order term capturing inertia and of the fractional-order term capturing the other forces share sign, implying stability. This is discussed in [23]. Optimization within this space of equations to find the particular order that best fits the process remains an open question. However, frequency-domain data could forge a strong connection between the modeling and monitoring outlined in this work and a segment of industry where fractional-order dynamics are suspected but not yet verified.

An additional area where the ideas presented in this work may acquire practical traction is structural health monitoring. Results from that field indicating fractional-order dynamics could enhance the transparency of the relevance of these contributions. Furthermore, the existing emphasis on frequency response in structural health monitoring suggests that the field may be in position to benefit from the incorporation of measurement of fractional order.

The foregoing discussion is not assumed to be complete. From a higher-level perspective, other experimental settings in industry ripe for innovation in light of this work certainly exist. The breadth of applications that stand to benefit from novel insights extracted from calculus, a veritable pillar of engineering, is vast.

7.3 Modeling and Design Implications

Exhaustively testing models of real and imagined mechanical systems through the lens of fractional order measurement is beyond the scope of finite time. Instead, the benefit of system monitoring by fractional order to modelers and control designers primarily lies in the transparency of the shifts in frequency response that are caused by damage. It is desired to extract information about how to construct mechanical models so that the systems respond at some arbitrary order, implying compatibility with the monitoring proposed in this work.

Preliminary examinations into constructions of tree network systems other than those in this dissertation have been made. For instance, one may alternate component patterns from one layer to the next, with the first layer having one spring and one damper but the second having all (four) components as springs, and so on. The transfer function of an infinite version of this system would be

$$G_\infty(s) = \frac{1}{\dfrac{1}{G_k(s) + \dfrac{1}{\dfrac{1}{G_k(s)+G_\infty(s)} + \dfrac{1}{G_k(s)+G_\infty(s)}}} + \dfrac{1}{G_b(s) + \dfrac{1}{\dfrac{2}{G_k(s)+G_\infty(s)}}}};$$

this is self-similar, as in the robot formation example.

A closed-form expression for $G_\infty(s)$ can be found algebraically. For completeness, it is given by

$$G_\infty(s) = \frac{1}{3}\left(-2G_k(s) - G_b(s) \pm \sqrt{13(G_k(s))^2 + 22G_k(s)G_b(s) + (G_b(s))^2}\right),$$

from which no affirmative conclusion about fractional order can be drawn. Future work, however, could explore reverse-engineering this algebra, turning a transfer function of some desired order into a corresponding combination of individual components.

7.4 Concluding Remarks

This dissertation has established new principles for monitoring of high-order mechanical systems. Fractional order is a transparent lens through which to view dynamical changes experienced by such a system. The benefits of this type of monitoring that specifically depend on the mathematics of fractional calculus are twofold. First, detection of a problem in the domain of frequency response leads immediately to the determination of a governing equation for the system as it is currently operating. This means that if it is desired to continue using the system after damage or some other modification, the new governing equation can be employed in testing the new system on various types of inputs in simulation.

In turn, the second benefit is that these simulations can be computationally efficient because of the model simplification from high order to fractional order. From the outset, this has been the primary motivation for seeking to extract insights from fractional calculus. The flexibility afforded to the modeler by the choice of dynamical order among all real numbers allows for the generation of system models with virtually any set of response characteristics, without having to include an expensively large number of terms in the governing equation.

In the evolution of a system, modeling is followed by control and design. Indeed, the advances in modeling presented in this dissertation affect the other two areas as well. Reductions in simulation time can easily propagate into development of a control strategy, but the variety of options for this control strategy itself may be expanded to include fractional-order methods as well. The inverse problem discussed just before this section, which seeks a way to produce mechanical system models of

arbitrary order, is specifically motivated by the area of design. If there is a benefit to be had in a particular engineering setting by creating a fractional-order component from some combination of others that are available, these advances can further that pursuit.

This work extends mathematically into the concept of implicit operators as models for complex systems. The possibility of closed-form models for systems previously reserved for numerical approaches is appealing. Additionally, this work extends practically into fractional-order control. If that concept can be beneficial in an application not suggestive of fractional-order dynamics whatsoever, such as two-legged walking, its promise is certainly no less evident for control of fractional-order systems. As that class of systems grows, so too does the potential of fractional order as an influential parameter in modeling and control.

Perhaps optimistically, there will be benefits of unknown nature that follow from this work as well. This is likely to be the case because of the intellectual proximity of the advances presented here to the building blocks of calculus. A complete list of all applications of calculus that have helped civilization would exceed the limits of the human mind. This work is presented with the intention of expanding that list.

BIBLIOGRAPHY

1. J. Alastruey, K. Parker, J. Peiró, and S. Sherwin. Analysing the pattern of pulse waves in arterial networks: a time-domain study. *Journal of Engineering Mathematics*, 64(4):331–351, 2009.

2. Y. Altintas, C. Brecher, M. Weck, and S. Witt. Virtual machine tool. *CIRP Annals-Manufacturing Technology*, 54(2):115–138, 2005.

3. D. Baleanu, J. A. T. Machado, and A. C. J. Luo. *Fractional Dynamics and Control*. Springer Publishing Company, Inc., New York, 2011.

4. J. Cao, S. Xue, J. Lin, and Y. Chen. Nonlinear dynamic analysis of a cracked rotor-bearing system with fractional order damping. *Journal of Computational and Nonlinear Dynamics*, 8(3):031008, 2013.

5. Y. Cao and W. Ren. Distributed formation control for fractional-order systems: Dynamic interaction and absolute/relative damping. *Systems & Control Letters*, 59(34):233–240, 2010.

6. Y. Cao, Y. Li, W. Ren, and Y. Q. Chen. Distributed coordination of networked fractional-order systems. *IEEE Transactions on Systems, Man, and Cybernetics; Part B: Cybernetics*, 40(2):362–370, 2010.

7. Y. Cao, W. Yu, W. Ren, and G. Chen. An overview of recent progress in the study of distributed multi-agent coordination. *IEEE Transactions on Industrial Informatics*, 9(1):427–438, 2013.

8. S. Celikovsky, J. Zikmund, and C. Moog. Partial exact linearization design for the Acrobot walking. In *Proceedings of the 2008 American Control Conference*, pages 874–879. IEEE, 2008.

9. E. N. Chatzi and A. W. Smyth. The unscented Kalman filter and particle filter methods for nonlinear structural system identification with non-collocated heterogeneous sensing. *Structural Control and Health Monitoring*, 16(1):99–123, 2009.

10. M. N. Chatzis and E. N. Chatzi. A discontinuous unscented Kalman filter for non-smooth dynamic problems. *Frontiers in Built Environment*, 3, 2017. doi: 10.3389/fbuil.2017.00056. URL `https://doi.org/10.3389/fbuil.2017.00056`.

11. C.-W. Chen, J.-N. Juang, and G. Lee. Frequency domain state-space system identification. In *Proceedings of the 1993 American Control Conference*, pages 3057–3061. IEEE, 1993.

12. Y. Chen and K. L. Moore. Analytical stability bound for a class of delayed fractional-order dynamic systems. *Nonlinear Dynamics*, 29(1-4):191–200, 2002.

13. A. K. Das, R. Fierro, V. Kumar, J. P. Ostrowski, J. Spletzer, and C. J. Taylor. A vision-based formation control framework. *IEEE Transactions on Robotics and Automation*, 18(5):813–825, 2002.

14. S. Das. *Functional Fractional Calculus*. Springer Science & Business Media, 2011.

15. H. Delavari, P. Lanusse, and J. Sabatier. Fractional order controller design for a flexible link manipulator robot. *Asian Journal of Control*, 15:783–795, 2013.

16. P. Derler, E. A. Lee, and A. S. Vincentelli. Modeling cyber–physical systems. *Proceedings of the IEEE*, 100(1):13–28, 2012.

17. M. Di Paola, G. Failla, and M. Zingales. Physically-based approach to the mechanics of strong non-local linear elasticity theory. *Journal of Elasticity*, 97(2): 103–130, 2009.

18. M. Di Paola, F. P. Pinnola, and M. Zingales. Fractional differential equations and related exact mechanical models. *Computers & Mathematics with Applications*, 66(5):608–620, 2013.

19. J. A. Fax and R. M. Murray. Information flow and cooperative control of vehicle formations. *IEEE Transactions on Automatic Control*, 49(9):1465–1476, 2004.

20. J. Flores, J. Alastruey, and P. E. Corvera. A novel analytical approach to pulsatile blood flow in the arterial network. *Annals of Biomedical Engineering*, 44(10): 3047–3068, 2016.

21. B. Goodwine. Fractional-order dynamics in a random, approximately scale-free network of agents. In *Proceedings of the IEEE Conference on Control, Automation, Robotics & Vision*, pages 1581–1586, 2014.

22. B. Goodwine. Modeling a multi-robot system with fractional-order differential equations. In *Proceedings of the IEEE International Conference on Robotics and Automation*, pages 1763–1768, 2014.

23. B. Goodwine and K. Leyden. Recent results in fractional-order modeling in multi-agent systems and linear friction welding. *IFAC-PapersOnLine*, 48(1):380–381, 2015. Extended abstract, 8th Vienna International Conference on Mathematical Modelling.

24. S. K. Goumas, M. E. Zervakis, and G. S. Stavrakakis. Classification of washing machines vibration signals using discrete wavelet analysis for feature extraction. *IEEE Transactions on Instrumentation and Measurement*, 51(3):497–508, 2002.

25. T. T. Hartley and C. F. Lorenzo. Fractional-order system identification based on continuous order-distributions. *Signal Processing*, 83(11):2287–2300, 2003.

26. A. Hereid, E. A. Cousineau, C. M. Hubicki, and A. D. Ames. 3D dynamic walking with underactuated humanoid robots: A direct collocation framework for optimizing hybrid zero dynamics. In *Proceedings of the 2016 IEEE International Conference on Robotics and Automation (ICRA)*, pages 1447–1454. IEEE, 2016.

27. N. Heymans and J.-C. Bauwens. Fractal rheological models and fractional differential equations for viscoelastic behavior. *Rheologica Acta*, 33:210–219, 1994.

28. K. Hirai, M. Hirose, Y. Haikawa, and T. Takenaka. The development of Honda humanoid robot. In *Proceedings of the 1998 IEEE International Conference on Robotics and Automation*, volume 2, pages 1321–1326. IEEE, 1998.

29. C. M. Ionescu, J. Tenreiro Machado, and R. De Keyser. Modeling of the lung impedance using a fractional-order ladder network with constant phase elements. *IEEE Transactions on Biomedical Circuits and Systems*, 5(1):83–89, 2011.

30. I. W. Jamaludin, N. A. Wahab, N. S. Khalid, S. Sahlan, Z. Ibrahim, and M. F. Rahmat. N4SID and MOESP subspace identification methods. In *Proceedings of the 2013 IEEE 9th International Colloquium on Signal Processing and its Applications (CSPA)*, pages 140–145. IEEE, 2013.

31. J.-N. Juang and R. S. Pappa. An eigensystem realization algorithm for modal parameter identification and model reduction. *Journal of Guidance, Control, and Dynamics*, 8(5):620–627, 1985.

32. S. Kagami, T. Kitagawa, K. Nishiwaki, T. Sugihara, M. Inaba, and H. Inoue. A fast dynamically equilibrated walking trajectory generation method of humanoid robot. *Autonomous Robots*, 12(1):71–82, 2002.

33. T. Kalmár-Nagy, G. Stépán, and F. C. Moon. Subcritical hopf bifurcation in the delay equation model for machine tool vibrations. *Nonlinear Dynamics*, 26(2): 121–142, 2001.

34. G. Karsai and J. Sztipanovits. Model-integrated development of cyber-physical systems. In *Proceedings of the IFIP International Workshop on Software Technologies for Embedded and Ubiquitous Systems*, pages 46–54. Springer, 2008.

35. J. F. Kelly and R. J. McGough. Fractal ladder models and power law wave equations. *The Journal of the Acoustical Society of America*, 126(4):2072–2081, 2009.

36. E. A. Lee. CPS foundations. In *Proceedings of the 2010 47th ACM/IEEE Design Automation Conference (DAC)*, pages 737–742. IEEE, 2010.

37. N. E. Leonard and E. Fiorelli. Virtual leaders, artificial potentials, and coordinated control of groups. In *Proceedings of the 40th IEEE Conference on Decision and Control*, pages 2968–2973, December 2001.

38. K. Leyden and B. Goodwine. Using fractional-order differential equations for health monitoring of a system of cooperating robots. In *Proceedings of the 2016 IEEE International Conference on Robotics and Automation (ICRA)*, pages 366–371. IEEE, 2016.

39. K. Leyden and B. Goodwine. Fractional-order system identification for health monitoring. *Nonlinear Dynamics*, 2018. doi: 10.1007/s11071-018-4128-y. URL `https://doi.org/10.1007/s11071-018-4128-y`.

40. K. Leyden, M. Sen, and B. Goodwine. Models from an implicit operator describing a large mass-spring-damper network. *IFAC-PapersOnLine*, 2018. In press from 9th Vienna International Conference on Mathematical Modelling.

41. D.-Y. Liu, T.-M. Laleg-Kirati, O. Gibaru, and W. Perruquetti. Identification of fractional order systems using modulating functions method. In *Proceedings of the IEEE American Control Conference (ACC)*, pages 1679–1684, 2013.

42. J. T. Machado, V. Kiryakova, and F. Mainardi. Recent history of fractional calculus. *Communications in Nonlinear Science and Numerical Simulation*, 16 (3):1140–1153, 2011.

43. A. E. Martin and J. P. Schmiedeler. Predicting human walking gaits with a simple planar model. *Journal of Biomechanics*, 47(6):1416–1421, 2014.

44. J. Mayes. *Reduction and Approximation in Large and Infinite Potential-Driven Flow Networks*. PhD thesis, University of Notre Dame, 2012.

45. J. Mayes and M. Sen. Approximation of potential-driven flow dynamics in large-scale self-similar tree networks. *Proceedings of the Royal Society A*, 467:2810–2824, 2011.

46. C. A. Monje, B. M. Vinagre, V. Feliu, and Y. Chen. Tuning and auto-tuning of fractional order controllers for industry applications. *Control Engineering Practice*, 16(7):798–812, 2008.

47. K. Murphy, G. Hunt, and D. P. Almond. Evidence of emergent scaling in mechanical systems. *Philosophical Magazine*, 86(21-22):3325–3338, 2006.

48. R. M. Murray. Recent research in cooperative control of multivehicle systems. *Journal of Dynamic Systems, Measurement, and Control*, 129(5):571, 2007.

49. A. Narang, S. L. Shah, and T. Chen. Continuous-time model identification of fractional-order models with time delays. *IET Control Theory & Applications*, 5 (7):900–912, 2011.

50. K. B. Oldham and J. Spanier. *The Fractional Calculus*. Academic Press, New York, 1974.

51. M. D. Ortigueira. An introduction to the fractional continuous-time linear systems: the 21st century systems. *Circuits and Systems Magazine, IEEE*, 8(3): 19–26, 2008.

52. M. D. Ortigueira. *Fractional Calculus for Scientists and Engineers*, volume 84 of *Lecture Notes in Electrical Engineering*. Springer, 2011.

53. M. D. Ortigueira and J. Tenreiro Machado. What is a fractional derivative? *Journal of Computational Physics*, 293:4–13, 2015.

54. A. Oustaloup. *La Dérivation Non Entière*. Hermes, Paris, 1995.

55. B. Peeters and G. De Roeck. Reference-based stochastic subspace identification for output-only modal analysis. *Mechanical Systems and Signal Processing*, 13 (6):855–878, 1999.

56. I. Podlubny. *Fractional Differential Equations*. Academic Press, San Diego, 1998.

57. D. C. Post and J. P. Schmiedeler. Velocity disturbance rejection for planar bipeds walking with HZD-based control. In *Proceedings of the 2014 IEEE/RSJ International Conference on Intelligent Robots and Systems (IROS)*, pages 4882–4887. IEEE, 2014.

58. I. Poulakakis and J. W. Grizzle. Modeling and control of the monopedal robot Thumper. In *Proceedings of the 2009 IEEE International Conference on Robotics and Automation*, pages 3327–3334. IEEE, 2009.

59. C. Rainieri and G. Fabbrocino. Development and validation of an automated operational modal analysis algorithm for vibration-based monitoring and tensile load estimation. *Mechanical Systems and Signal Processing*, 60:512–534, 2015.

60. W. Ren, R. W. Beard, and E. M. Atkins. Information consensus in multivehicle cooperative control. *IEEE Control Systems Magazine*, pages 71–82, April 2007.

61. E. Reynders, J. Houbrechts, and G. De Roeck. Fully automated (operational) modal analysis. *Mechanical Systems and Signal Processing*, 29:228–250, 2012.

62. M. J. Roemer and G. J. Kacprzynski. Advanced diagnostics and prognostics for gas turbine engine risk assessment. In *2000 IEEE Aerospace Conference Proceedings*, volume 6, pages 345–353. IEEE, 2000.

63. A. H. Shirdel, K.-M. Björk, and H. T. Toivonen. Identification of linear switching system with unknown dimensions. In *Proceedings of the 2014 47th Hawaii International Conference on System Sciences (HICSS)*, pages 1344–1352. IEEE, 2014.

64. F. Silva and V. Santos. Towards an autonomous small-size humanoid robot: Design issues and control strategies. In *Proceedings of the 2005 IEEE International Symposium on Computational Intelligence in Robotics and Automation*, pages 87–92. IEEE, 2005.

65. M. F. Silva, J. A. T. Machado, and A. M. Lopes. Fractional order control of a hexapod robot. *Nonlinear Dynamics*, 38(1-4):417–433, 2004.

66. M. C. Smith. Synthesis of mechanical networks: the inerter. *IEEE Transactions on Automatic Control*, 47(10):1648–1662, 2002.

67. K. Sreenath, H.-W. Park, I. Poulakakis, and J. W. Grizzle. Embedding active force control within the compliant hybrid zero dynamics to achieve stable, fast running on MABEL. *The International Journal of Robotics Research*, 32(3): 324–345, 2013.

68. V. E. Tarasov. *Fractional Dynamics: Applications of Fractional Calculus to Dynamics of Particles, Fields and Media*. Springer Science & Business Media, 2011.

69. S. Türkay and H. Akçay. A study of random vibration characteristics of the quarter-car model. *Journal of Sound and Vibration*, 282(1):111–124, 2005.

70. E. R. Westervelt, J. W. Grizzle, and D. E. Koditschek. Hybrid zero dynamics of planar biped walkers. *IEEE Transactions on Automatic Control*, 48(1):42–56, 2003.

71. E. R. Westervelt, J. W. Grizzle, C. Chevallereau, J. H. Choi, and B. Morris. *Feedback Control of Dynamic Bipedal Robot Locomotion*. CRC Press, 2007.

72. J. Yamaguchi, E. Soga, S. Inoue, and A. Takanishi. Development of a bipedal humanoid robot-control method of whole body cooperative dynamic biped walking. In *Proceedings of the 1999 IEEE International Conference on Robotics and Automation*, volume 1, pages 368–374. IEEE, 1999.

73. A. H. Zemanian. *Infinite Electrical Networks*, volume 101 of *Cambridge Tracts in Mathematics*. Cambridge University Press, 1991.

74. C. Zhai, D. Hanaor, and Y. Gan. Universality of the emergent scaling in finite random binary percolation networks. *PLOS ONE*, 12(2), 2017. doi: 10.1371/journal.pone.0172298. URL `https://doi.org/10.1371/journal.pone.0172298`.

75. C. Zhao, D. Xue, and Y. Chen. A fractional order PID tuning algorithm for a class of fractional order plants. In *Proceedings of the IEEE International Conference on Mechatronics & Automation*, 2005.

76. S. Zhou, J. Cao, and Y. Chen. Genetic algorithm-based identification of fractional-order systems. *Entropy*, 15(5):1624–1642, 2013.

This document was prepared & typeset with pdfLaTeX*, and formatted with* NDdiss2$_\varepsilon$ *classfile (v3.2013[2013/04/16]) provided by Sameer Vijay and updated by Megan Patnott.*